

**A LIQUID FERTILIZER CONCENTRATION
MEASUREMENT SYSTEM BASED ON THE
MICROWAVE SENSOR AND INTERNET OF
THINGS (IOT) TECHNOLOGY**

LIM ZHENG YOONG

UNIVERSITI TUNKU ABDUL RAHMAN

**A LIQUID FERTILIZER CONCENTRATION MEASUREMENT
SYSTEM BASED ON THE MICROWAVE SENSOR AND INTERNET
OF THINGS (IOT) TECHNOLOGY**

LIM ZHENG YOONG


**A project report submitted in partial fulfilment of the
requirements for the award of Bachelor of Engineering
(Honours) Mechatronics Engineering**

**Lee Kong Chian Faculty of Engineering and Science
Universiti Tunku Abdul Rahman**

September 2022

DECLARATION

I hereby declare that this project report is based on my original work except for citations and quotations which have been duly acknowledged. I also declare that it has not been previously and concurrently submitted for any other degree or award at UTAR or other institutions.

Signature :  _____

Name : Lim Zheng Yoong

ID No. : 18UEB00409

Date : 12-9-2022

APPROVAL FOR SUBMISSION

I certify that this project report entitled “**A LIQUID FERTILIZER CONCENTRATION MEASUREMENT SYSTEM BASED ON THE MICROWAVE SENSOR AND INTERNET OF THINGS (IOT) TECHNOLOGY**” was prepared by **LIM ZHENG YOONG** has met the required standard for submission in partial fulfilment of the requirements for the award of Bachelor of Engineering (Honours) Mechatronics Engineering at Universiti Tunku Abdul Rahman.

Approved by,

Signature : 

Supervisor : Ir Dr Mun Hou Kit

Date : 29/9/2022

Signature : 

Co-Supervisor : Dr Kwan Ban Hoe

Date : 30 Sep 2022

The copyright of this report belongs to the author under the terms of the copyright Act 1987 as qualified by Intellectual Property Policy of Universiti Tunku Abdul Rahman. Due acknowledgement shall always be made of the use of any material contained in, or derived from, this report.

© 2022, Lim Zheng Yoong. All right reserved.

ACKNOWLEDGEMENTS

I would like to thank everyone who had contributed to the successful completion of this project. I would like to express my gratitude to my research supervisor and co-supervisor, Dr. Mun Hou Kit and Dr. Kwan Ban Hoe for their invaluable advice, guidance and enormous patience throughout the development of the research.

In addition, I would also like to express my gratitude to my loving parents and friends who had helped and given me encouragement in this project.

ABSTRACT

Many people are suffering from hunger, especially in the region of Africa. This shows that agricultural production is not enough to supply the food demand. Due to global warming, rising sea levels will reduce the land for agriculture and extreme weather event will occur more frequently. This will decrease the total crop yields and affect the global food supply. To overcome this problem, crop production must increase. By using a suitable concentration of liquid fertilizer on the crops, crop yields can rise significantly. Determination of the liquid fertilizer concentration accurately and fast is one of the ways to increase crop yields. All the system proposed by previous researchers does not integrate with Internet of Things (IoT) technology. The microwave sensor has the advantages of fast response time, non-intrusive and non-invasive which is suitable to use for liquid fertilizer concentration real time monitoring. This study proposed a planar microwave sensor to measure the urea and monoammonium phosphate (MAP) liquid fertilizer. The sensor characteristic is measured by a vector network analyser (VNA) to determine the frequencies that have a linear trend between the transmission coefficient (S_{21}) and the concentration of liquid fertilizers. The sensitivity of urea is 3.20 dB/(g/mL) at 2.37 GHz and MAP is 1.13 dB/(g/mL) at 2.54 GHz. The liquid fertilizer concentration measurement system has been developed. The calibration equation is obtained by measuring the power detector output voltage. Next, the validation test is carried out by using the calibration equation. The validation result shows that the coefficient of determination (R^2) is higher than 0.9 and the root mean square error (RMSE) is less than 0.1 for both fertilizers. IoT technology is integrated into this system. The measured concentration can be monitored using the developed android mobile application and web application while the data is stored in the Firebase Realtime Database.

TABLE OF CONTENTS

| | | |
|--|--|-------------|
| DECLARATION | | i |
| APPROVAL FOR SUBMISSION | | ii |
| ACKNOWLEDGEMENTS | | iv |
| ABSTRACT | | v |
| TABLE OF CONTENTS | | vi |
| LIST OF TABLES | | ix |
| LIST OF FIGURES | | x |
| LIST OF SYMBOLS / ABBREVIATIONS | | xiii |
| LIST OF APPENDICES | | xv |
| | | |
| CHAPTER | | |
| 1 | INTRODUCTION | 1 |
| 1.1 | General Introduction | 1 |
| 1.2 | Importance of the Study | 2 |
| 1.3 | Problem Statement | 4 |
| 1.4 | Aim and Objectives | 6 |
| 1.5 | Scope and Limitation of the Study | 6 |
| 1.6 | Contribution of the Study | 7 |
| 1.7 | Outline of the Report | 8 |
| 2 | LITERATURE REVIEW | 9 |
| 2.1 | Introduction | 9 |
| 2.2 | Fertilizer concentration measurement sensor | 9 |
| 2.2.1 | Conductivity sensor | 9 |
| 2.2.2 | Ion selective sensor | 9 |
| 2.2.3 | Ultraviolet-visible spectroscopy | 10 |
| 2.2.4 | Colorimeter | 10 |
| 2.2.5 | Comparison of the fertilizer concentration measurement sensor | 11 |
| 2.3 | Planar microwave sensor | 14 |

| | | |
|----------|---|-----------|
| 2.4 | Liquid fertilizer concentration | 18 |
| 2.5 | IoT architectures | 18 |
| 2.6 | Wireless communication protocol | 21 |
| 2.7 | IoT agriculture system | 24 |
| 3 | METHODOLOGY AND WORK PLAN | 27 |
| 3.1 | Project Planning and Milestones | 27 |
| 3.2 | Design workflow and system architecture | 28 |
| 3.3 | Design and simulation of microwave sensor | 29 |
| 3.4 | Fabrication of microwave sensor | 31 |
| 3.5 | Evaluation method of microwave sensor | 31 |
| 3.6 | Hardware Components | 34 |
| | 3.6.1 Microwave sensor | 34 |
| | 3.6.2 Power detector | 35 |
| | 3.6.3 Voltage controlled oscillator (VCO) | 35 |
| | 3.6.4 ESP32 DEVKIT V1 Board | 35 |
| | 3.6.5 Analogue to digital converter | 36 |
| | 3.6.6 OLED display | 37 |
| 3.7 | Software | 38 |
| | 3.7.1 Firebase Cloud Server | 38 |
| | 3.7.2 Arduino IDE | 38 |
| | 3.7.3 Visual Studio Code | 39 |
| | 3.7.4 Expo | 39 |
| | 3.7.5 Proteus | 40 |
| 3.8 | Evaluation method of the sensor with the developed prototype | 40 |
| 4 | RESULTS AND DISCUSSION | 42 |
| 4.1 | Result of simulated microwave sensor | 42 |
| 4.2 | Comparison between simulated and measured characteristics of microwave sensor | 45 |
| 4.3 | Evaluation of microwave sensor by using VNA | 46 |
| 4.4 | Software design | 51 |
| | 4.4.1 MCU program | 51 |
| | 4.4.2 Firebase Realtime Database | 52 |

| | | |
|----------|--|------------|
| 4.4.3 | Data monitoring via browser and mobile application | 53 |
| 4.5 | Hardware design | 55 |
| 4.5.1 | Circuit Diagram and Pin Connection | 55 |
| 4.5.2 | PCB design | 57 |
| 4.5.3 | Project Prototype | 58 |
| 4.6 | Evaluate prototype of liquid fertilizer concentration measurement system | 59 |
| 4.7 | Problem Encountered and Improvement | 65 |
| 4.8 | Summary | 66 |
| 5 | CONCLUSIONS AND RECOMMENDATIONS | 67 |
| 5.1 | Conclusions | 67 |
| 5.2 | Recommendations for future work | 68 |
| | REFERENCES | 69 |
| | APPENDICES | 78 |
| | LIST OF PUBLICATIONS | 106 |

LIST OF TABLES

| | | |
|------------|---|----|
| Table 1.1: | The function of macronutrients, deficiency symptoms and effect (Uchida, 2014). | 2 |
| Table 2.1: | Comparison of various sensors for liquid fertilizer concentration measurement | 13 |
| Table 2.2: | Summary of different microwave sensor designs with the concentration of liquid under test | 16 |
| Table 2.3: | Concentration of liquid fertilizer used for irrigation or hydroponic solution | 18 |
| Table 2.4: | Comparison of different wireless communication protocols (Saad et al., 2014; Al-Sarawi et al., 2017; Poursafar, Alahi and Mukhopadhyay, 2017; Sinha, Wei and Hwang, 2017) | 22 |
| Table 2.5: | Different designs of IoT agriculture system | 24 |
| Table 3.1: | Gantt chart of part I project | 27 |
| Table 3.2: | Gantt chart of part II project | 27 |
| Table 3.3: | Design specifications of microwave sensor | 30 |
| Table 3.4: | Concentration of urea solution used in this experiment | 32 |
| Table 3.5: | Concentration of MAP solution used in this experiment | 34 |
| Table 4.1: | Dimensions of the microwave sensor | 42 |
| Table 4.2: | Summary of the sensor characteristics between simulation and measurement result | 46 |
| Table 4.3: | Comparison of various sensors for liquid fertilizer concentration measurement | 64 |

LIST OF FIGURES

| | | |
|--------------|---|----|
| Figure 1.1: | Fertilizer consumption in the world from 1961 to 2019 (International Fertilizer Association, 2019). | 1 |
| Figure 1.2: | Number of people faced hunger in the world (FAO et al., 2021). | 3 |
| Figure 2.1: | Five layers of IoT architecture | 20 |
| Figure 2.2: | Classification of wireless communication technology | 21 |
| Figure 3.1: | Workflow of methodology | 28 |
| Figure 3.2: | Block diagram of the liquid fertilizer concentration measurement system | 28 |
| Figure 3.3: | Geometry of planar transmission lines (a) microstrip line, (b) stripline and (c) coplanar waveguide | 30 |
| Figure 3.4: | Measurement setup | 33 |
| Figure 3.5: | Power detector | 35 |
| Figure 3.6: | VCO | 35 |
| Figure 3.7: | ESP32 DEVKIT V1 board | 36 |
| Figure 3.8: | ESP32 DEVKIT V1 board pinout (Random Nerd Tutorials, 2022) | 36 |
| Figure 3.9: | ADS1115 ADC | 37 |
| Figure 3.10: | OLED display | 38 |
| Figure 3.11: | Arduino IDE interface | 39 |
| Figure 3.12: | Prototype measurement setup | 41 |
| Figure 4.1: | Layout of planar microwave sensor (a) top view and (b) side view | 42 |
| Figure 4.2: | Simulated S parameters results of microwave sensor | 43 |
| Figure 4.3: | Direction of signal and power flow | 43 |
| Figure 4.4: | Electric field distribution at the resonance frequency (2.425GHz) for (a) isometric view, (b) front view, (c) transverse cross-section view in the middle of the x-axis | |

| | | |
|--------------|---|----|
| | and (d) transverse cross-section view in the middle of the y-axis | 44 |
| Figure 4.5: | Comparison of S parameter between simulated and fabricated sensor | 45 |
| Figure 4.6: | Graph of S_{21} against the frequency for different urea concentrations | 47 |
| Figure 4.7: | Graph of S_{21} against urea concentration at (a) 2.09 GHz and (b) 2.37 GHz | 48 |
| Figure 4.8: | Graph of S_{21} against the frequency for different MAP concentrations | 49 |
| Figure 4.9: | Graph of S_{21} against urea concentration at (a) 2.54 GHz and (b) 2.92 GHz | 50 |
| Figure 4.10: | Flow chart of the main loop program and power detector output voltage measurement program | 51 |
| Figure 4.11: | Flow chart of the concentration conversion program | 52 |
| Figure 4.12: | Firestore Realtime Database | 53 |
| Figure 4.13: | Android mobile application layouts (a) home page, (b) graph page and (c) history page | 54 |
| Figure 4.14: | Web application layouts (a) home page, (b) graph page and (c) history page | 55 |
| Figure 4.15: | Schematic diagram of the liquid fertilizer monitoring system | 55 |
| Figure 4.16: | PCB Layout | 57 |
| Figure 4.17: | Bottom View of fabricated PCB | 58 |
| Figure 4.18: | PCB with soldered electronic components | 58 |
| Figure 4.19: | Inner view of the junction box | 59 |
| Figure 4.20: | Outer view of the junction box | 59 |
| Figure 4.21: | Graph of voltage against concentration for urea fertilizer | 60 |
| Figure 4.22: | Graph of voltage against concentration for MAP fertilizer | 61 |
| Figure 4.23: | Comparison of the predicted and actual concentration of urea fertilizer | 62 |

| | | |
|--------------|--|----|
| Figure 4.24: | Comparison of the predicted and actual concentration of MAP fertilizer | 63 |
| Figure 4.25: | Repeatability test of the 0.435 g/ml urea solution without averaging | 65 |
| Figure 4.26: | Repeatability test of the 0.435 g/ml urea solution with the averaging method | 66 |

LIST OF SYMBOLS / ABBREVIATIONS

| | |
|-------------------|---|
| $ T $ | voltage transmission coefficient |
| $ \Gamma $ | voltage reflection coefficient |
| c | speed of light (m/s) |
| c_1 | concentration of the stock solution (g/ml) |
| c_2 | final concentration of the diluted solution (g/ml) |
| f | volume fraction of inclusions (m^3) |
| f_r | resonance frequency (Hz) |
| N_{OC} | number of output code |
| r | outer ring resonator radius (m) |
| R^2 | coefficient of determination |
| S_{11} | reflection coefficient |
| S_{21} | transmission coefficient |
| v_1 | volume of the stock solution (ml) |
| v_2 | volume of the final diluted solution (ml) |
| V_{CH} | measurement channel voltage level (V) |
| ϵ_{eff} | effective permittivity of substrate and liquid under test (F/m) |
| ϵ_{effc} | effective permittivity of a composite (F/m) |
| ϵ_h | host medium permittivity (F/m) |
| ϵ_i | inclusions permittivity (F/m) |
| ADC | analogue to digital converter |
| BJT | bipolar junction transistor |
| CLI | command line interface |
| DC | direct current |
| GUI | graphical user interface |
| I2C | Inter-Integrated circuit |
| I2S | integrated Inter-IC sound bus |
| IDE | integrated development environment |
| IoT | Internet of Things |
| MAP | monoammonium phosphate |
| MCU | microcontroller |
| MPU | microprocessor |

| | |
|------|---|
| NPK | nitrogen, phosphorus, and potassium |
| OLED | organic light emitting diode |
| PCA | principal component analysis |
| PCB | printed circuit board |
| PVC | polyvinyl chloride |
| RMSE | root mean square error |
| SMA | SubMiniature version A |
| SPI | serial peripheral interface |
| SRR | split ring resonator |
| UART | universal asynchronous receiver-transmitter |
| USB | universal serial bus |
| VCO | voltage controlled oscillator |
| VNA | vector network analyser |

LIST OF APPENDICES

| | |
|-------------------------------------|----|
| Appendix A: MCU program code | 78 |
| Appendix B: Mobile app program code | 85 |
| Appendix C: Web app program code | 99 |

CHAPTER 1

INTRODUCTION

1.1 General Introduction

It is estimated that humans have used manure as the organic fertilizer to increase their crop yields for more than 8000 years (University of Nebraska–Lincoln, 2015). Starting from the 19th century, many types of chemical fertilizers were invented and used in commercial farming (Russel and Williams, 1977). Nitrogen, phosphorus and potassium (NPK) are the three primary nutrients that are required by crops. In 1961, the total amount of NPK fertilizer consumed in the world is 31,657 kt. The consumption of fertilizer has increased to 190,808 kt in the year 2019. According to the International Fertilizer Association (2021), fertilizer consumption is expected to grow annually with a growth rate of 1% in the next four years.

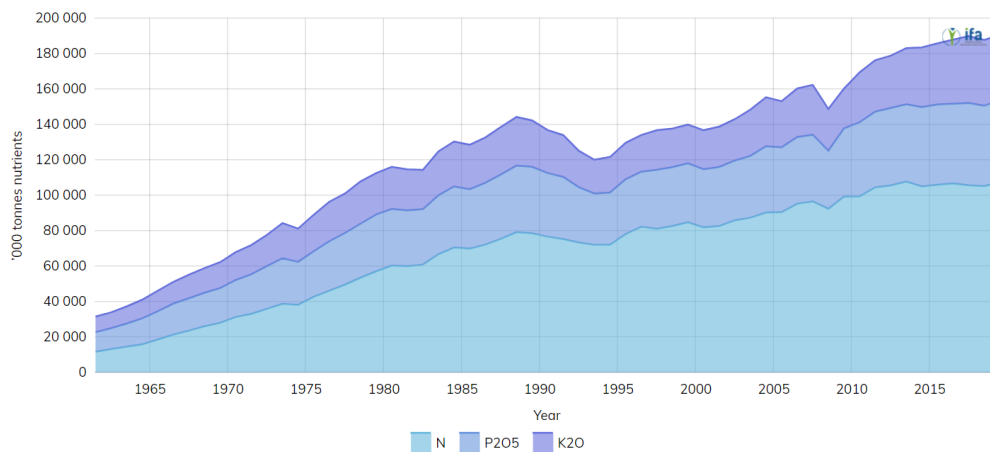


Figure 1.1: Fertilizer consumption in the world from 1961 to 2019 (International Fertilizer Association, 2019).

Liquid fertilizer has become popular nowadays due to the development of precision agriculture (Bongiovanni and Lowenberg-Deboer, 2004). The crops can absorb the liquid fertilizer faster than the dry or granular fertilizer because the granular fertilizer takes some time to dissolve in water. Besides, the nutrients of the liquid fertilizer can be sprayed evenly across the crops. Spreading of

granular fertilizer tends to be uneven due to the composition of each granule being different to another granule.

Liquid fertiliser can mix and regulate the concentration of NPK easily. The growth rate of the crops is significantly affected by the composition and concentration of the fertilizer used. The amounts of nutrients required are also varying among the plants. Thus, the liquid fertilizer can be easily combined with different types of nutrients to obtain the optimal amount of NPK for the particular crop.

Table 1.1: The function of macronutrients, deficiency symptoms and effect (Uchida, 2014).

| Macronutrient | Function | Deficiency symptoms | Effect of crop |
|---------------|--|---|---|
| Nitrogen | Plants require nitrogen to synthesize enzymes. | Chlorosis happens at the tips of leaves. | Lack of nitrogen can cause early maturity. |
| Phosphorus | Plants require phosphorus for energy storage and root development. | Colour of the leaves changes from green to dark blue. | Lack of phosphorus can cause poor fruit and seed development. |
| Potassium | Plants require potassium to promote metabolism. | Chlorosis happens along the edges of leaves. | Lack of potassium can cause a smaller size of fruits and seeds. |

1.2 Importance of the Study

Due to the COVID-19 pandemic in 2020, world hunger is projected to increase by 18% compared to 2019 and reach a total amount of 768 million people (FAO et al., 2021). This shows that agriculture production is not enough to supply the food demand. In order to reduce the number of people who are facing hunger, agriculture and food production need to increase.

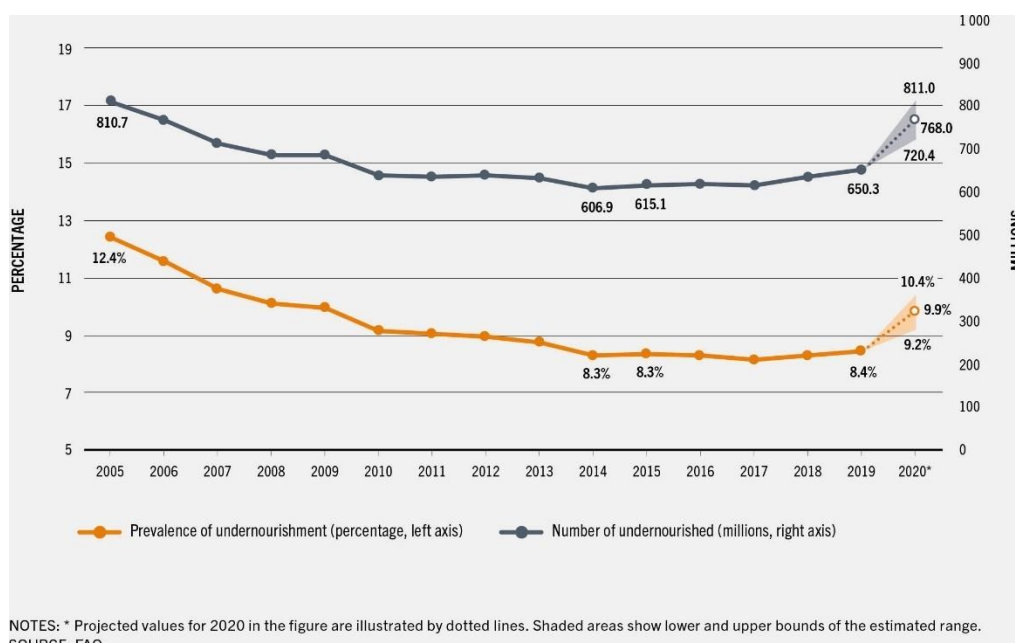


Figure 1.2: Number of people faced hunger in the world (FAO et al., 2021).

By using a suitable concentration of liquid fertilizer on the crops, the crop yields can rise significantly. For example, using the NPK fertilizer in the ratio of 100 : 50 : 50 kg ha⁻¹, the cucumber yield is 26% more than the ratio of 60 : 30 : 30 kg ha⁻¹ (Jilani et al., 2009). Excessive use of fertilizer not only affects the quality of crops but also causes environmental pollution. Therefore, it is crucial to measure the concentration of liquid fertilizer in order to provide a suitable amount of nutrients to the crops.

In recent years, precision agriculture has been promoted by the government in every country. Precision agriculture is utilising scientific knowledge and IoT technology to improve crop yields. Precision agriculture is the combination of monitoring, analysis, and assisting management to increase productivity, reduce labour, as well as improve the quality of crops. The cost and accuracy of the sensor will directly affect efficiency and profitability. By integrating the liquid fertilizer measurement system with IoT, the NPK concentration can be monitored and controlled automatically. This can provide the crops with an optimum amount of nutrients and prevent excessive fertilizer used on the crops which will ultimately cause water pollution in the nearby river.

1.3 Problem Statement

There are many people suffering from hunger, especially in the region of Africa. Due to global warming, rising sea level will reduce the land for agriculture and the extreme weather event will occur more frequently. This will decrease the total crop yields and affect the global food supply. To overcome this problem, crop production must increase. Determination of the liquid fertilizer concentration accurately and fast is one of the ways to increase crop yields. By applying the concept of precision agriculture, the concentration of liquid fertilizer can be monitored remotely. This ultimately can reduce labour time and provide nutrients more effectively.

Measuring and monitoring the liquid fertilizer accurately is one of the challenges in the agriculture sector. The atomic absorption spectrophotometric has been used in the lab to determine the element and concentration of the liquid. Atomic absorption spectrophotometry has the disadvantages of low sensitivity due to the electromagnetic wave interference, costly, large volumes of samples are required and it is recommended to measure one element at one time to obtain higher accuracy (Hussain and Keçili, 2020). Another method that can determine the liquid concentration is liquid chromatography. The main limitations of the liquid chromatography method are low measurement speed due to the compound separation process is required, expensive and bulky (Moldoveanu and David, 2016).

Rocher, et al. (2019) have proposed a conductivity sensor based on magnetic coil to monitor the liquid fertilizer for the irrigation system. This conductivity sensor consists of induced coil and powered coil. A predetermined frequency and voltage are applied to the powered coil. The induced coil will induce current and change the conductivity. In this experiment, the best prototype is having an average percentage error of 2.15%. However, it is tested by using magnesium nitrate as the fertilizer. If different fertilizer is used, the electrical conductivity is different. Thus, the sensitivity and accuracy of the sensor will drop and the combination of NPK fertilizer has not been tested.

Richa, Fizir and Touil (2021) have done a review to measure the concentration of macronutrients by using ion selective electrodes as the sensor. The main components for the ion selective electrodes system are the sensor electrode, internal electrolyte solution, ion selective material, reference

electrode, reference electrolyte solution and voltmeter. The voltmeter value will be used to determine the concentration. The response time of this sensor is slow, and the sensitivity of this sensor will decrease over time, so recalibration is required. Therefore, it is obvious that the ion selective electrodes sensor is not recommended to apply in the IoT application due to its short lifetime and regular maintenance is required.

Ultraviolet–visible spectroscopy also can be used to measure the concentration of liquid fertilizer. If the liquid fertilizer is having more than one compound, interference will exist in this mixture solution. This interference in the spectrum will cause the spectroscopy measurement result to be inaccurate. Self-learning artificial intelligence methods can be used to overcome this issue (Monteiro-Silva, Jorge and Martins, 2019; Silva et al., 2021). However, time for collecting data and analysing data are the limitations. Besides, the cost of spectroscopy is high.

Another type of optical method to measure the concentration is using colorimetric approach. This approach requires a colour reagent to measure the concentration. A reference colour chart will be used to compare the colour change. In order to obtain higher accuracy results, the photocell or camera is needed to detect the colour change and artificial intelligence techniques will be used to analyse the colour change (Potdar et al., 2021). The sample for testing concentration needs to be properly disposed to avoid contamination.

Based on the literature reviews, the conductivity sensor, ion selective sensor, colorimetric approach and ultraviolet-visible spectroscopy are not integrated with IoT to monitor the liquid fertilizer concentration. The conductivity sensor and ion selective sensor have the potential to be integrated with IoT technology but the conductivity sensor is invasive and intrusive, so not all fertilizers are suitable. The ion selective sensor required recalibration over time, this makes the sensor hard to integrate with the IoT system for monitoring the fertilizer for a long duration. Without integrated with IoT technology, the farmers cannot monitor the liquid fertilizer concentration automatically in real time. This will reduce crop productivity and increase labour costs. With IoT technology, the optimum amount of liquid fertilizer can be applied to the crops accurately during irrigation. This can promote the crop growth rate and reduce the waste of fertilizer.

Planar microwave sensor has the advantages of low cost, small size, non-contact, easy to fabricate, high sensitivity, low weight, design flexibility, high reliability, fast response time and robustness against harsh environments (Mohammadi et al., 2020; Harnsoongnoen and Wanthong, 2021). In the four-industrial revolution, sensors which have the characteristics of low cost, low weight and small size are becoming more popular as these types of sensors are suitable to integrate with IoT technology. Microwave sensors have been used in various areas with different applications. Planar microwave sensors can be used for liquid concentration measurement (Velez et al., 2019), gas detection (Bailly et al., 2017), monitoring the growth of bacteria (Narang et al., 2018), angular velocity measurement (Su et al., 2017), blood glucose level detection (Omer, Shaker and Safavi-Naeini, 2020), and soil moisture measurement (Keshavarz et al., 2021).

1.4 Aim and Objectives

In this project, the aim is to develop a liquid fertilizer concentration measurement system based on the microwave sensor and integrate this system with IoT technology so that the concentration of liquid fertilizer can be monitored in real time and the data can be accessed worldwide. The objectives of the project are:

- i) Design and fabricate a planar microwave sensor to measure liquid fertilizer concentration.
- ii) Design and develop a liquid fertilizer concentration measurement system by using a planar microwave sensor.
- iii) Integrating IoT into the liquid fertilizer concentration measurement system which can perform data collecting and monitoring.
- iv) Develop a graphical user interface (GUI) for mobile application and web application to display the liquid fertilizer concentration in graphical format for better visualisation.

1.5 Scope and Limitation of the Study

The scope of this study is to develop an embedded system that is able to perform real time liquid fertilizer concentration monitoring by using microwave sensor with the integration of IoT technology. This project is separated into four parts.

The first part is to design, simulate and fabricate the microwave sensor. The second part is to determine the sensitivity of the planar microwave sensor in liquid fertilizer measurement by using a vector network analyser. The third part is developing and testing the hardware system by integrating the microwave sensor with IoT technology. The last part is to develop a mobile application and web application GUI for users to monitor the system and have a better visualisation. The liquid fertilizers used in this study are urea and MAP. A planar microwave sensor with a circular ring design will be used to measure the concentration of liquid fertilizer.

The limitations of this study are that this system will be affected by changes in the surrounding temperature. This is because the voltage controlled oscillator (VCO) output frequency will be affected when temperature increases or decreases. Besides, the measurement of liquid concentration accuracy might be affected when the liquid is not at room temperature and atmospheric pressure. A similar dimension of the bottle must be used for the measurement and the position of the bottle put on the microwave sensor must be consistent to obtain a consistent result.

1.6 Contribution of the Study

This project will develop a liquid fertilizer measurement system that can provide farmers to measure and monitor the liquid fertilizer concentration in real time. The contributions of this project are:

- i) Review and discuss the existing liquid fertilizer concentration measurement system.
- ii) Design, simulate and fabricate a planar microwave sensor to measure liquid fertilizer concentration.
- iii) Propose and develop a portable and convenient system to measure the liquid fertilizer.
- iv) Apply the Firebase Realtime Database to store the fertilizer concentration.
- v) Develop a mobile application and web application for better visualisation.

1.7 Outline of the Report

This report consists of five chapters. Chapter 1 introduces the crucial of liquid fertilizer to overcome the food shortage, the pros of liquid fertilizer, the problems faced by the current liquid fertilizer measurement system, the aim and objectives to solve the problems, the scope and limitation of the study and the contribution of the study in order to offer an overview to the reader about the importance of this project. Chapter 2 reviews the types of sensors to measure the fertilizer, different designs of planar microwave sensors and IoT concepts that are required to accomplish this project. In Chapter 3, the methodology of the project is discussed comprehensively to complete this project. The timeline of the project planning, simulation and fabrication procedure, sensor and prototype evaluation method are mentioned. Chapter 4 concentrates on the sensor design, performance of the sensor, software and hardware design as well as the accuracy of the prototype. The result obtained is discussed in depth in this chapter. Lastly, Chapter 5 concludes the overall study and proposes the future direction of this study.

CHAPTER 2

LITERATURE REVIEW

2.1 Introduction

In this literature review, the front part will emphasise the different types of sensors that are used to measure the liquid fertilizer including conductivity sensor, ion selective sensor, ultraviolet–visible spectroscopy and colorimeter. A comparison of the advantages and limitations of these sensors will be discussed. After that, different microwave sensor designs as well as the liquid fertilizer concentration used in agriculture are mentioned. Apart from that, the architecture of the IoT system and the wireless communication protocol will be introduced. Finally, a comparison of different IoT agriculture systems will be reviewed.

2.2 Fertilizer concentration measurement sensor

2.2.1 Conductivity sensor

A conductivity sensor based on magnetic coil has been studied to determine the concentration of sodium chloride salt and magnesium nitrate fertilizer. This sensor is made of copper wire and polyvinyl chloride (PVC) tube. This sensor consists of an induced coil and powered coil. The different number of spires and layers on the induced coil and powered coil is tested to determine which spire number will obtain the highest sensitivity and accuracy. For the sodium chloride, forty spires of powered coil and eighty spires of induced coil with eight layers obtain a better correlation between concentration and conductivity. However, when tested with magnesium nitrate, the same spires number of powered coil and induced coil with four layers can obtain better correlation and accuracy (Rocher et al., 2019).

2.2.2 Ion selective sensor

Ion selective sensor has been used for monitoring the nutrient concentration in a hydroponic nutrient management system. To determine the phosphate concentration, a cobalt based electrode is used. The sensing electrode is made of cobalt rod solder with a copper wire and placed inside the polyethylene plastic

case that will be filled with silicone. For the measurement of nitrate concentration, a silver chloride (AgCl) electrode is immersed in sodium nitrate (NaNO₃) and sodium chloride (NaCl) solution and PVC is used as the ion-selective membrane. For potassium, the AgCl electrode is immersed in potassium chloride (KCl) solution and PVC is used as the ion-selective membrane. Orion 9320BN ion selective electrode is used for the calcium concentration measurement. Orion 900200 is used as the reference electrode for all the sensor electrodes. The RMSE of nitrate is 25.2 mg/L, potassium is 19.1 mg/L, calcium is 11.5 mg/L and phosphate is 10.9 % (Jung et al., 2019).

2.2.3 Ultraviolet-visible spectroscopy

Ultraviolet-visible spectroscopy has been used to monitor the NPK concentration in hydroponic nutrient solutions. A miniature deuterium light source which can emit the light spectrum from 185 nm to 1100 nm and a miniaturised spectrometer which can detect the spectrum from 190 nm to 650 nm is used in this system. The light will pass through the sample solution and the spectrometer will determine the light attenuation. Different types of molecules will absorb different wavelengths and cause light attenuation. The Hoagland solution which contains macronutrients and micronutrients is used as the sample solution. In order to obtain different concentrations of NPK value, the NPK are added separately. Due to the sample solution having a lot of different atoms, constructive or destructive interferences will occur and cause the output data harder to identify the concentration of NPK. The principal component analysis (PCA) self-learning artificial intelligence method is used to classify the data and identify the concentration accurately (Silva et al., 2021).

2.2.4 Colorimeter

A small colorimeter chip based on Beer-Lambert's Law has been proposed to measure the NPK concentration in soil. This colorimeter system consists of a microfluidic channel, light source, processing circuit and display. The chromogenic agent mixed with nutrient solution flows through the microfluidic channel. For the light source, blue light is used to detect potassium and red light is used to detect nitrogen and phosphorus. In the processing circuit, a photoelectric sensor is used to detect the reflected light intensity and convert it

to the current signal for further processing. There are some constraints in this system. The atoms must be able to absorb incident light, so varying the NPK concentration will affect the reflected light intensity. The solution must not be able to generate fluorescence or carry out photochemical reactions. To avoid light interference, measurements taken in a dark environment will obtain higher accuracy compared to a light environment (Liu et al., 2016).

2.2.5 Comparison of the fertilizer concentration measurement sensor

Table 2.1 presents the comparison among conductivity sensor, ion selective sensor, ultraviolet-visible spectroscopy and colorimeter. The measurement concentration range of the conductivity sensor is between 0 to 45000 mg/L which is much higher than the other types of sensors. The R^2 value for all types of sensors is higher than 0.9 which indicates that the measured concentration is highly correlated. However, the R^2 of using ultraviolet-visible spectroscopy to measure phosphate is 0.82 which illustrates a weak correlation.

The response time of the conductivity sensor and ultraviolet-visible spectroscopy is faster while the ion selective sensor and colorimeter are having a slow response time. This is because the ion selective sensor spends some time on the reaction between the test solution and electrode. For the colorimeter, the chromogenic agent also spends some time reacting with the test solution to change the colour of the test solution for concentration measurement.

The ultraviolet-visible spectroscopy and colorimeter are non-invasive and non-intrusive as compared to the conductivity sensor and ion selective sensor which are intrusive and invasive. A non-invasive sensor will not contact with the liquid fertilizer during the measurement which can avoid the possibility of sample or sensor contamination. A non-intrusive sensor can be placed outside the pipe if the sensor integrates with the irrigation system which causes no blocking of liquid fertilizer flow inside the pipe. A non-invasive and non-intrusive sensor is preferred over an invasive and intrusive sensor as non-invasive and non-intrusive sensor is easier to operate and maintain.

Colorimeter requires the chromogenic agent to change the colour of the test solution. After mixing with the chromogenic agent, the test solution might become a hazardous solution. All the sensors mentioned above are not intergraded with IoT technology. The cost of the conductivity sensor is lower

than the ion selective sensor, ultraviolet-visible spectroscopy and colorimeter. In a nutshell, a low cost, fast response time, non-invasive and non-intrusive sensor with IoT technology that can measure liquid fertilizer in real time is imperative to develop.

Table 2.1: Comparison of various sensors for liquid fertilizer concentration measurement

| Sensor | Liquid under test | Concentration | R ² | Response time | Non-invasive | Non-intrusive | Additional chemical | Integrated with IoT | Cost |
|---|---|---|--|---------------|--------------|---------------|---------------------|---------------------|----------|
| Conductivity sensor (Rocher et al., 2019) | sodium chloride and magnesium nitrate | 0 - 0.045 g/mL | NaCl: 0.9113 Mg(NO ₃) ₂ : 0.9735 | Fast | No | No | No | No | Low |
| Ion selective sensor (Jung et al., 2019) | NO ₃ , K, Ca and PO ₄ solution | 3 - 1200 mg/L | 0.96 | Slow | No | No | No | No | Moderate |
| Ultraviolet-visible spectroscopy (Silva et al., 2021) | Hoagland solutions | N (103.17-554.85 mg/L) P (15.06-515.35 mg/L) K (113.78-516.45 mg/L) | N: 0.9942 P: 0.8240 K: 0.9748 | Fast | Yes | Yes | No | No | High |
| Colorimeter (Liu et al., 2016) | Ammonium nitrogen, phosphorus solution and potassium solution | N (0 – 27 mg/L) P (0 - 24 mg/L) K (0 – 27 mg/L) | NA | Slow | Yes | Yes | Yes | No | Moderate |

2.3 Planar microwave sensor

There are many techniques proposed by other researchers to measure the concentration of liquid fertiliser such as conductivity sensor, ion selective sensor, ultraviolet-visible spectroscopy, colorimetric sensor and others. Planar microwave sensor has become more popular nowadays because it is easy to manufacture, low cost and small in size. Many researchers have proposed various designs of the microwave sensor and it is applicable in various fields.

A planar microwave sensor with the microstrip line and split ring resonator (SRR) design can be used to measure the concentration of the salt solution. This sensor is made of DiClad 880 and copper metal. A polypropylene tube is placed on the SRR middle hole. This is a non-contact sensor that can avoid contamination or chemical reaction between the sensor and salt sample. Four resonance peak frequencies are obtained in the range of 0.5 GHz to 2.2 GHz. Logarithmic regression and PCA method are used to determine the concentration of salt and classify the types of salt groups. The result shows that higher concentrations of the salt solution have a higher resonance frequency and lower reflection coefficient as the relative permittivity and reflected power decrease when concentration increases (Harnsoongnoen and Wanthong, 2021). To increase the resolution and sensitivity, an active loop feedback loop with a bipolar junction transistor (BJT) is added to the planar microwave sensor. This can reduce the effect of reflected power loss (Zarifi et al., 2015).

A double ring resonator microwave sensor can be used for real time monitoring of water contamination. The contaminants of glucose, acetate, and potassium hydrogen phthalate are successfully detected by the microwave sensor due to different concentrations and types of contaminants will influence the dielectric properties. A microwave sensor can monitor the resonant frequency and amplitude of the transmission coefficient to identify the concentration of contaminants. This sensor is made of copper metal and Duroid 5880 which has a uniform electrical property over frequency. A copolyester microfluidic channel is placed over the ring gap to have a better electrical field interaction to improve sensitivity. This sensor is capable to distinguish different types of contaminants as each contaminant has a different resonance frequency. However, low concentrations of the contaminants in water cannot be detected (Mohammadi et al., 2020).

A good microwave sensor requires the characteristics of large shifts in resonance frequency and amplitude to have a higher sensitivity, operate at a lower frequency to avoid substrate absorption and a linearity output model. A planar double-sided spiral SRR contains four spiral rings, two on top and two at bottom. The drive loop is on the top middle to produce a larger magnetic field to improve the quality factor. This sensor is made of Duroid 5880 and copper metal. An acrylic coating is used on the sensor to prevent damage. This sensor has a compact design, a small sensing area and a lower operating frequency but increasing the copper conductor length causes higher power loss (Benkhaoua et al., 2016).

A planar microwave sensor with a complementary double SRR design has been used to measure the concentration of ammonia and iron in water to prevent water contamination. It contains two rectangular rings with a split gap. This sensor is made of FR-4 substrate and copper metal. Double-sided tape is stuck on the sensing area. The result shows that the resonance frequency decreases when the concentration increases. Due to nonlinearity, the Fourier curve fitting model is used as the predictive function in order to obtain an error lesser than 0.01 for the sensor (Yee et al., 2021).

A microstrip line coupled square complementary SRR is proposed to measure the concentration of phosphate and nitrate. The square design can reduce the resonance frequency and increase the electric field strength in order to increase the sensitivity. This sensor is made of Duroid 6002 and copper. Nevertheless, the sensitivity decreases when concentration increases due to nonlinear functions among the concentration, resonance frequency and transmission coefficient (Harnsoongnoen, 2021).

A differential open complementary SRR is proposed to measure the concentration of sodium solution. This sensor consists of a pair of symmetrical open complementary SRR sensing areas where one area is used for reference and the other one is used for measurement. This sensor is made of FR-4 substrate and copper. The difference between the reference and measurement transmission coefficient is used to determine the concentration of the solution. This differential sensor can reduce the effect of surrounding factors such as temperature and pressure (Velez et al., 2018). A differential SRR microwave sensor has been proposed as it can improve the sensor resolution (Velez et al.,

2019). However, the differential sensor is harder to fabricate and has a larger size. This is because if the fabrication process causes the resonator to become asymmetrical, the problem of frequency splitting will arise.

An interdigital capacitor loaded electric LC resonator planar microwave sensor is used to detect the concentrations of nitrate and phosphate. The vertical spiral design obtains the highest sensitivity among horizontal spiral, vertical fingered and horizontal fingered designs. This sensor is made of DiClad 880 and copper (Harnsoongnoen et al., 2019).

Interdigitated electrodes microwave sensor is developed to detect zinc pollution in water. This sensor consists of a gold eight-pair interdigitated electrode that is printed on a polytetrafluoroethylene substrate. The bismuth (III) oxide is coated on the interdigitated electrode to increase the sensitivity. This is because the coating is able to absorb the zinc ions in water but the time for adsorption to reach an equilibrium state is estimated at 10 minutes (Frau et al., 2019).

Table 2.2: Summary of different microwave sensor designs with the concentration of liquid under test

| Planar Microwave Sensor Design | Liquid under test | Concentration (mg/L) | Frequency (GHz) | Reference |
|--------------------------------|--|----------------------|-----------------|------------------------------------|
| Microstrip with SRR | CaCl ₂ , NaCl, KCl, MgCl ₂ and Na ₂ CO ₃ | 40 - 200 | 0.5 - 2.2 | (Harnsoongnoen and Wanthong, 2021) |
| Double ring resonator | Potassium hydrogen phthalate, glucose-acetate mix, glucose, and acetate | 50 - 800 | 4 - 5 | (Mohammadi et al., 2020) |

| | | | | |
|---|---|---------------------|-----------|------------------------------|
| Double-sided spiral SRR | Ethanol and Methanol | $0 - 1 \times 10^6$ | 0.1 - 0.2 | (Benkhaoua et al., 2016) |
| complementary double SRR | Ammonia and Iron | 0 - 53 | 1.5 - 2.6 | (Yee et al., 2021) |
| Microstrip line coupled square complementary SRR | phosphate, nitrate, and phosphate-nitrate mix | 0 - 1000 | 1.0 - 1.2 | (Harnsoongnoen, 2021) |
| Differential open complementary SRR | Sodium | 0 - 80000 | 0.7-1.2 | (Velez et al., 2018) |
| Differential SRR | NaCl, KCl and CaCl ₂ | 0 - 60000 | 0.7 - 1.2 | (Velez et al., 2019) |
| Interdigital capacitor loaded electric LC resonator | Nitrate and Phosphate | 0 - 1000 | 1 - 5 | (Harnsoongnoen et al., 2019) |
| Interdigitated electrodes | zinc | 0 - 100 | 0.1-3.25 | (Frau et al., 2019) |

In short, the planar microwave sensor is used to determine different types of liquid concentration. The liquid under test will affect the power loss of the microwave signal. Ordinarily, the reflective coefficient or transmission coefficient will be used to determine the strength of the microwave reflective or transmission power. After that, the reflective coefficient or transmission coefficient will be used to determine the liquid concentration. From the review, the microwave sensor can detect various ranges of concentration from 0 g/ml to

1g/ml. As a result, the microwave sensor is possible to measure numerous types of liquid fertilizers concentration accurately in this project.

2.4 Liquid fertilizer concentration

Liquid fertilizer usually is in the form of powder, granular or concentrated liquid. Hence, dilution with water is required to obtain an optimum concentration of liquid fertilizer for the plants. Too concentrated liquid fertilizer used not only harms the growth of plants but also causes environmental pollution. Table 2.3 shows the concentration of liquid fertilizers used by different plants.

Table 2.3: Concentration of liquid fertilizer used for irrigation or hydroponic solution

| Plant | Fertilizer | Concentration |
|---|---|--|
| Sorghum bicolor (L.) Moench (GutierrezMiceli et al., 2008) | NPK triple 17 fertilizer | 0.14 – 0.17 g/ml |
| Cucumis sativus L. (Yan et al., 2012) | Hoagland's solution | 0.30 g/l KNO ₃ 0.33 g/l Ca(NO ₃) ₂ 0.06 g/l NH ₄ H ₂ PO ₄ 0.12 g/l MgSO ₄ |
| Lactuca sativa (Jung et al., 2019) | KNO ₃ , NH ₂ PO ₄ , Ca(NO ₃) ₂ , K ₂ SO ₄ , MgSO ₄ , and Mg(NO ₃) ₂ | 0.43 g/l NO ₃ 0.15 g/l K 0.12 g/l PO ₄ |

2.5 IoT architectures

IoT does not have a standard architecture. Various types of IoT architectures have been published by different researchers. There are two most common IoT architectures that have been applied in the agricultural sector which are three layers of IoT architecture and five layers of IoT architecture. Other than these two architectures, cloud based architecture and fog based architecture have gained attention from some researchers.

Fu (2016) has proposed a three layers IoT architecture to monitor the environmental conditions and growth rate of the crops on the farms. The first

layer is the perception layer. This layer can be considered as a sensing layer where various types of sensors will be deployed on the farm to obtain data of the surrounding temperature, humidity, light intensity as well as soil pH value and moisture level. The second layer is the transportation layer. The data from each sensor will be collected by the central control unit via wireless communication technology such as Bluetooth. After that, the collected data will be transmitted to the backend server. The third layer is the application layer. This layer will analyse the collected data and report the result to the farmer.

Three layers of IoT architecture only focus on the main concept of the IoT and are not enough to represent all the functions of IoT. Thus, five layers of IoT architecture have been adopted by some researchers. The five layers of IoT architecture have two extra layers which are the middleware layer at the third layer and the business layer at the fifth layer. The function of the perception layer and transport layer is the same as the three layers of IoT architecture. The middleware layer will obtain the sensor data from the transport layer to carry out analysis and storage. This layer also will process the commands from the application layer and communicate with the actuators to carry out the response. The application layer provides the end user with an interface for better visualisation and control. The business layer will include the business costs, security risks and benefits (Virupaxappa and Thangam, 2021).

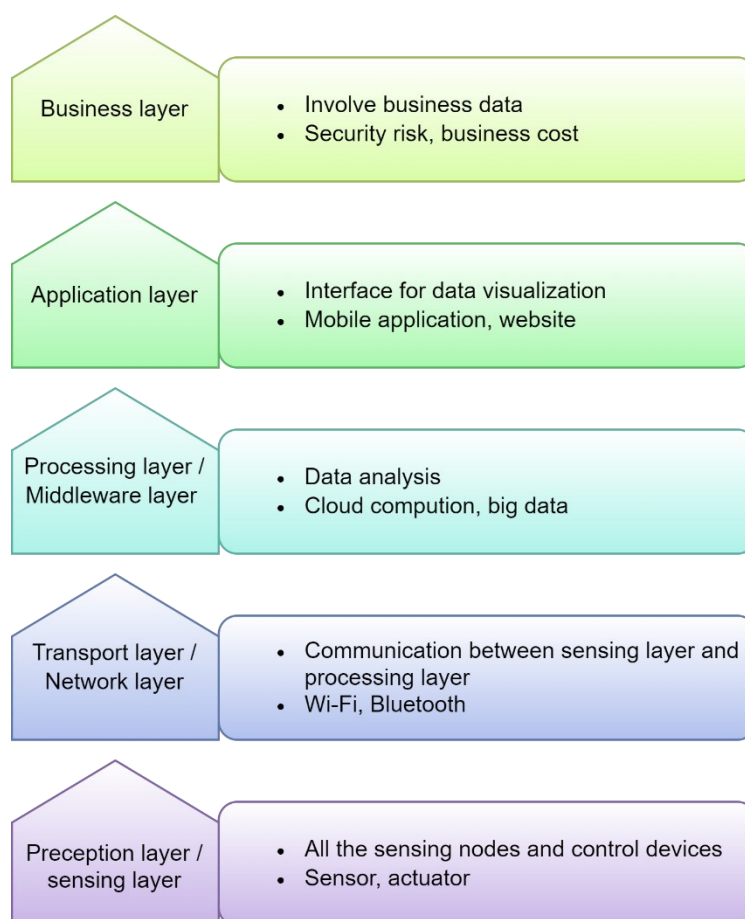


Figure 2.1: Five layers of IoT architecture

Cloud based architecture consists of a perception layer, gateway layer and application layer. The gateway layer will collect all the perception layer data for local storage and preprocessing before sending it to the application layer (Araby et al., 2019). Cloud based architecture employs a centralised backend server, so the latency will be higher. Fog based architecture has been developed to overcome this issue. The fog based architecture employs a decentralised backend server. Thus, the server that is closer to the end user will be used in order to reduce the latency. When the internet connection is interrupted, fog based architecture can provide the service to users independently (Chiang and Zhang, 2016).

2.6 Wireless communication protocol

The wireless communication protocol is used to transmit data between two devices. In IoT applications, wireless communication will be more preferred than wire communication when data is transmitted between two devices because wireless communication is much easier to install, scalable and lower costs. IoT wireless communication protocol can be categorised into personal area network, local area network, wide area network and metropolitan area network (Sharma and Dhir, 2014). To reduce the maintenance of the sensors, battery life is one of the most vital factors that should be considered when designing the IoT sensor node. Thus, low power consumption wireless communication technology is more beneficial to IoT applications. Furthermore, a small amount of data is transferred between node and gateway, so a low transmission rate of the wireless communication technology is enough for IoT applications (Mahmoud and Mohamad, 2016).

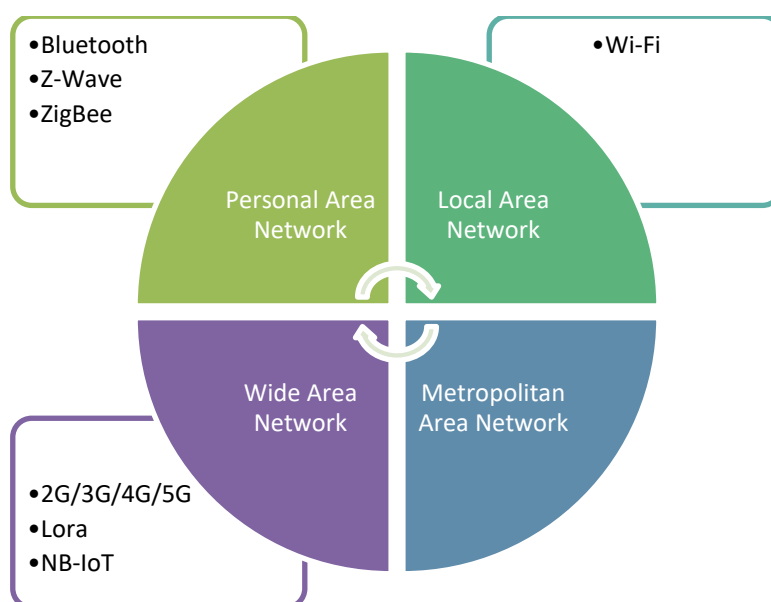


Figure 2.2: Classification of wireless communication technology

Table 2.4: Comparison of different wireless communication protocols (Saad et al., 2014; Al-Sarawi et al., 2017; Poursafar, Alahi and Mukhopadhyay, 2017; Sinha, Wei and Hwang, 2017)

| | Wi-Fi | Bluetooth | ZigBee | LoRa | Z-Wave | NB-IoT | 2G |
|--------------------|-------------------------------------|---------------------------------------|--|-------------------------------------|-----------------------------|--------------------------|------------------------------|
| Standard | IEEE 802.11 g | IEEE 802.15.4 | IEEE 802.15.4 | IEEE 802.15.4 | Z-Wave | 3GPP | 3GPP |
| Frequency band | 2.4 GHz | 868/915 MHz & 2.4 GHz | 2.4 GHz | 868/915 MHz & 433 MHz | 868 MHz & 908 MHz | 700/800/900 MHz | 850/900 MHz & 1800/1900 MHz |
| Transmission rate | 54 Mbps | 1 Mbps | 250 kbps | 50 Kbps | 100 Kbps | 200 Kbps | 168 Kbps |
| Distance | 10 – 100 m | 15 - 30 m | 10 – 100 m | 15km | 30 -100 m | 35km | 2 – 35 km |
| Energy consumption | High | Low | Low | Low | Low | Low | High |
| Application | Data network, Internet, Monitoring, | Wireless headsets, Audio Applications | Home industry monitoring and controlling | industry monitoring and controlling | Home Monitoring and Control | Home industry monitoring | Internet, Machine to machine |

Based on the comparison table, the transmission rate of Wi-Fi is the highest compared to other types of wireless communication protocols. Nevertheless, the power consumption of Wi-Fi and 2G is considered high as compared to Bluetooth, ZigBee, LoRa, Z-Wave and NB-IoT. The Wi-Fi, Bluetooth, ZigBee and Z-Wave are having a shorter data transmission distance while LoRa, NB-IoT and 2G have a longer data transmission distance.

In a word, Wi-Fi is suitable to use in the application which required a high data transmission rate, low latency and short range. The Bluetooth wireless communication protocol has a lower power usage and moderate data transmission rate which is apt for application in wireless headsets and audio applications. The ZigBee and Z-Wave wireless communication protocols are purposely designed for the IoT application that required a low data transmission range and speed but longer operating duration, especially for the systems that are powered by batteries. LoRa and the NB-IoT are also intentionally designed for IoT applications. The main difference is LoRa and NB-IoT have a longer data transmission range. For the 2G communication protocol, the power consumption is high and the data transmission range is long. However, the data can be directly sent to the cell tower, unlike other wireless communication protocols which required to install an intermediate router and gateway to transmit data to the server via the internet. Due to the Wi-Fi is the most common wireless communication protocol, the liquid fertilizer measurement system for this project will be based on Wi-Fi technology.

2.7 IoT agriculture system

Table 2.5: Different designs of IoT agriculture system

| Application | MCU / MPU | Wireless communication | Cloud/ GUI development platform | Reference |
|--|--|------------------------|---|--------------------------------------|
| Monitoring environment, soil moisture, irrigation and fertilization | Arduino Uno | Wi-Fi module (ESP8266) | Android OS and Web | (Saini and Saini, 2020) |
| Soil moisture and irrigation | Raspberry Pi | ZigBee | ThingSpeak IoT | (Boobalan et al., 2018) |
| An automated fertilizer system for monitoring, analysing and controlling | Arduino Nano is used for environment monitoring, Raspberry Pi 4 used for main controlling unit | unknown | Android studio 4.0 for mobile application | (Madanayaka and Thilakarathne, 2021) |
| Liquid fertilizer control automatically in the aquaponic system | Arduino Uno (Wemos D1 Mini) | Wi-Fi (ESP8266) | Antares | (Wibowo et al., 2019) |

| | | | | |
|--|----------------------|-------|--|---------------------------------------|
| Monitoring environmental condition | Texas CC3200 | Wi-Fi | unknown | (Prathibha, Hongal and Jyothi, 2017) |
| Weather, soil and area monitoring for farm | Arduino Mega 2560 R3 | GSM | SMS | (Menon and Prabhakar, 2021) |
| LoRa agriculture system | Raspberry Pi 3 B+ | LoRa | The Things Network and Cayenne dashboard | (Gutierrez et al., 2019) |
| Hydroponics monitoring system | Raspberry Pi 3 | Wi-Fi | Ubidots | (Joshitha et al., 2021) |
| Greenhouse farming monitoring system | Node MCU ESP32 | Wi-Fi | Firebase | (Lara, Gutierrez and Rodriguez, 2019) |

Recently, IoT technology has been applied in many agriculture applications including irrigation systems, fertilizer monitoring systems and so forth to increase crop production and reduce labour costs. Table 2.5 shows the summary of different IoT agriculture system designs. Arduino, Texas CC3200 and Node MCU ESP32 can be categorised as the microcontroller (MCU) but the Raspberry Pi is categorised as the microprocessor (MPU). MPU have higher computational power compared to MCU while the price of MPU is higher than MCU.

The Arduino Uno, Arduino Mega and Arduino Nano are not integrated with the Wi-Fi module, thus an external Wi-Fi module such as ESP8266 is required in order to connect with the cloud server to provide a real time monitoring function. However, Raspberry Pi 3 and Node MCU ESP32 are integrated with Wi-Fi and Bluetooth modules so an external wireless communication module is not required. For this reason, the ESP32 microcontroller has a better advantage for a low computational IoT system that required a Wi-Fi communication protocol.

One of the notable highlights in the summary is most of the researchers are preferred to use Wi-Fi as compared the other wireless communication technology. This is due to the fact that the home Wi-Fi router can be used as the gateways for the IoT system which is designed by using Wi-Fi communication protocol. In contrast, LoRa and ZigBee protocols required an external communication module and gateway. For GSM protocol, an external GSM module and SIM card are necessary. As a result, using Wi-Fi does not require extra cost to purchase a new gateway module. ThingSpeak IoT, Antares, The Things Network, Ubidots and Firebase are the cloud servers that are preferable for IoT applications. Hence, the microcontroller that uses for this project will be based on the Wi-Fi integrated ESP32 microcontroller and the Firebase will be chosen as the cloud development platform.

CHAPTER 3

METHODOLOGY AND WORK PLAN

3.1 Project Planning and Milestones

This project is separated into two parts. Part I of this project is emphasising problem formulation, literature review, preliminary testing of microwave sensor and conceptual design of the IoT system, whereas part II of this project is focusing on prototype development, software design and prototype testing.

Table 3.1: Gantt chart of part I project

| No. | Project Activities | W1 | W2 | W3 | W4 | W5 | W6 | W7 | W8 | W9 | W10 | W11 | W12 | W13 | W14 |
|-----|--|----|----|----|----|----|----|----|----|----|-----|-----|-----|-----|-----|
| 1 | Problem formulation & Project planning | | | | | | | | | | | | | | |
| 2 | Introduction and overview | | | | | | | | | | | | | | |
| 3 | Literature review | | | | | | | | | | | | | | |
| 4 | Methodology and Work Plan | | | | | | | | | | | | | | |
| 5 | Preliminary Result | | | | | | | | | | | | | | |
| 6 | Report writing and Presentation | | | | | | | | | | | | | | |

Table 3.2: Gantt chart of part II project

| No. | Project Activities | W1 | W2 | W3 | W4 | W5 | W6 | W7 | W8 | W9 | W10 | W11 | W12 | W13 | W14 |
|-----|-------------------------------------|----|----|----|----|----|----|----|----|----|-----|-----|-----|-----|-----|
| 1 | Hardware development | | | | | | | | | | | | | | |
| 2 | Software development | | | | | | | | | | | | | | |
| 3 | Prototype testing and Data analysis | | | | | | | | | | | | | | |
| 4 | Poster preparation | | | | | | | | | | | | | | |
| 5 | Report writing and Presentation | | | | | | | | | | | | | | |

3.2 Design workflow and system architecture

To accomplish this project, the main progression will separate into three stages. The first stage is performing planning and research to understand the concept of this liquid fertilizer monitoring system. The second stage is choosing the right design of the microwave sensor and testing the sensitivity of the sensor. The third stage is integrating the microwave sensor with IoT technology and building a prototype to verify this system.

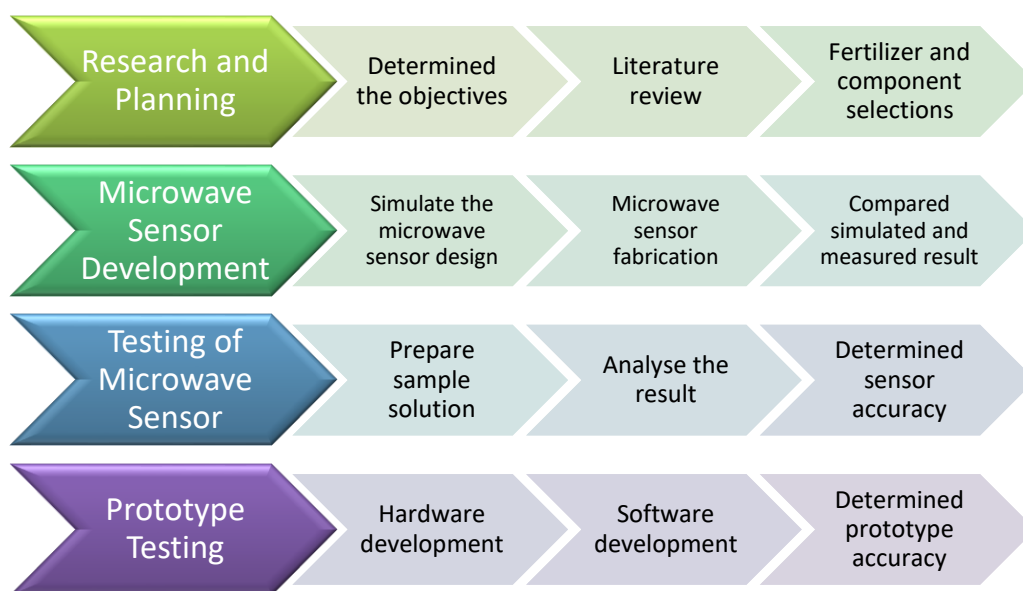


Figure 3.1: Workflow of methodology

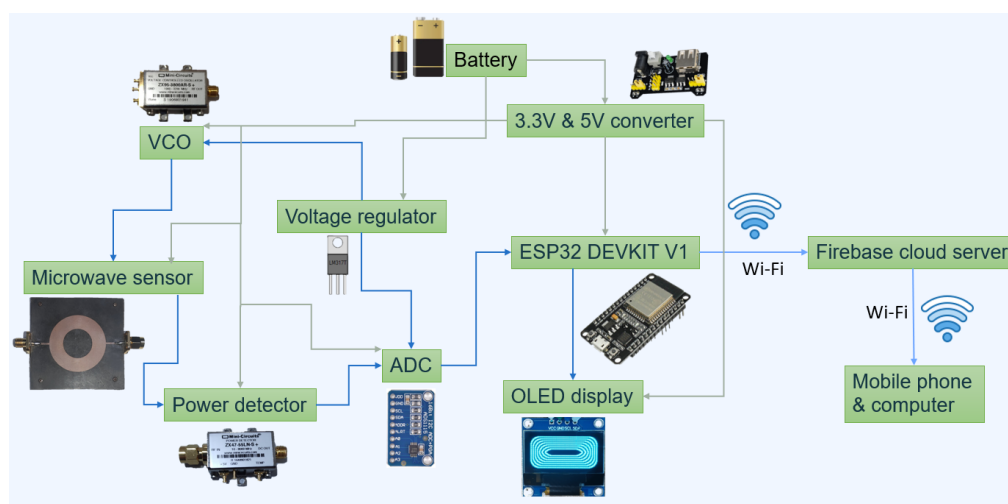


Figure 3.2: Block diagram of the liquid fertilizer concentration measurement system

This main controlling unit is the ESP32 DEVKIT V1 board. A linear voltage regulator is applied to control the output voltage. A potentiometer is used to adjust the voltage regulator output voltage. The output voltage of the linear voltage regulator will determine the frequency generated by the VCO. The frequency signal will transmit across the microwave sensor to the power detector via coaxial cable. The power detector will convert the power at that frequency to the corresponding voltage level. The analogue to digital converter (ADC) will convert the analogue signal to digital signal and send it to the microcontroller via I2C. The organic light emitting diode (OLED) display will show the concentration value. The microcontroller will communicate with the Firebase cloud server and the user can view the result by using mobile phone or computer via Wi-Fi.

3.3 Design and simulation of microwave sensor

The CST microwave studio is used to simulate the microwave sensor before fabrication to avoid waste of materials. Some specifications should be considered during the simulation process. The RT/Duroid 5880 glass microfiber PTFE composite is chosen as the substrate because it has low dielectric constant and dielectric loss which is 2.2 and 0.0009 respectively, so it is suitable to use in high frequency applications as well as resistant to etching solvents and reagents. The thickness of the RT/Duroid 5880 is 0.502 mm and it is laminate with electrodeposited copper with the thickness of 0.035 mm on both sides of the substrate. The microwave sensor is required to operate between 1.9 GHz to 3.7 GHz as the VCO can only produce frequency within this range. The insertion loss of the sensor should be as small as possible to ensure the power detector can detect the power changes. Lastly, two ports are required to measure the S_{21} of the microwave sensor.

Table 3.3: Design specifications of microwave sensor

| Parameter | Requirement |
|---------------------|-------------------|
| Substrate | RT/Duroid 5880 |
| Patch | Copper |
| Operating frequency | 1.9 GHz - 3.7 GHz |
| Resonant frequency | 2.45 GHz |
| Insertion loss | < 2 dB |
| Area | 60 mm × 60 mm |
| Number of ports | 2 |

There are three types of common planar transmission line designs which are microstrip line, stripline and coplanar waveguide. In this design, the microstrip line is chosen because this design is easier to fabricate as compared to the stripline and coplanar waveguide. The microstrip line is an open structure where a narrow straight conductor line is placed on a substrate with a ground plane so this design can be fabricated by a photolithographic method. Unlike the stripline geometry, the conductor is located between the top and bottom ground plates and the stripline design is not appropriate to measure high permittivity and low loss substances. The coplanar waveguide has a conductor located in the middle and it is separated from a pair of ground planes on both sides. The heat sink capability of this design is low and a thick substrate is required to reduce losses (Abd Rahman et al., 2017).

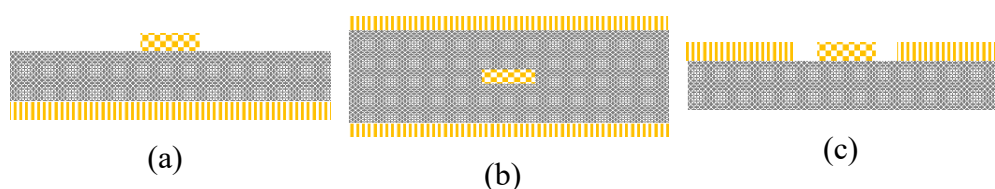


Figure 3.3: Geometry of planar transmission lines (a) microstrip line, (b) stripline and (c) coplanar waveguide

The circular ring cavity geometry is one of the common designs for resonator microwave sensors. This design will introduce a high electric field

concentration in the cavity. The resonance frequency of the circular ring cavity can be calculated by using Equation 3.1 (Bogner et al., 2017).

$$f_r = \frac{c}{2\pi r \sqrt{\epsilon_{eff}}} \quad (3.1)$$

where

f_r = resonance frequency (Hz)

c = speed of light (m/s)

r = outer ring resonator radius (m)

ϵ_{eff} = effective permittivity of substrate and liquid under test (F/m)

3.4 Fabrication of microwave sensor

The design of the microwave sensor that is drawn in the CST studio is exported to the Gerber file format and the sensor layout is printed on tracing paper which functions as a mask for photolithography. A photoresist is laminated on the copper board by using a Photonex 325 laminator at 110 °C. After that, the tracing paper with the printed layout is pressed tightly on the laminated copper board and exposed to a UV light source for 40 seconds. Sodium Carbonate is mixed with water as the developer solution. Then, the copper board is immersed into the developer solution to remove the photoresist. After that, the copper board is immersed in the ferric chloride etching solution for 1 hour to remove the exposed region of copper. Next, the copper board is soaked into the sodium hydroxide solution to remove the photoresist. Finally, the microwave sensor is screwed on an aluminium plate and the microwave sensor is soldered with the SubMiniature version A (SMA) ports.

3.5 Evaluation method of microwave sensor

The first step is the preparation of test solutions. Urea is one of the fertilizers used in this project. The NPK value of urea is 46-0-0 which contains 46% of nitrogen. 86.957 g of granular urea fertilizer is dissolved in 200 ml of distilled water to acquire the concentration of 0.435 g/ml urea solution. The mass is measured by precision balance with the model FX-300i. After the urea fertilizer is fully dissolved, the different volumes of urea solution with a concentration of 0.435 g/ml are diluted in the different volumes of distilled water to obtain the urea concentration ranging from 0.326 g/ml to 0.022 g/ml. The plastic bottles

are used to store the solution and syringes are used to measure the volume. The final volume of the diluted solution is fixed at 12 ml. The final concentration of the dilution can be determined by using the dilution formula shown in Equation 3.2.

$$c_1 v_1 = c_2 v_2 \quad (3.2)$$

where

c_1 = concentration of the stock solution (g/ml)

v_1 = volume of the stock solution (ml)

c_2 = final concentration of the diluted solution (g/ml)

v_2 = volume of the final diluted solution (ml)

Table 3.4: Concentration of urea solution used in this experiment

| Concentration of urea (g/ml) | Volume of urea stock solution (0.435 g/ml) added (ml) | Volume of distilled water added (ml) | Volume of final diluted solution (ml) |
|------------------------------|---|--------------------------------------|---------------------------------------|
| 0.435 | 12.0 | 0.0 | 12.0 |
| 0.326 | 9.0 | 3.0 | 12.0 |
| 0.218 | 6.0 | 6.0 | 12.0 |
| 0.109 | 3.0 | 9.0 | 12.0 |
| 0.022 | 0.6 | 11.4 | 12.0 |
| 0.000 | 0.0 | 12.0 | 12.0 |

The second step is the microwave sensor measurement setup. The model of VNA used in the experiment is ROHDE & SCHWARZ ZVL. This is a two ports network analyser that can measure the frequency ranges from 9 kHz to 13.6 GHz. For this experiment, the measurement frequency is from 1.5 GHz to 4 GHz. The Through – Open – Short – Match calibration is done before measuring the microwave sensor to correct the systematic error. The resolution of 1001 frequency points is swapped across the frequency ranges.

The microwave sensor is connected to the VNA by using the coaxial cable via the SMA ports. The plastic bottle is put on the centre of the microwave sensor and the S_{21} value is recorded. This process is repeated by changing the concentration of 0.435 g/ml to 0.326, 0.218, 0.109, 0.022 and 0 g/ml urea

solution. Each concentration is repeated five times to reduce the measurement error. After that, the average value of S_{21} is calculated. The graph of S_{21} against frequency for different concentrations is plotted. The R^2 values of S_{21} against different concentrations for all the frequency points are calculated. By comparing the R^2 value and analysing the graph of S_{21} against frequency, the two best frequencies are chosen where the R^2 value is higher than 0.9 and the graph shows a linear trend of S_{21} with respect to the solution concentrations. The graphs of S_{21} against different concentrations at the selected frequencies are plotted.

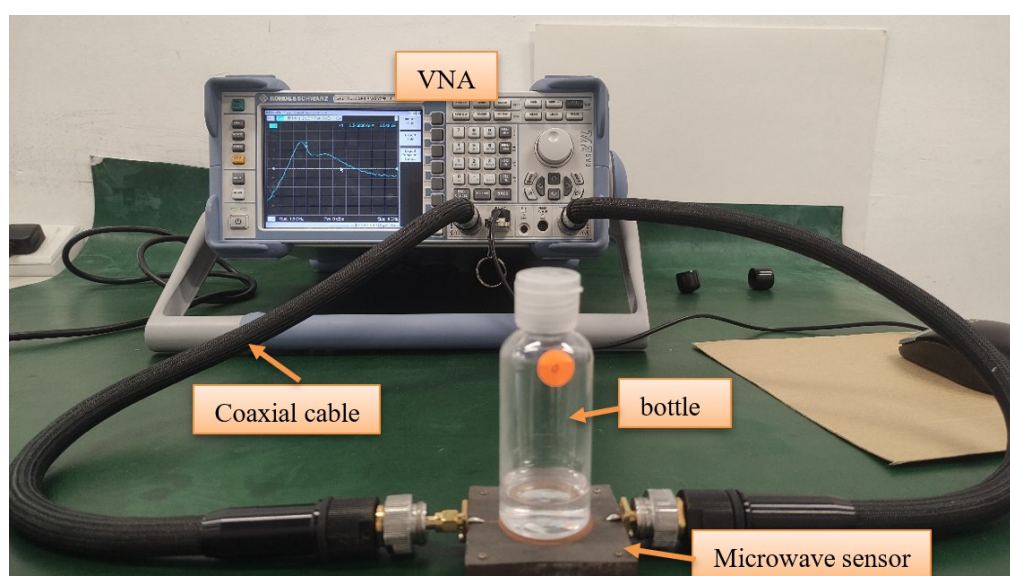


Figure 3.4: Measurement setup

The urea fertilizer is replaced with the MAP. A 40.000 g of powder MAP fertilizer is dissolved in 200 ml of distilled water to acquire the concentration of 0.200 g/ml MAP solution. After the MAP is fully dissolved, the different volumes of MAP solution with a concentration of 0.200 g/ml are diluted in the different volumes of distilled water to obtain the MAP concentration ranging from 0.150 g/ml to 0.010 g/ml. The microwave sensor measurement process is similar to the urea solution.

Table 3.5: Concentration of MAP solution used in this experiment

| Concentration of MAP (g/ml) | Volume of MAP stock solution (0.200 g/ml) added (ml) | Volume of distilled water added (ml) | Volume of final diluted solution (ml) |
|-----------------------------|--|--------------------------------------|---------------------------------------|
| 0.200 | 12.0 | 0.0 | 12.0 |
| 0.150 | 9.0 | 3.0 | 12.0 |
| 0.100 | 6.0 | 6.0 | 12.0 |
| 0.050 | 3.0 | 9.0 | 12.0 |
| 0.010 | 0.6 | 11.4 | 12.0 |

3.6 Hardware Components

3.6.1 Microwave sensor

The working theory of the planar microwave sensor is based on the variation of the test sample's dielectric properties and can be explained by Maxwell-Garnet mixing theory. The Maxwell-Garnet mixing theory can be defined in Equation 3.3. The ϵ_{eff} is defined as the composite effective permittivity, ϵ_h is the host medium (water) permittivity and ϵ_i is the inclusions permittivity. The f is the volume fraction of inclusions inside the host which depends on the liquid fertilizer concentration (Mohammadi et al., 2020).

$$\epsilon_{eff} = \epsilon_h \frac{\epsilon_h + \frac{1+2f}{3}(\epsilon_i - \epsilon_h)}{\epsilon_h + \frac{1-f}{3}(\epsilon_i - \epsilon_h)} \quad (3.3)$$

where

ϵ_{effc} = effective permittivity of a composite (F/m)

ϵ_h = host medium permittivity (F/m)

ϵ_i = inclusions permittivity (F/m)

f = volume fraction of inclusions (m^3)

The changing of the host medium permittivity, inclusions permittivity and volume fraction of the test sample will amend the effective permittivity and therefore affect the planar microwave sensor's resonant frequency and resonant amplitude or amplitude of the S_{21} . Therefore, the liquid fertilizer concentration can be identified by examining the amplitude of the S_{21} parameter when different test samples are applied to the sensor.

3.6.2 Power detector

The model of power detector used in this system is ZX47-55LN-S+ which is manufactured by Mini-Circuits. This power detector has an operating voltage of 5 V. The measuring input power ranges from -55 dBm to 10 dBm at the frequency ranges from 10 MHz to 8000 MHz. This sensor consists of a built-in temperature sensor to reduce the fluctuation of output voltage due to the changing of the surrounding temperature.



Figure 3.5: Power detector

3.6.3 Voltage controlled oscillator (VCO)

The model of VCO used in this system is ZX95-3800AR-S+ which is manufactured by Mini-Circuits. This VCO has a normal operating voltage of 5 V and it can generate an output frequency from 1.9 GHz to 3.7 GHz by changing the turning voltage from 0.5 V to 20 V. Typically, this VCO provides an output power of 6 dBm.



Figure 3.6: VCO

3.6.4 ESP32 DEVKIT V1 Board

The main processing unit used in this system is NodeMCU ESP32. This processing unit consists of built-in Wi-Fi and Bluetooth modules. It has a dual core 32-bit processor, 4 MB flash memory, 520 KB random access memory and

thirty general purpose input output pins. The total number of input output pins is more than enough for this application. Moreover, this processing unit supports integrated Inter-IC sound bus (I2S), universal asynchronous receiver-transmitter (UART), serial peripheral interface (SPI) and Inter-Integrated circuit (I2C) communication protocols. There is one universal serial bus (USB) type B micro for power and program flashing. The normal operating voltage is 3.3 V.

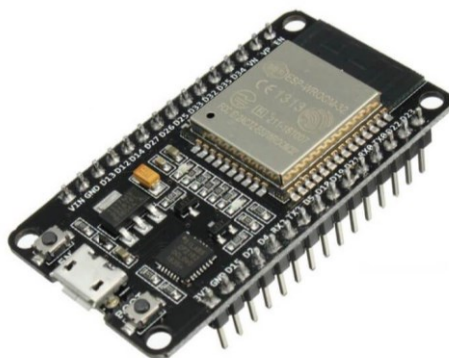


Figure 3.7: ESP32 DEVKIT V1 board

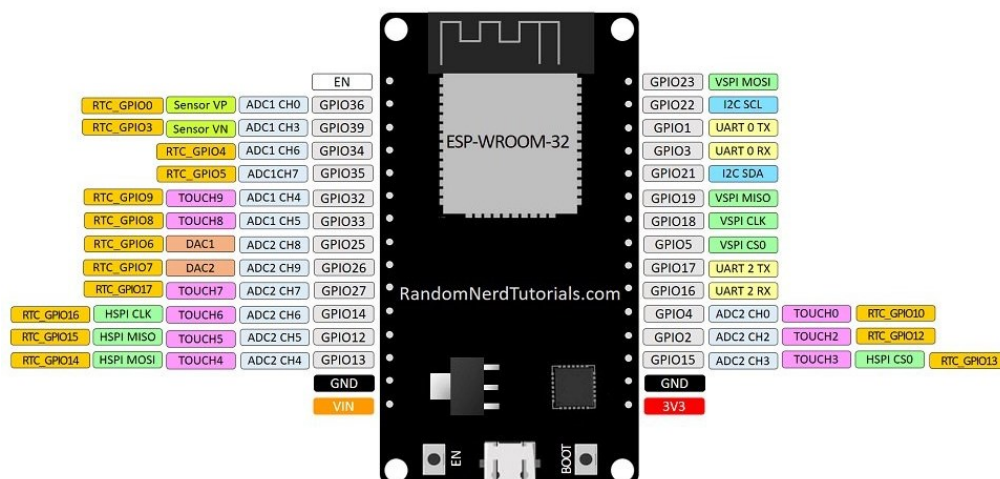


Figure 3.8: ESP32 DEVKIT V1 board pinout (Random Nerd Tutorials, 2022)

3.6.5 Analogue to digital converter

The ADS1115 is a delta-sigma ADC with I2C communication protocol. The maximum programmable data rate is 860 samples per second with 16 bits resolution. The programmable gain amplifier provides an input voltage measurement range from ± 0.256 V to ± 6.144 V. This ADC provides four single-ended or two differential inputs for the voltage measurement and operates

in either continuous conversion mode or single-shot mode. This ADC operating voltage is ranging from 2 V to 5.5 V and it can enter idle mode when analogue to digital conversion is not performed in order to reduce the power consumption. The measurement voltage can be calculated by using Equation 3.4, if 16 bits resolution with ± 2.048 V is applied.

$$N_{OC} = 16000 \times V_{CH} \quad (3.4)$$

where

N_{OC} = number of output code

V_{CH} = measurement channel voltage level (V)

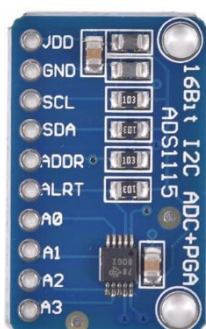


Figure 3.9: ADS1115 ADC

3.6.6 OLED display

Organic light emitting diode (OLED) display which has SSD1306 driver to control the graphic display. This OLED has 128×64 pixels at the display dimension of $26.7 \times 19.3 \times 1.7$ mm. This monochromatic OLED will display white colour and the built-in I2C interface will be used to communicate with the microcontroller.



Figure 3.10: OLED display

3.7 Software

3.7.1 Firebase Cloud Server

Firebase cloud server is a backend server developed by Google developers. It can be used for data storage, analysis, monitoring, data visualisation and remote configuration. It has a real time database that is suitable for IoT applications and it is easy to configure the microcontroller to connect with the cloud server. It also includes the services such as data management across different operating platforms, cloud messaging as well as authentication. Integrating the real time database with firebase authentication, the user identity can be determined and the user can only access its data. This platform provides a simple way to develop mobile applications and web applications. With real time synchronization, the user can obtain the data from any device immediately. Firebase also includes web hosting services. By using firebase hosting, the web app can be deployed easily. The end user can access the website around the world as all the deployed files are stored on the solid state drive at the content delivery network all around and the website is having the secure sockets layer certificate to increase the security.

3.7.2 Arduino IDE

In this project, the Arduino integrated development environment (IDE) is used to write code, compile, and upload the code to the ESP32 microcontroller. The Arduino IDE is open source software and can be written in C or C++ programming language. Arduino programming consists of a lot of open source libraries which cause easier and faster in the development process. Arduino IDE

is widely used to compile the code for microcontrollers because it can be operated on Windows, macOS and Linux operating systems and many different types of microcontroller development boards are compatible with this IDE.

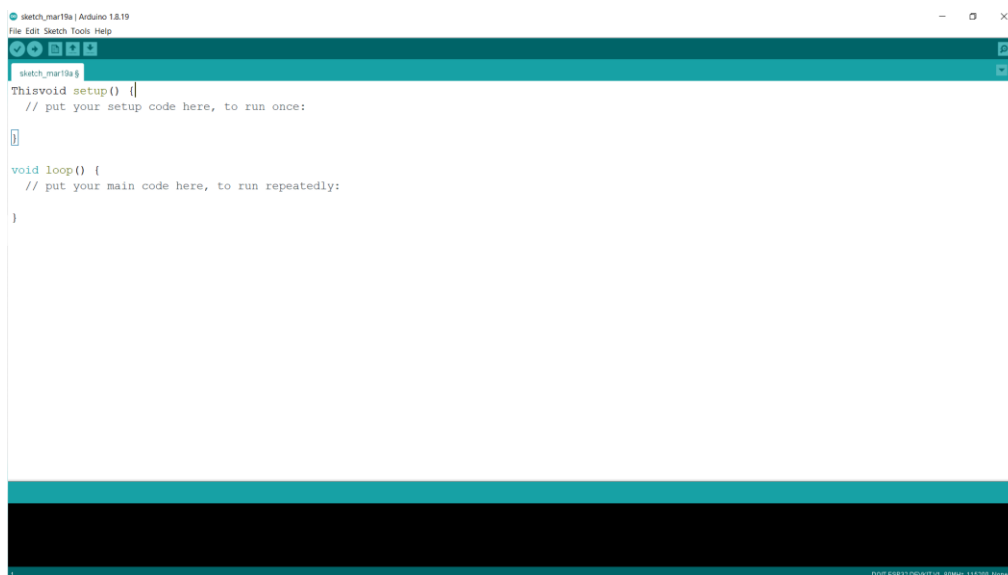


Figure 3.11: Arduino IDE interface

3.7.3 Visual Studio Code

Visual Studio Code is a code editor which provides a space for the programmer to write code. This software can be used across the Window, Mac and Linux platform and support almost all programming language including javascript, typescript, python, C, C++ and so on. The extension in this software provides many features like detecting the syntax error automatically, suggesting the common code, automatic imports the library to the coding, providing default code formatting and others. Therefore, this code editor is very user-friendly. In this project, Visual Studio Code is used to develop mobile applications and webpage.

3.7.4 Expo

Expo is a framework to build react native apps by using javascript so all the react native library is compatible in the Expo. Expo software development kit provides a lot of well-tested, consistent and comprehensive libraries which make it easier to develop mobile applications. The Expo command line interface (CLI) allows the programmer to debug the program locally by simulating it on

the computer and remotely via the Expo client app during the development phase. The Expo CLI can be used to publish the app on the Expo server. By using the Expo framework, developers do not need to be familiar with native iOS or Android code, the Expo CLI can compile the code to run on iOS and Android in the background. With one Expo code, it not only can run on iOS and Android mobile platforms but it also can run in Windows, macOS and Web by installing respective source files for compilation.

3.7.5 Proteus

Proteus is a powerful development platform for circuit design and simulation. There are many components like resistors, capacitors, microcontrollers, switches and et cetera in the library which let the user draws the schematics diagram easily. This software provides measurement and analysis tools such as voltmeter, ammeter, and oscilloscope for real time simulation. This software can be used to design the printed circuit board (PCB) as well. The PCB design in this software provides the function of automatic components placement and wire routing, design rule checking, viewing the 3D design and exporting the PCB layout to the Gerber file.

3.8 Evaluation method of the sensor with the developed prototype

A prototype of the liquid fertilizer concentration measurement system is developed. The VNA is replaced by the power detector and VCO to measure the liquid fertilizer concentration due to the VNA is costly and bulky. By replacing the VNA, the liquid fertilizer concentration measurement system will become small, light and portable. The same concentration of urea sample solutions that use to evaluate the microwave sensor is prepared to evaluate the sensitivity of the prototype. The VCO tuning voltage will be determined when analysing the microwave sensor. Each concentration is repeated three times to reduce the measurement error. After that, the average output voltage from the power detector is calculated. The graph of power detector output voltage against concentration is plotted. The best fit line is plotted on the graph to show the relationship between voltage and concentration. The R^2 value is calculated to evaluate the correlation between voltage and concentration. The best fit line

equation is obtained and used as the calibration equation in the software to determine the liquid fertilizer concentration.

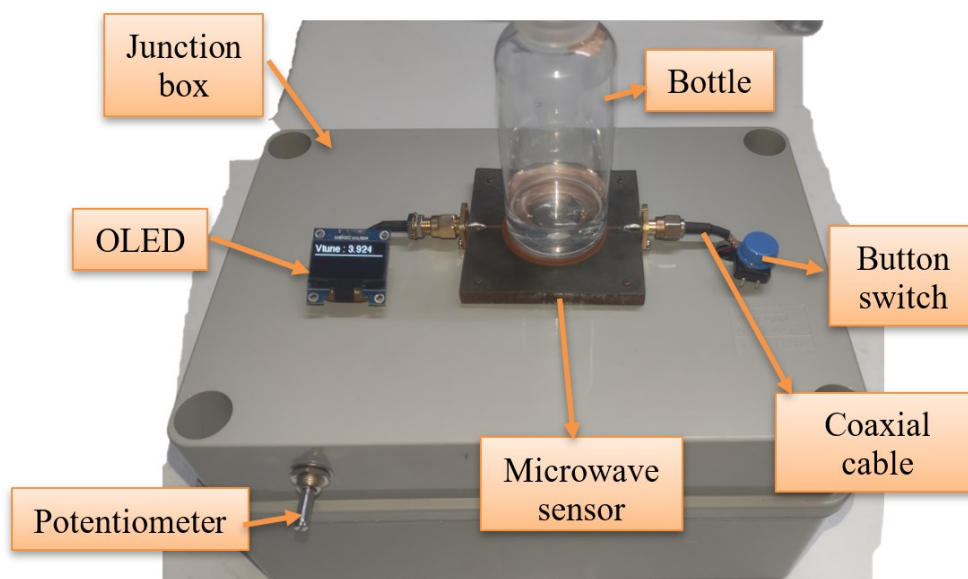


Figure 3.12: Prototype measurement setup

CHAPTER 4

RESULTS AND DISCUSSION

4.1 Result of simulated microwave sensor

By using the CST microwave studio to simulate and optimise the microwave sensor, the final design and dimension of the planar microwave sensor are shown in Figure 4.1. The simulation result of resonant frequency and insertion loss shows that the patch design with the dimension in Table 4.1 is the closest to the design requirement.

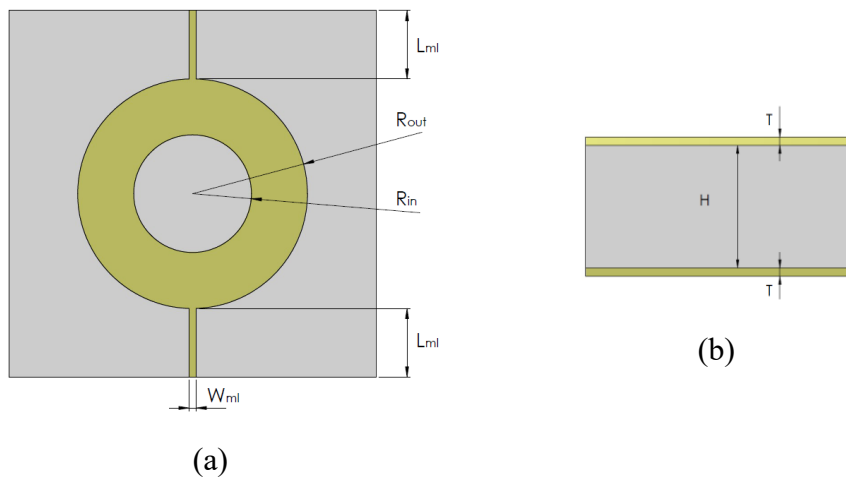


Figure 4.1: Layout of planar microwave sensor (a) top view and (b) side view

Table 4.1: Dimensions of the microwave sensor

| Parameter | Description | Dimension (mm) |
|-----------|-------------------------------|----------------|
| R_{out} | Radius of the outer ring | 18.51 |
| R_{in} | Radius of the inner ring | 9.48 |
| L_{ml} | Length of the microstrip line | 11.04 |
| W_{ml} | Width of the microstrip line | 1.14 |
| t | Thickness of copper patch | 0.035 |
| h | Thickness of substrate | 0.502 |

Figure 4.2 shows the simulated result of S_{11} and S_{21} of the microwave sensor and the resonance frequency is about 2.425 GHz. At the resonance frequency, the S_{11} is -28.094 dB which is the lowest point of the S_{11} . In contrast,

at the resonance frequency, the S_{21} is -0.385 dB which is the highest point of the S_{21} .

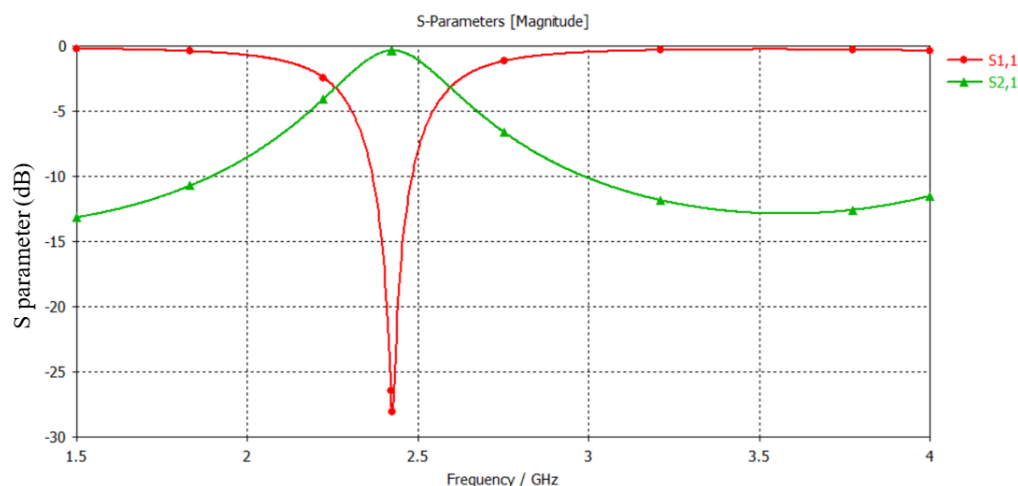


Figure 4.2: Simulated S parameters results of microwave sensor

Return loss can be expressed as a ratio of the incident power to the reflected power in decibels (dB) while insertion loss can be defined as a ratio of the incident power to the transmitted power in dB. A high return loss indicates less signal is reflected, so the S_{11} parameter's value will be lower. On the other hand, the low insertion loss indicates more signal is transmitted across the microwave sensor, so the S_{21} parameter's value will be higher. At the resonance frequency, 95.7 % of the signal power is transmitted across the microwave sensor, 3.9 % of power is reflected and 0.4 % of the power is dissipated in the conducting surfaces and dielectric materials. The relationship between the incident power, reflected power, transmitted power, return loss and insertion loss is shown in Figure 4.3. The reflection coefficient and transmission coefficient can be calculated by using Equations 4.1 and 4.2.

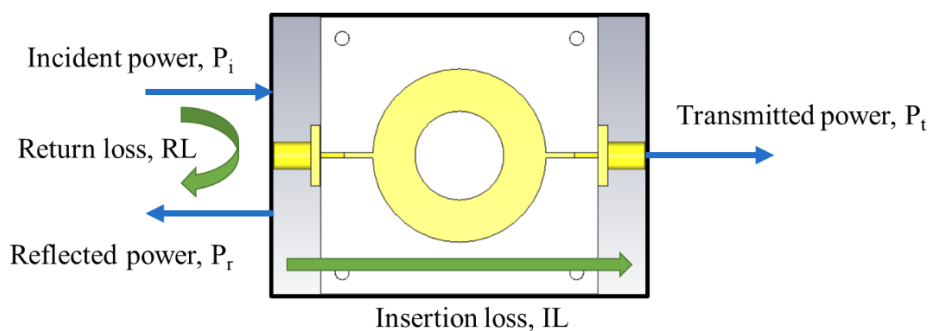


Figure 4.3: Direction of signal and power flow

$$S_{11} = 20 \log|\Gamma| \quad (4.1)$$

$$S_{21} = 20 \log|T| \quad (4.2)$$

where

$|\Gamma|$ = voltage reflection coefficient

$|T|$ = voltage transmission coefficient

S_{11} = reflection coefficient (dB)

S_{21} = transmission coefficient (dB)

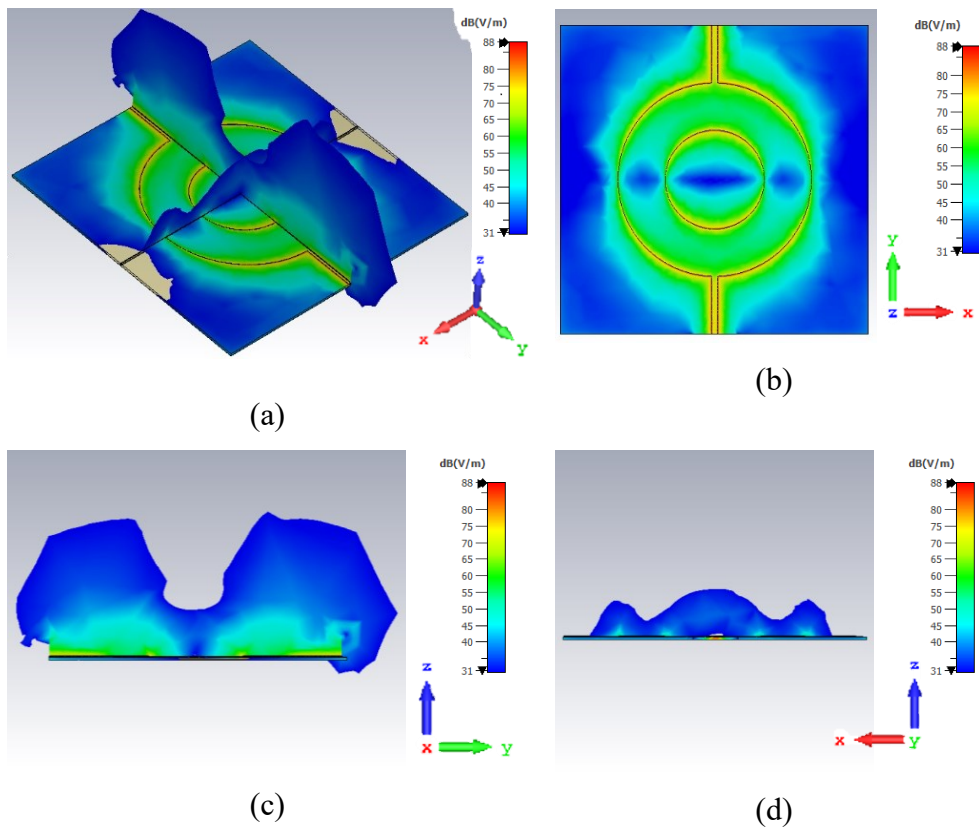


Figure 4.4: Electric field distribution at the resonance frequency (2.425GHz) for (a) isometric view, (b) front view, (c) transverse cross-section view in the middle of the x-axis and (d) transverse cross-section view in the middle of the y-axis

Figure 4.4 shows the electric field distribution on the planar microwave sensor when port 1 is excited and port 2 is matched. On the circular ring of the microwave sensor, the electric field is highly concentrated in this area. The higher the electric field concentration, the higher the sensitivity of the

microwave sensor due to the higher variation of the permittivity. Due to this microwave sensor being designed for non-invasive and non-intrusive measurement, the electric field distributed away from the planar microwave sensor should be considered too. Figure 4.3 (c) and (d) show a strong electric field distribution away from the circular ring surface. Thus, the liquid under test is suitable to put on this area in order to obtain higher sensitivity.

4.2 Comparison between simulated and measured characteristics of microwave sensor

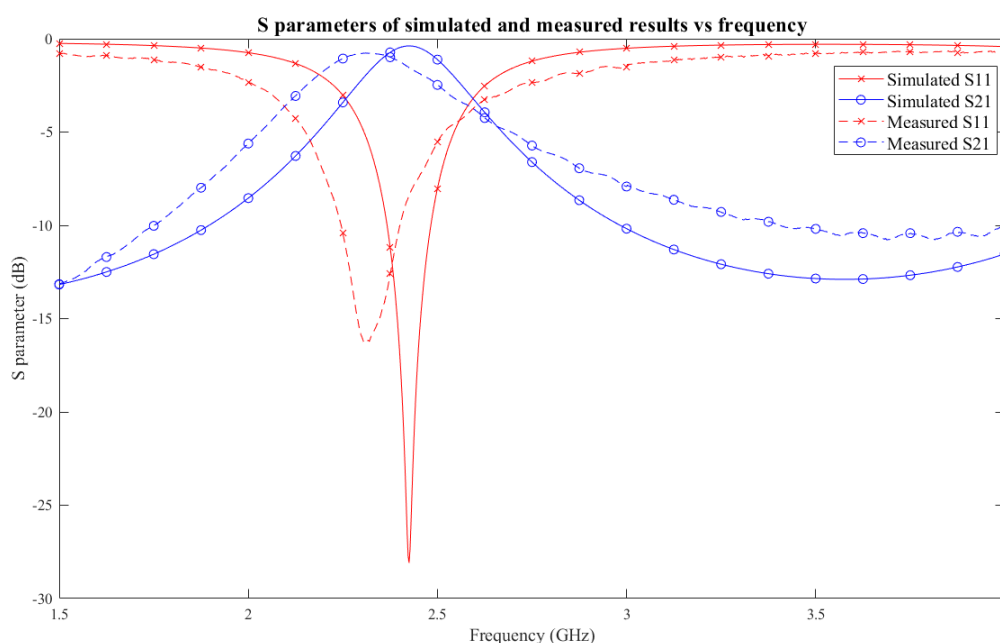


Figure 4.5: Comparison of S parameter between simulated and fabricated sensor

The deviation between simulation and experimental measurement results of the microwave sensor without any liquid under test is demonstrated in Figure 4.5. The result shows the simulated and measured S parameter is in close agreement with each other. The simulated resonance frequency is 2.425 GHz while the measured resonance frequency is 2.313 GHz. The simulated S_{11} and S_{21} at resonance frequency are -28.094 dB and -0.385 dB respectively but the measured S_{11} and S_{21} are -23.687 dB and -0.680 dB respectively. The main factor that causes the shifting of resonance frequency and discrepancy in the S parameter is the effect of soldering between the SMA port and microwave

sensor. Other than this factor, the dimension tolerance of the fabricated sensor, mismatch of the SMA port, measurement error and environment permittivity variation will also affect the result. Table 4.2 presents the summary of the sensor characteristics between simulation and measurement results.

Table 4.2: Summary of the sensor characteristics between simulation and measurement result

| Characteristic | Simulation | Measurement |
|---------------------------|------------|-------------|
| Resonance frequency (GHz) | 2.425 | 2.313 |
| S_{11} (dB) | - 28.09 | - 16.25 |
| S_{21} (dB) | - 0.385 | - 0.777 |
| $ \Gamma $ | 0.039 | 0.154 |
| $ T $ | 0.957 | 0.914 |

By observing the power loss at the resonance frequency, the measured $|T|$ is 0.154 and the measured $|T|$ is 0.914. The $|\Gamma|$ is much lower compared to the $|T|$. This show that less signal is reflected and more power is transmitted across the microwave sensor. Consequently, the S_{21} parameter is chosen for the liquid fertilizer measurement. The selected power detector in this prototype can only measure the power between - 55 dBm to 10 dBm. However, the insertion loss is 0.777 dB so it has a minimum effect on the power detector to detect the liquid fertilizer concentration.

4.3 Evaluation of microwave sensor by using VNA

The experiments were performed in real time and the results were ready when the bottle filled with the sample solution was put on the sensor. Figure 4.6 illustrates the measured S_{21} of the sensor for urea solution with the concentration ranging from 0 g/ml to 0.435 g/ml. By referring to Figure 4.6, a linear trend of S_{21} can be observed at the frequency around 2.09 GHz and 2.37 GHz. The variation of the S_{21} as a function of the sample's concentration at 2.09 GHz and 2.37 GHz is plotted in Figure 4.7 (a) and (b). The amplitude of the S_{21} parameter linearly decreases with the increment of concentration at 2.09 GHz while at 2.37 GHz, the amplitude of the S_{21} parameter linearly increases with the increment

of concentration. The variations of measurements were expressed as error bars in the plots. The R^2 is higher than 0.9 and RMSE is less than 0.1 at both frequencies. The gradient of the linear model shows the sensitivity of the sensor. The sensitivity at 2.09 GHz is 1.97 dB/(g/mL) which is lower than the sensitivity at 2.37 GHz which is 3.20 dB/(g/mL). Thus, the frequency of 2.37 GHz is chosen as the frequency to measure the concentration of urea solution.

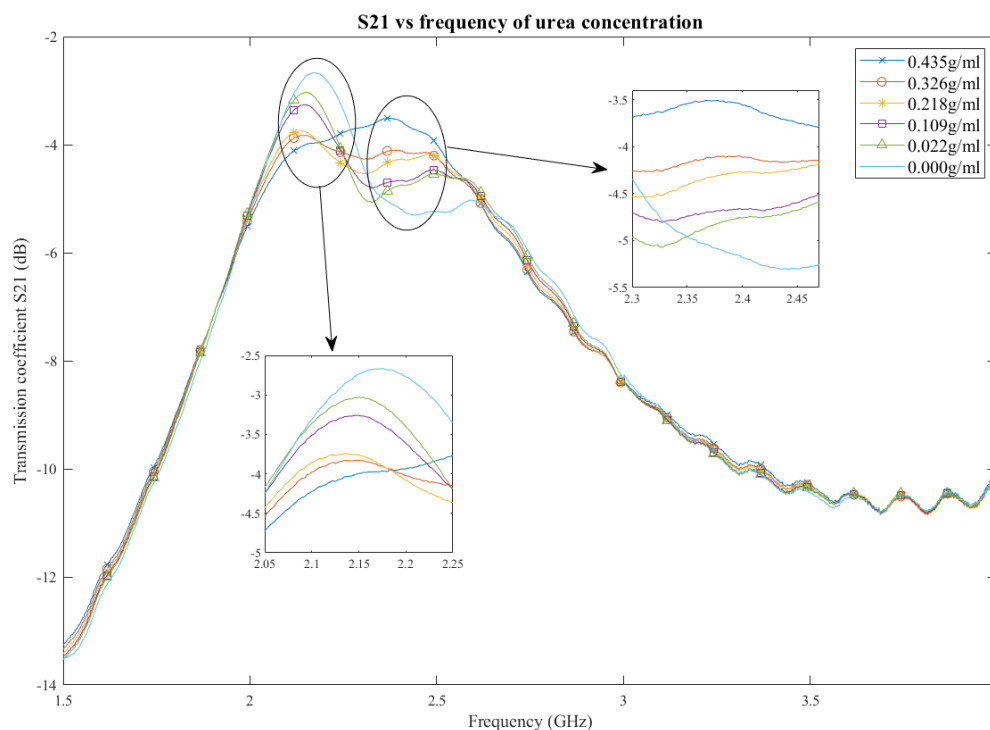
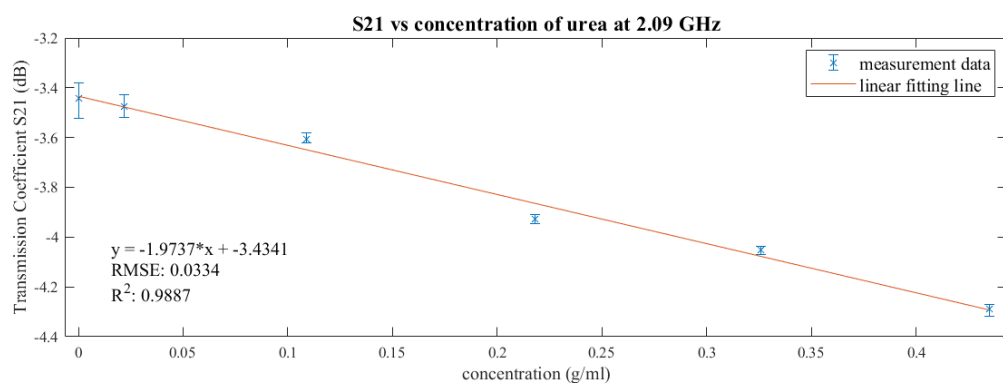
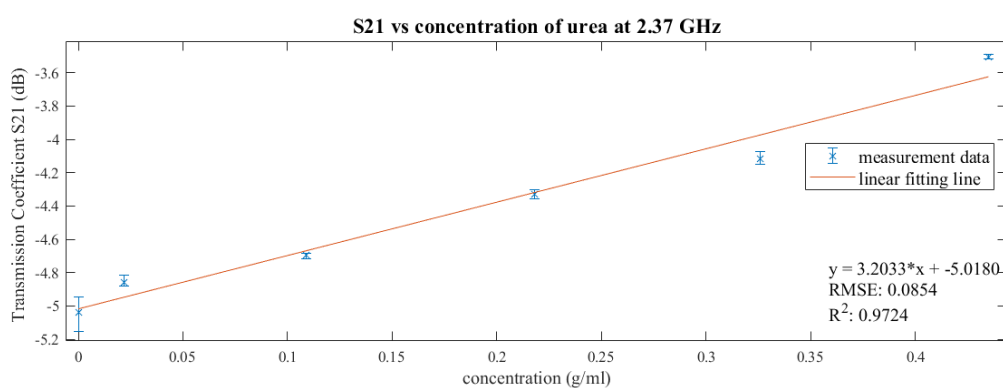


Figure 4.6: Graph of S_{21} against the frequency for different urea concentrations



(a)



(b)

Figure 4.7: Graph of S₂₁ against urea concentration at (a) 2.09 GHz and (b) 2.37 GHz

Figure 4.8 illustrates the measured microwave S₂₁ of the sensor for MAP solution with the concentration ranging from 0.01 g/ml to 0.2 g/ml. By referring to Figure 4.8, a linear trend of S₂₁ can be observed at the frequency around 2.54 GHz and 2.92 GHz. The variation of the S₂₁ as a function of the sample's concentration at 2.54 GHz and 2.92 GHz is plotted in Figure 4.9 (a) and (b). The amplitude of the S₂₁ parameter linearly increases with the increment of concentration. The variations of measurements are expressed as error bars in the plots. The R² is higher than 0.9 and RMSE is less than 0.1 at both frequencies. The gradient of the linear model shows the sensitivity of the sensor. The sensitivity at 2.54 GHz is 1.13 dB/(g/mL) which is slightly higher than the sensitivity at 2.92 GHz which is 1.00 dB/(g/mL). Therefore, the frequency of 2.54 GHz is chosen as the frequency to measure the concentration of MAP solution.

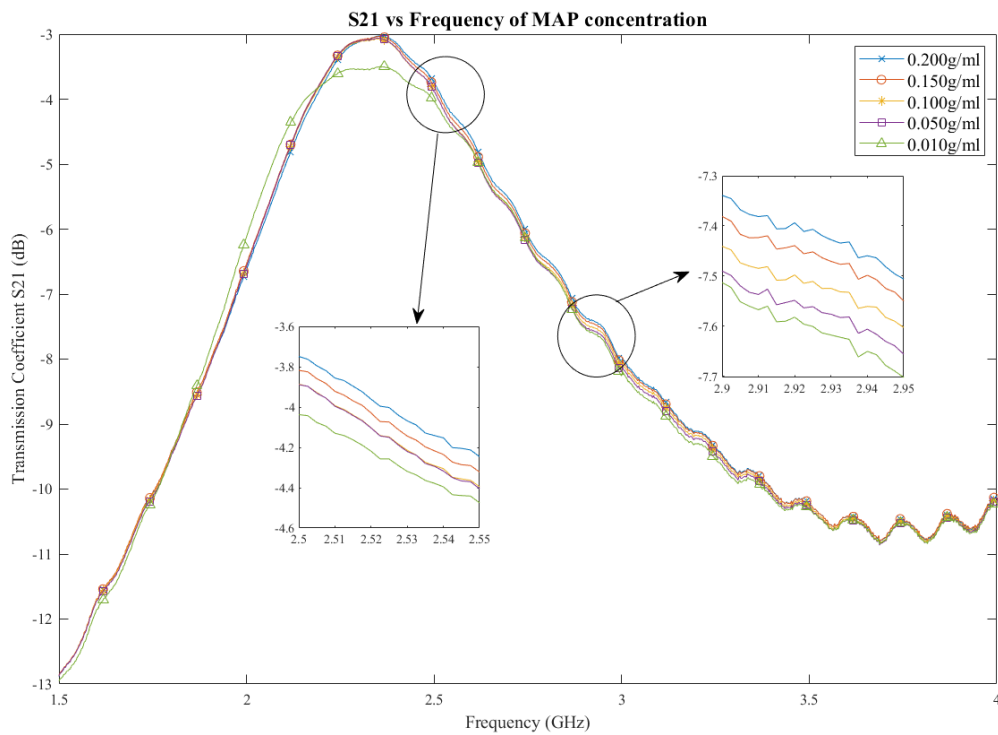
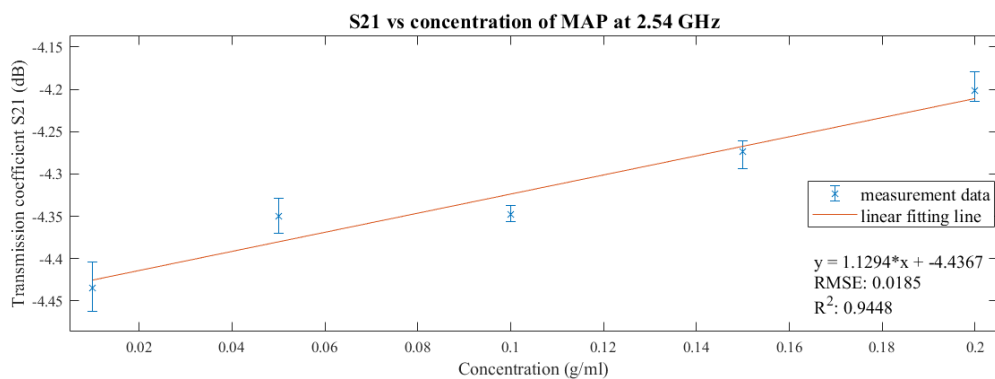
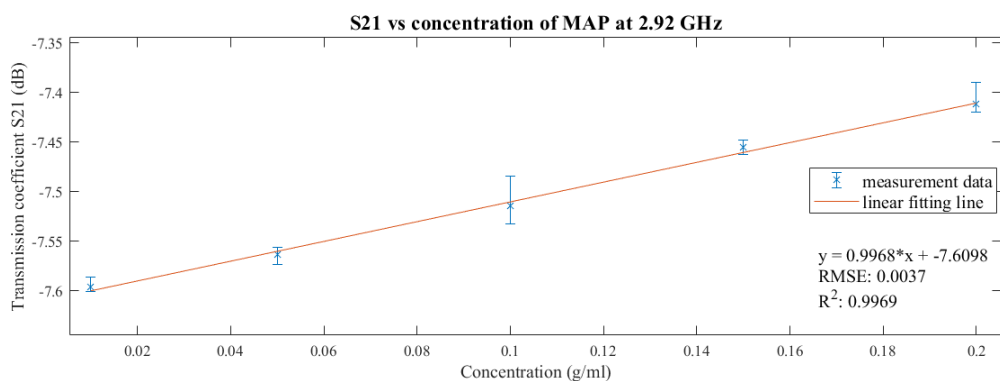


Figure 4.8: Graph of S_{21} against the frequency for different MAP concentrations



(a)



(b)

Figure 4.9: Graph of S_{21} against urea concentration at (a) 2.54 GHz and (b) 2.92 GHz

The error bars in Figure 4.7 and Figure 4.9 indicates the measurement uncertainty which is due to the sample preparation process, differences in plastic bottles due to uncontrollable variation during the manufacturing process and differences in location between the bottles and the circular ring of microwave sensor that may have occurred during the experiment.

4.4 Software design

4.4.1 MCU program

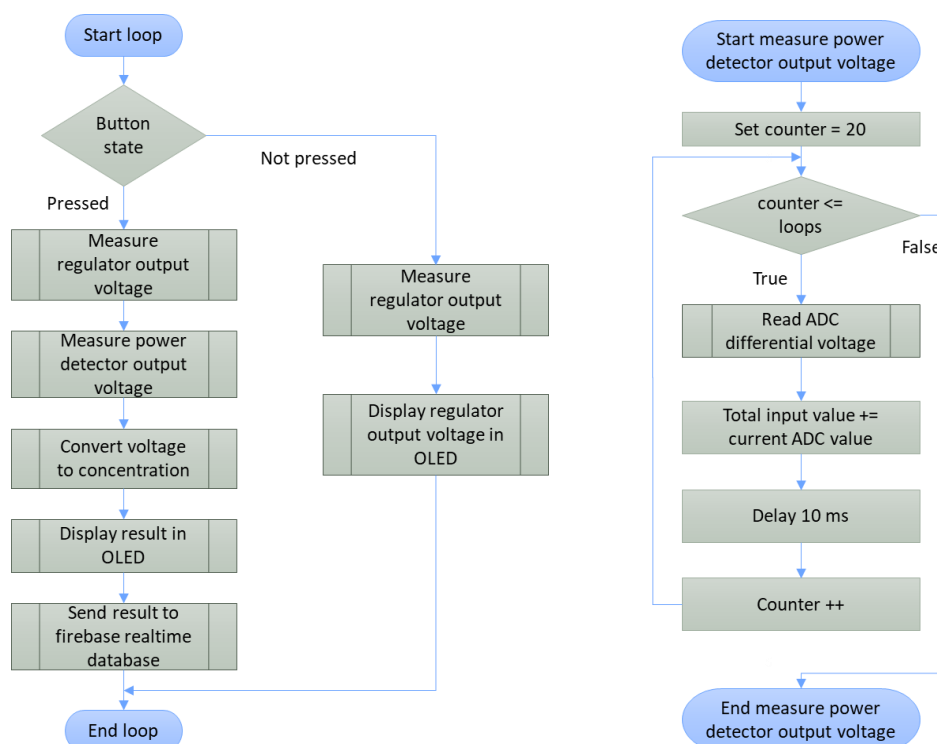


Figure 4.10: Flow chart of the main loop program and power detector output voltage measurement program

Figure 4.10 illustrates the flow chart of the main loop program and power detector output voltage measurement program. First of all, the MCU will detect whether the button is pressed or not. If the button is pressed, the tuning voltage and power detector output voltage are measured by ADC and the data is transmitted to the microcontroller. Then, the MCU will identify the type of fertilizer and its concentration. The value of tuning voltage is analysed to figure out the fertilizer type of the measurement. Next, the power detector output voltage is used to calculate the liquid fertilizer concentration by using the corresponding calibration equation. The calibration equation is depending on the type of fertilizers. After that, the result is displayed on the OLED and sent to the Firebase Realtime Database to monitor the fertilizer concentration in real time. If the button is not pressed, the MCU will collect the regulator output voltage and display the voltage on the OLED so that the user can adjust the regulator output voltage to the appropriate value.

For the power detector output voltage measurement algorithm, the MCU is repeated 20 times to acquire the power detector differential voltage for one measurement. After that, the MCU will calculate the average voltage level to reduce the voltage fluctuation caused by the environmental noise and the noise produced when electronic components are operating.

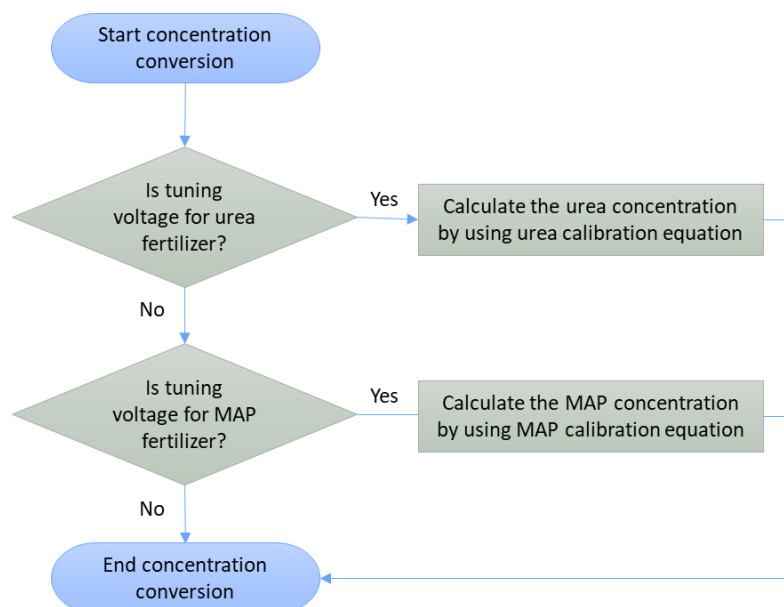


Figure 4.11: Flow chart of the concentration conversion program

Figure 4.11 presents the concentration conversion algorithm, the MCU will check whether the tuning voltage is in the acceptable range for the urea fertilizer measurement or MAP fertilizer measurement. The tuning voltage of the urea fertilizer and MAP fertilizer is determined in section 4.3. If the tuning voltage is within the acceptable range, the MCU will calculate the urea concentration or MAP concentration by using the respective calibration equation. The calibration equation will be determined in section 4.6. The Arduino program code for the ESP32 microcontroller is given in Appendix A.

4.4.2 Firebase Realtime Database

Firebase Realtime Database is the cloud server used to store data for this project. The real time database is stored in the javascript object notation file format. When new data is added, a new node is created in the existing JSON structure. Users can allocate any name to the node and all the data inside the node with

variables and values are considered members. The no cost plan of the Firebase cloud storage provides 1 GB of data storage which is enough for this project. Figure 4.12 shows part of the data stored in the Firebase Realtime Database.

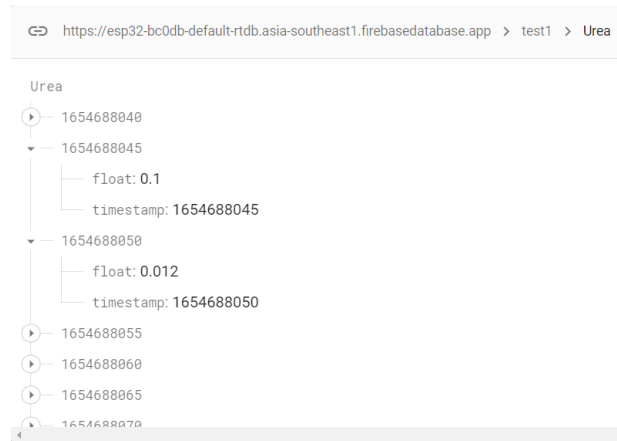


Figure 4.12: Firebase Realtime Database

In this project, Firebase Realtime Database starts with a test1 node which can be described as the identity of the fertilizer concentration measurement system. If more than one system is used, different identity names can be assigned. The identity name also can be used as an authentication identity to prevent other systems modified this system data. The second branch of the node is named Urea in order to store the urea fertilizer concentration. The name of the third branch node is the timestamp value of the system measurement time which is uploaded by the MCU. This node's name is set as the epoch timestamp to prevent two identical names are created which will cause errors in the program. The data members of the third branch nodes have the variable name of float and timestamp. This illustrates that the concentration is stored in the float variable. The epoch timestamp value of 1654688045 can be converted to a human readable date and time of 8 June 2022 at 19:34:05 UTC+8. The data can be described as the urea fertilizer was measured on 8 June 2022 at 19:34:05 where the urea concentration was 0.1 g/ml.

4.4.3 Data monitoring via browser and mobile application

The data can be monitored by using the computer or mobile phone via browser or android application. The expo framework is used to create the android

application and web application. The JavaScript program code for the mobile application and web application is given in Appendix B and Appendix C. By viewing the data via the android application or web application, the user can experience a more friendly interface instead of reading through columns and rows of data in JSON format.

Figure 4.13 shows the mobile application layouts. The main page will be the home page. The home page will show the latest liquid fertilizer concentration in real time. When new data is received by the Firebase database, the mobile application will update to the latest result automatically. At the bottom navigation bar, the user can choose to view the area graph and history urea concentration measurement data.

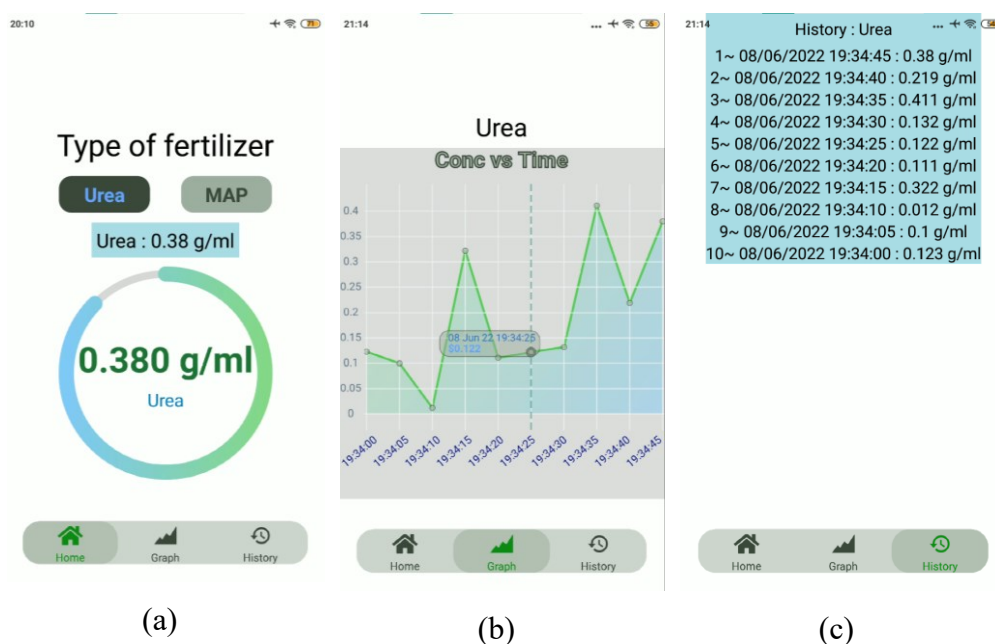


Figure 4.13: Android mobile application layouts (a) home page, (b) graph page and (c) history page

Firestore is used to deploy the web application. For the Firestore hosting, the no cost plan provides 10 GB of storage. The source code of the web app is uploaded to the firestore hosting server. Thus, the user can access the data via the browser by entering the website address. The GUI and the functions of the application for both the mobile application and web application are almost the same in order to let the user easily handle both of these applications. Figure 4.14 shows the web application layouts.

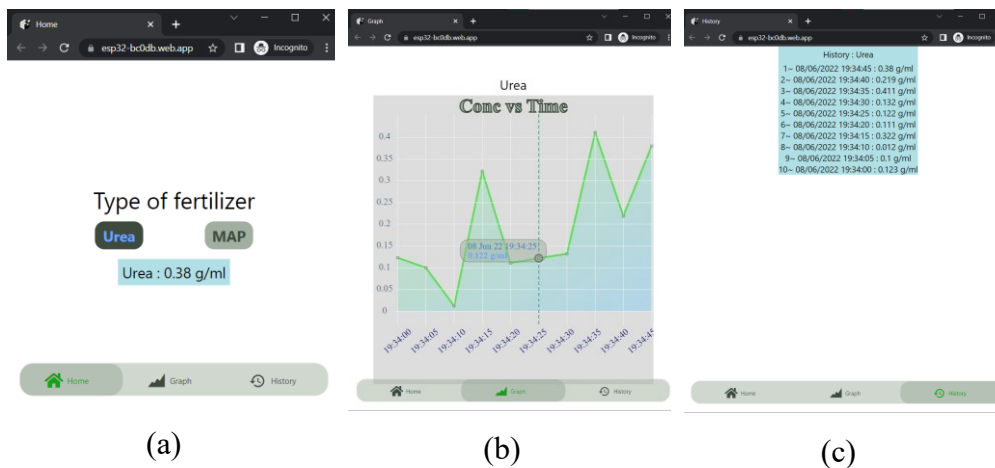


Figure 4.14: Web application layouts (a) home page, (b) graph page and (c) history page

4.5 Hardware design

4.5.1 Circuit Diagram and Pin Connection

A 9 V and 12 V battery is used to supply the power to this system. A breadboard power supply converter will convert the voltage to 3.3 V and 5 V. The ESP32 DEVKIT V1 board, OLED display and ADC required a 3.3 V power supply to operate. The power supply for the VCO and power detector is 5 V.

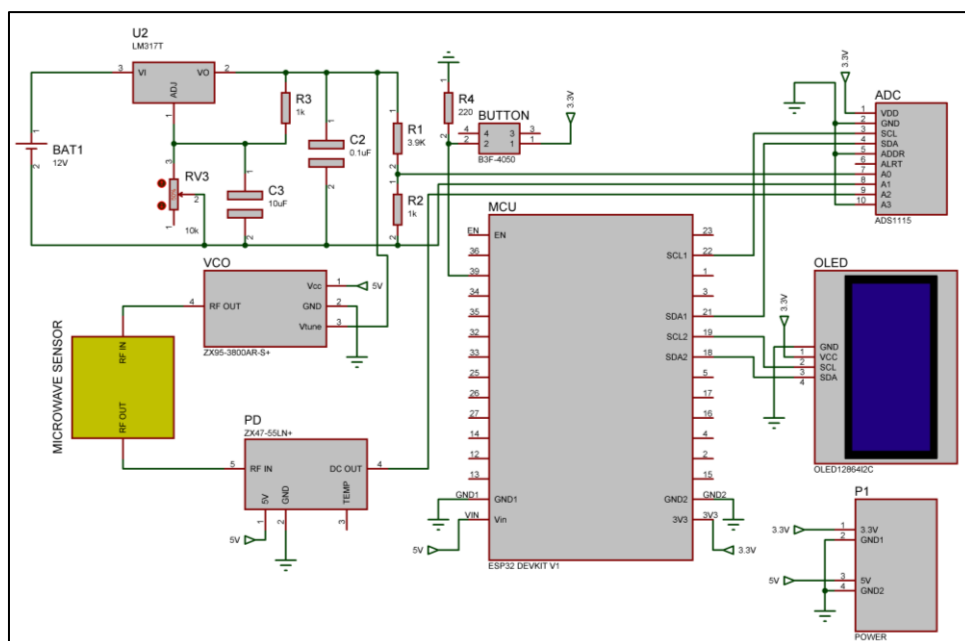


Figure 4.15: Schematic diagram of the liquid fertilizer monitoring system

The LM315 linear voltage regulator is constructed to control the tuning voltage of the VCO. With the potentiometer in the feedback circuit, the output voltage is adjustable from 1.25 V to 10.5 V and the maximum output current is 1.5 A which is much more than the current required by the VCO tuning current. The 1 μ F ceramic capacitor in this circuit is used to improve the transient response of output voltage. The 10 μ F tantalum capacitor is used to prevent amplification of the ripple voltage when the output voltage is adjusted higher. The ESP32 microcontroller has a maximum 3.3 V input and output voltage for all the general purpose input output pins.

From the datasheet of the VCO, the VCO generates the radio frequency output of 2092.6 MHz at 2 V and 3168.1 at 10 V. Hence, this adjustable voltage regulator is designed to supply the output voltage from 2 V to 10 V. The voltage divider circuit is used to reduce the regulator output voltage level and become lesser than 2.048 V for the ADS1115 ADC to measure the actual voltage level. The ADS1115 ADC will convert the voltage level from the analogue signal to the digital signal. If the voltage level is different from the predetermined value, a potentiometer is used to adjust the regulator output voltage.

The power detector output voltage is ranging from 0.5 V to 2 V. The ADC of the microcontroller is 12 bits resolution so the minimum change of voltage that can be detected by the microcontroller is 0.81 mV. From the datasheet of this power detector, the output voltage changed by one decibel is – 25 mV/dB typically. If 0.01 dB change from the microwave sensor output is required to be detected by the microcontroller, the microcontroller needs to detect the 0.25 mV of voltage changes. Thus, 12 bits resolution of ADC is not enough. A 16 bits delta sigma ADS1115 ADC is selected. This ADC can detect 0.0625 mV change with a 16 bits resolution setting. This ADC is used I2C protocol to communicate with the microcontroller. The input voltage of ADC is 3.3 V.

The OLED display is chosen as it consumes lower power compared to the LCD display. This OLED communicates with the microcontroller by using the I2C protocol. After the measurement, the OLED will display the concentration of fertilizer and the ESP32 DEVKIT V1 board will send the result to the Firebase cloud server via Wi-Fi.

4.5.2 PCB design

Two layers PCB is designed by using Proteus software. Figure 4.16 shows the PCB layout of the liquid fertilizer centration measurement system. The size of the PCB is 17 cm by 11.5 cm which makes the PCB able to fit perfectly into a 21.5 cm length, 15 cm width and 11 cm high junction box together with batteries, ADC and power detector and other electronic components. The blue route represents the top layer routing while the red route represents the bottom layer routing. In this PCB design, the width of the trace route is 1.27 mm. The light blue colour in the PCB layout represents the PCB top silk which is used to identify the PCB components, sizes and symbols.

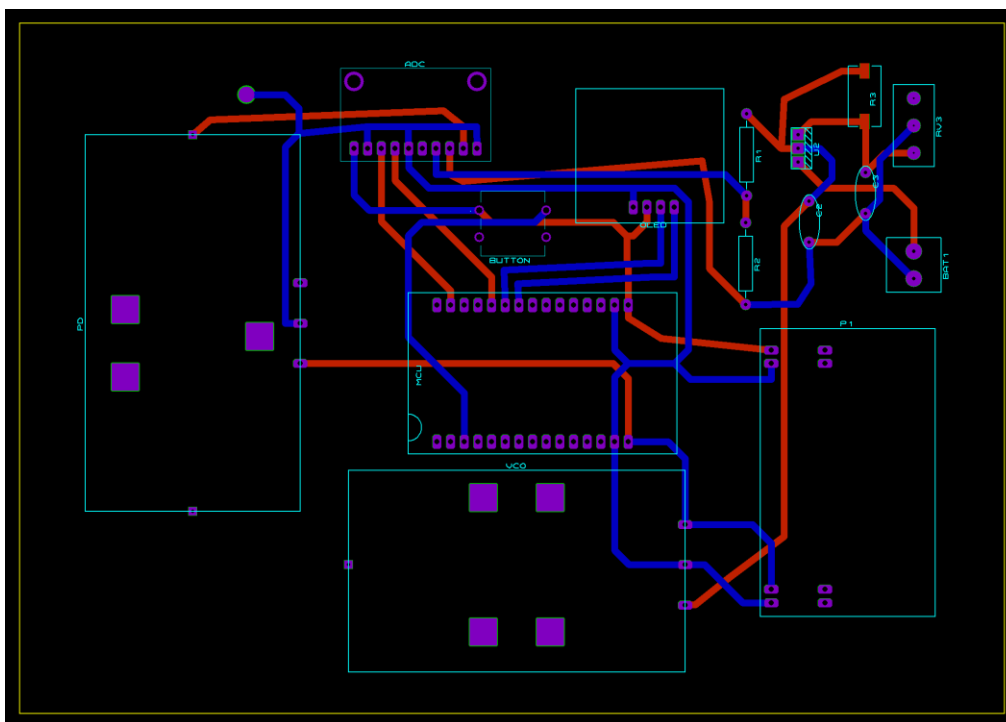


Figure 4.16: PCB Layout

The PCB was fabricated using photolithography and chemical etching methods. Figure 4.17 shows the bottom layer of the fabricated PCB and Figure 4.18 shows the PCB with electronic components soldered on it.

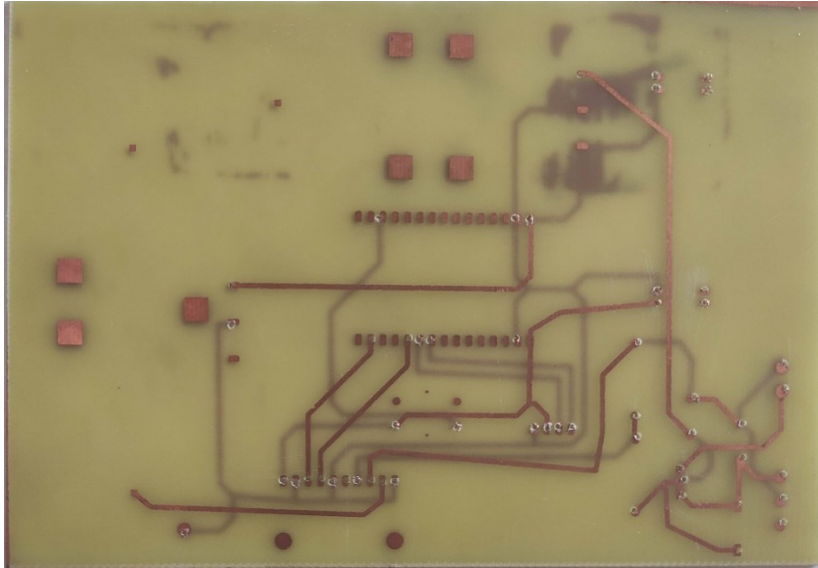


Figure 4.17: Bottom View of fabricated PCB

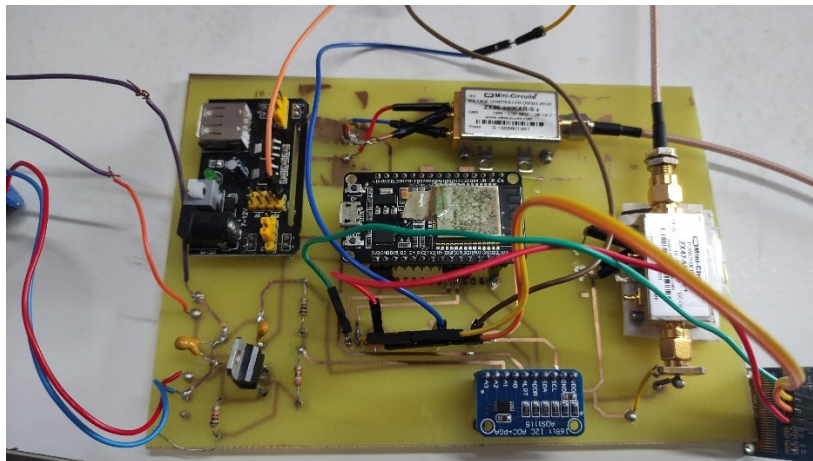


Figure 4.18: PCB with soldered electronic components

4.5.3 Project Prototype

A 21.5 cm × 15 cm junction box was used in this liquid fertilizer measurement system. The PCB, battery and electronic components were placed inside the junction box while the microwave sensor, OLED and button were placed on top of the junction box which was more convenient for the user to carry out the measurement and view the result. For the coaxial cables and wires to connect with the microwave sensor, OLED and button, two holes were drilled into the junction box. Figure 4.19 shows the components inside the junction box and Figure 4.20 shows the components outside the junction box.

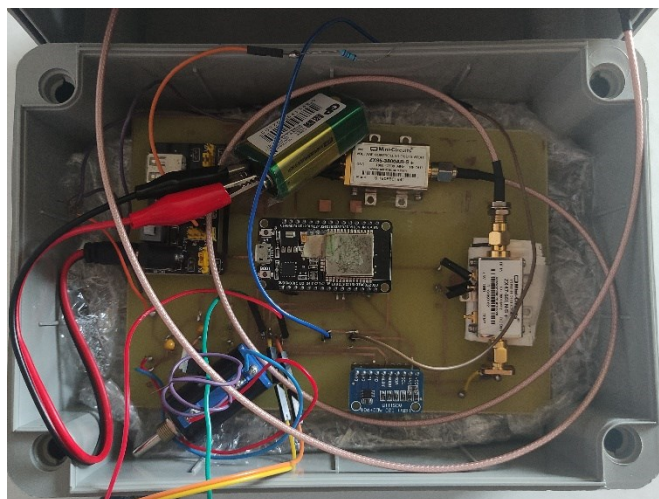


Figure 4.19: Inner view of the junction box

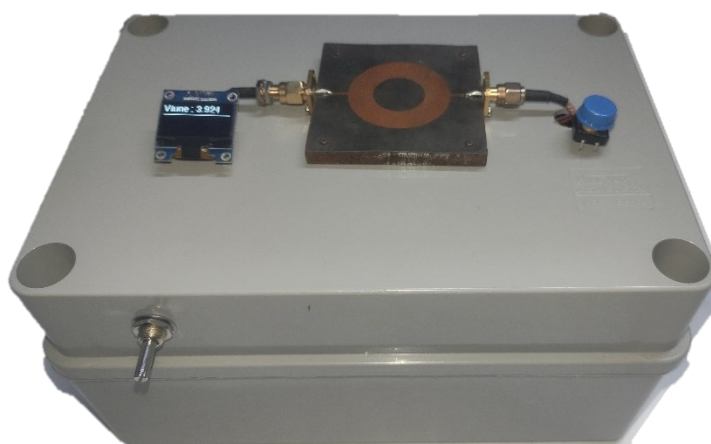


Figure 4.20: Outer view of the junction box

4.6 Evaluate prototype of liquid fertilizer concentration measurement system

For the urea fertilizer, the VCO tuning voltage was set to 3.92 V in order to obtain a 2.37 GHz frequency as this frequency obtained a positive linear trend with higher sensitivity when evaluating the microwave sensor performance in section 4.3. The trendline in Figure 4.21 shows the power detector output voltage linearly decreases with the increment of concentration. The sensitivity of the urea concentration measured with this prototype is 10.212 (g/ml)/V and the R^2 is 0.9829. The best fit line with the linear polynomial equation is expressed in Equation 4.3. This equation will be used as the calibration equation for the software to determine the urea concentration. The variations of measurements are expressed as error bars in the plots. The variation is due to

the differences in location between bottles and the circular ring of the microwave sensor during the prototype evaluation and caused by the heat sensitive electronic components.

$$c_{urea} = -10.212V_{pd} + 7.6903 \quad (4.3)$$

where

c_{urea} = concentration of urea solution (g/ml)

V_{pd} = power detector output voltage (V)

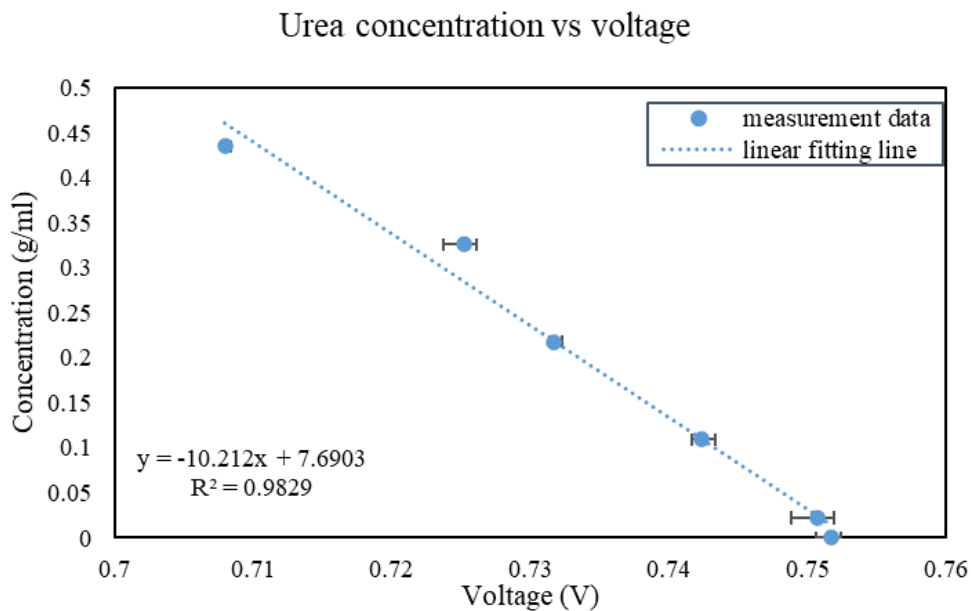


Figure 4.21: Graph of voltage against concentration for urea fertilizer

For the MAP fertilizer, the VCO tuning voltage was set to 5.11 V in order to obtain a 2.54 GHz frequency as this frequency obtained a positive linear trend with higher sensitivity when evaluating the microwave sensor performance. The trendline in Figure 4.22 shows the power detector output voltage decreases with the increment of concentration. The sensitivity equation of the MAP concentration measured with this prototype is expressed in Equation 4.4 and the R^2 is 0.9693. The best fit line with the quadratic polynomial equation is expressed in Equation 4.5. This equation will be used as the calibration equation for the software to determine the MAP concentration. The variations of measurements are expressed as error bars in the plots. The variation is due to the differences in location between bottles and the circular ring of the

microwave sensor during the prototype evaluation and caused by the heat sensitive electronic components.

$$\frac{dc_{MAP}}{dV_{pd}} = 4440.2V_{pd} + 3165.4 \quad (4.4)$$

$$c_{MAP} = 2220.1V_{pd}^2 - 3165.4V_{pd} + 1128.3 \quad (4.5)$$

where

c_{MAP} = concentration of MAP solution (g/ml)

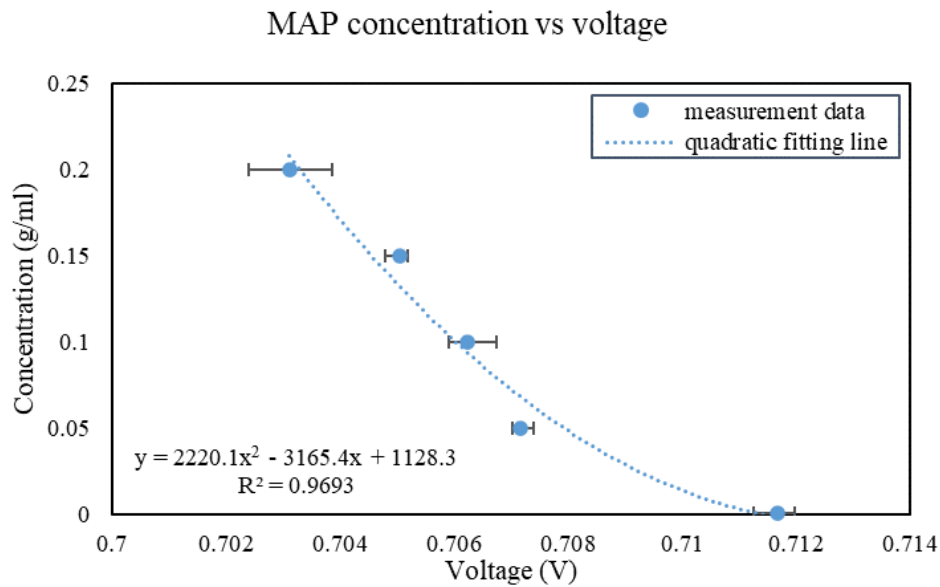


Figure 4.22: Graph of voltage against concentration for MAP fertilizer

The urea sample solution with the concentration between 0 g/ml and 0.435 g/ml and MAP sample solution with the concentration between 0.01 g/ml and 0.2 g/ml were prepared to validate the calibration equations for both liquid fertilizers. Figure 4.23 illustrates the comparison of the predicted and actual concentration of urea fertilizer. The predicted concentration of urea solutions was measured by using the microwave sensor. The MCU would predict the type of fertilizer according to the VCO tuning voltage and calculate the fertilizer concentration based on the urea calibration equations. Nevertheless, the actual concentration of the urea solutions was identified during the sample solution preparation process. The line of ideal fit indicates the best relationship between predicted and actual urea concentration. The predicted concentrations for this liquid fertilizer measurement system are close to the ideal fit line. For this urea fertilizer concentration prediction, the R^2 and RMSE are 0.9689 and 0.0433

respectively. The high R^2 and low RMSE indicate that this liquid fertilizer concentration measurement system exhibits great accuracy in urea concentration measurement.

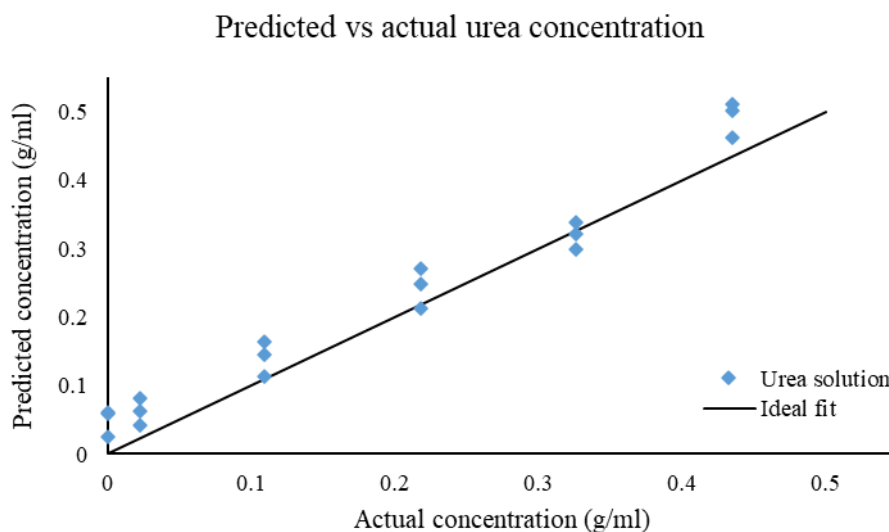


Figure 4.23: Comparison of the predicted and actual concentration of urea fertilizer

Figure 4.24 illustrates the comparison of the predicted and actual concentrations of MAP fertilizer. The predicted concentration of MAP solutions was measured by using the microwave sensor. The MCU would predict the type of fertilizer according to the VCO tuning voltage and calculate the fertilizer concentration based on the MAP calibration equations. Nevertheless, the actual concentration of the MAP solutions was identified during the sample solution preparation process. The line of ideal fit indicates the best relationship between predicted and actual MAP concentration. The predicted concentrations for this liquid fertilizer measurement system are close to the ideal fit line. For this MAP fertilizer concentration prediction, the R^2 and RMSE are 0.9256 and 0.0203 respectively. The high R^2 and low RMSE indicate that this liquid fertilizer concentration measurement system exhibits great accuracy in MAP concentration measurement.

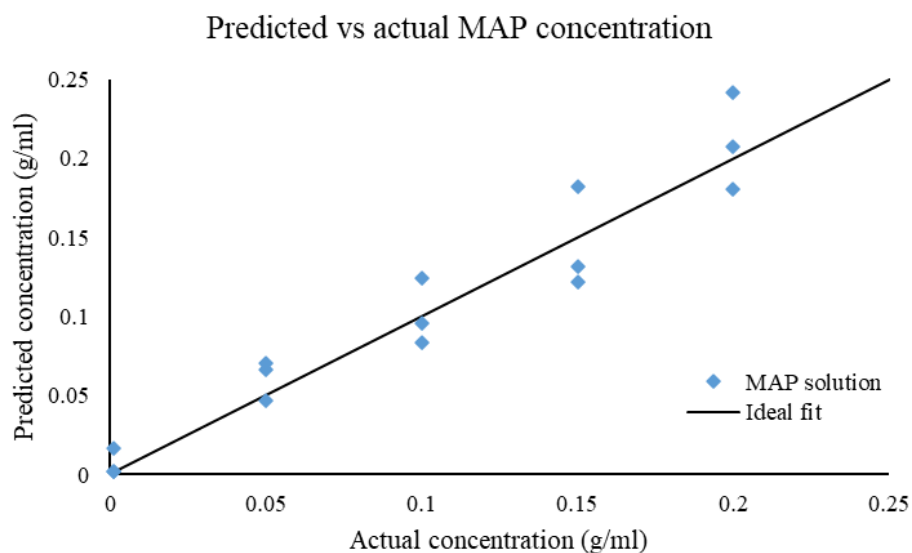


Figure 4.24: Comparison of the predicted and actual concentration of MAP fertilizer

Table 4.3 indicates the comparison among conductivity sensor, ion selective sensor, ultraviolet-visible spectroscopy, colorimeter and planar microwave sensor in liquid fertilizer concentration measurement. The measurement concentration range of the planar microwave sensor is higher than the other types of sensors. The R^2 value for all types of sensors is higher than 0.9 which indicates that the measured concentration is highly correlated with the actual concentration except for the measurement of phosphate by using ultraviolet-visible spectroscopy which is 0.82. The response time of the conductivity sensor, ultraviolet-visible spectroscopy and planar microwave sensor is faster than the ion selective sensor and colorimeter. The ultraviolet-visible spectroscopy, colorimeter and planar microwave sensor are non-invasive and non-intrusive as compared to conductivity sensor and ion selective sensor which are intrusive and invasive. Colorimeter requires chromogenic agent while the microwave sensor does not require the chromogenic agent and will not contaminate the liquid fertilizer during the measurement. The planar microwave sensor that is applied in this project is integrated with IoT technology while other types of sensors are not integrated with IoT technology. The cost of this sensor is relatively low compared to ultraviolet-visible spectroscopy, colorimeter and ion selective sensor.

Table 4.3: Comparison of various sensors for liquid fertilizer concentration measurement

| Sensor | Liquid under test | Concentration | R ² | Response time | Non-invasive | Non-intrusive | Additional chemical | Integrated with IoT | Cost |
|---|---|---|--|---------------|--------------|---------------|---------------------|---------------------|----------|
| Conductivity sensor (Rocher et al., 2019) | sodium chloride and magnesium nitrate | 0 - 0.045 g/mL | NaCl: 0.9113 Mg(NO ₃) ₂ : 0.9735 | Fast | No | No | No | No | Low |
| Ion selective sensor (Jung et al., 2019) | NO ₃ , K, Ca and PO ₄ solution | 3 - 1200 mg/L | 0.96 | Slow | No | No | No | No | Moderate |
| Ultraviolet-visible spectroscopy (Silva et al., 2021) | Hoagland solutions | N (103.17-554.85 mg/L) P (15.06-515.35 mg/L) K (113.78-516.45 mg/L) | N: 0.9942 P: 0.8240 K: 0.9748 | Fast | Yes | Yes | No | No | High |
| Colorimeter (Liu et al., 2016) | Ammonium nitrogen, phosphorus solution and potassium solution | N (0 - 27 mg/L) P (0 - 24 mg/L) K (0 - 27 mg/L) | NA | Slow | Yes | Yes | Yes | No | Moderate |
| Planar microwave sensor (this project) | Urea MAP | Urea (0 - 0.435 g/mL) MAP (0.01 - 0.2 g/ml) | Urea: 0.9656 MAP: 0.9289 | Fast | Yes | Yes | No | Yes | Low |

4.7 Problem Encountered and Improvement

To evaluate the repeatability of this liquid fertilizer concentration measurement system, the 0.435 g/ml urea solution was put on the microwave sensor. The power detector output voltage was recorded with an interval time of 1 s for a duration of 300 s long. Figure 4.25 depicts the repeatability test of the liquid fertilizer concentration measurement system without using the averaging method. The measured power detector output voltage was varying between 0.7283 V and 0.7322 V. The 0.0039 V voltage fluctuation was considered high and this fluctuation caused this system to become inaccurate. Thus, the averaging method is used to reduce the fluctuation.

By using a similar solution, the experiment was repeated by programming the MCU to calculate the average value for each measurement. A total of 20 voltage level was logged by the MCU. The average value of the 20 voltage levels was calculated by the MCU. The calculated average value was recorded with the interval time of 1 s for the duration of 300 s long. Figure 4.26 demonstrates, the repeatability test of the liquid fertilizer concentration measurement system by calculating the average value. The measured power detector output voltage was varying between 0.7274 V and 0.7283 V. By using the averaging method, the system fluctuation successfully declined to 0.0009 V voltage. As a result, the averaging method is used in this system.

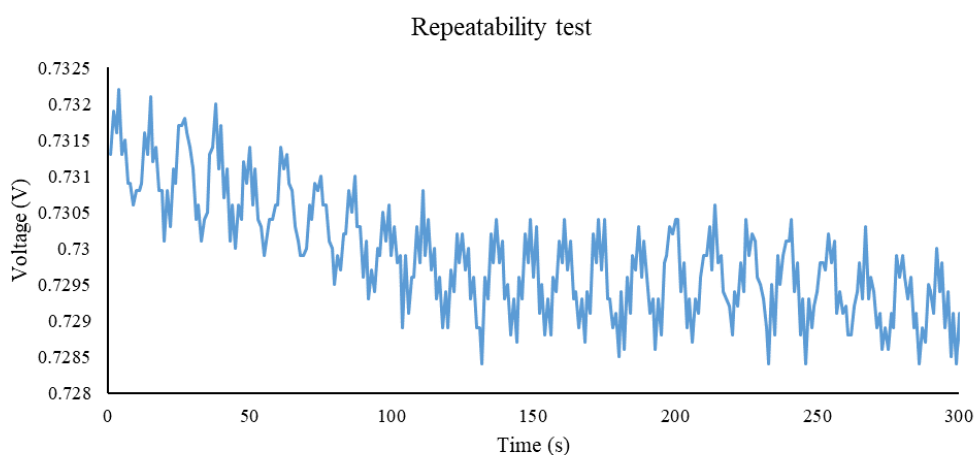


Figure 4.25: Repeatability test of the 0.435 g/ml urea solution without averaging

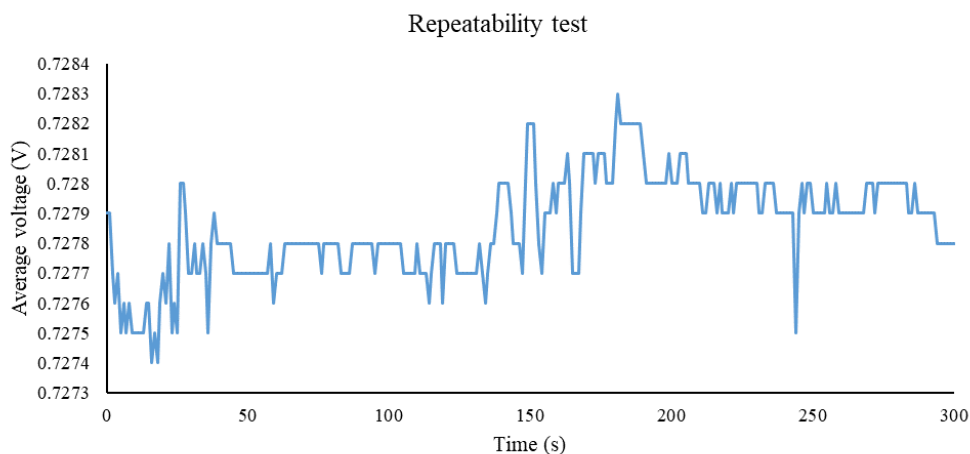


Figure 4.26: Repeatability test of the 0.435 g/ml urea solution with the averaging method

4.8 Summary

In this chapter, the circular ring resonance microwave sensor is designed to measure the liquid fertilizer concentration. The comparison of simulated and fabricated microwave sensor exemplifies that the simulated and measured S parameters have good agreement with each other. After that, the linear relationship between S_{21} and urea as well as MAP fertilizer have been found at 2.37 GHz and 2.54 GHz correspondingly. Next, a portable liquid fertilizer concentration measurement system which is connected to the microwave sensor for measuring the urea and MAP fertilizer concentration has been developed. The calibration equations for urea and MAP fertilizer have been identified by measuring the power detector output voltage. The validation tests have shown this microwave sensor can predict the fertilizer concentration accurately. The comparison of the liquid fertilizer measurement system with previous studies reveals that this system has the benefits of being small in size, low cost, user-friendly, non-destructive, non-intrusive, portable and integrated with IoT technology. Last but not least, the liquid fertilizer concentration measurement data can be viewed from the Firebase Realtime Database, website and mobile phone.

CHAPTER 5

CONCLUSIONS AND RECOMMENDATIONS

5.1 Conclusions

A planar microwave sensor based on a circular ring with the microstrip line design is developed to measure the liquid fertilizer concentration. The microwave sensor is simulated by the CST microwave studio and the fabricated sensor is measured by the VNA. By comparing the simulated and measured S parameters of the microwave sensor, the S parameters are having a close agreement between the simulation and measurement results. The electric field simulation shows the electric field is concentrated on the circular ring which is the appropriate location to measure the liquid fertilizer.

Urea and MAP fertilizers were used to evaluate the sensor performance. At the sensor's operating frequency of 2.37 GHz, a linear positive correlation between the concentration of urea fertilizer and S_{21} with a sensitivity of 3.20 dB/(g/mL) is obtained. For the MAP fertilizer, a linear positive correlation between concentration and S_{21} is obtained at 2.54 GHz with a sensitivity of 1.13 dB/(g/mL). The R^2 is higher than 0.9 and RMSE is lesser than 0.1 when evaluating the sensor performance for both the liquid fertilizer.

In addition, a portable liquid fertilizer concentration measurement system with integrated IoT technology is developed. The calibration equations for urea and MAP fertilizer have been identified by measuring the power detector output voltage. The operating tuning voltage for urea fertilizer is 3.92 V and for the MAP fertilizer is 5.11 V which are corresponding to the frequency of 2.37 GHz and 2.54 GHz. The validation results have shown that the urea and MAP concentration can be measured by this system with an R^2 of 0.9689 and 0.9256 as well as RMSE of 0.0433 and 0.0203 respectively.

By integrating the IoT technology, this liquid fertilizer concentration measurement system is able to send the data to the Firebase Realtime Database. The mobile application is installed on Android phones and the web application is hosted by using firebase hosting. The user can monitor the fertilizer concentration via the mobile application or web application.

5.2 Recommendations for future work

There are numerous recommendations for further investigations to improve this liquid fertilizer concentration measurement system. For future work, liquid fertilizers can be extended from urea and MAP to other types by recalibrating the proposed sensors and prototypes.

The second recommendation is the planar microwave sensor with different designs can be developed to increase the sensitivity of the sensor. In addition, different substrates of the sensor designs could be studied and explored to improve the sensitivity and accuracy of the sensor while diminishing the cost of the microwave sensor.

Other than that, the liquid fertilizer concentration measurement system can be modified and combined with the irrigation system for monitoring, analysing and determining the optimum concentration of the liquid fertilizer that should be applied to the crops during the irrigation process.

Lastly, the artificial intelligent enabled IoT system can be developed to process the historical data for optimum fertilizer concentration prediction and when the optimum concentration value is exceeded, an email or SMS will be sent to notify the user.

REFERENCES

Abd Rahman, N., Zakaria, Z., Abd Rahim, R., Dasril, Y. and Mohd Bahar, A.A., 2017. Planar Microwave Sensors for Accurate Measurement of Material Characterization: A Review. *TELKOMNIKA (Telecommunication Computing Electronics and Control)*, 15(3), p.1108. <https://doi.org/10.12928/telkomnika.v15i3.6684>.

Al-Sarawi, S., Anbar, M., Alieyan, K. and Alzubaidi, M., 2017. Internet of Things (IoT) communication protocols: Review. In: *2017 8th International Conference on Information Technology (ICIT)*. [online] Amman, Jordan: IEEE.pp.685–690. <https://doi.org/10.1109/ICITECH.2017.8079928>.

Araby, A.A., Abd Elhameed, M.M., Magdy, N.M., Said, L.A., Abdelaal, N., Abd Allah, Y.T., Darweesh, M.S., Fahim, M.A. and Mostafa, H., 2019. Smart IoT Monitoring System for Agriculture with Predictive Analysis. In: *2019 8th International Conference on Modern Circuits and Systems Technologies (MOCASST)*. Thessaloniki, Greece: IEEE.pp.1–4. <https://doi.org/10.1109/MOCASST.2019.8741794>.

Bailly, G., Harrabi, A., Rossignol, J., Michel, M., Stuerger, D. and Pribetich, P., 2017. Microstrip Spiral Resonator For Microwave-Based Gas Sensing. *IEEE Sensors Letters*, [online] 1(4), pp.1–4. <https://doi.org/10.1109/LSENS.2017.2716413>.

Benkhaoua, L., Benhabiles, M.T., Mouissat, S. and Riabi, M.L., 2016. Miniaturized Quasi-Lumped Resonator for Dielectric Characterization of Liquid Mixtures. *IEEE Sensors Journal*, 16(6), pp.1603–1610. <https://doi.org/10.1109/JSEN.2015.2504601>.

Bogner, A., Steiner, C., Walter, S., Kita, J., Hagen, G. and Moos, R., 2017. Planar Microstrip Ring Resonators for Microwave-Based Gas Sensing: Design Aspects and Initial Transducers for Humidity and Ammonia Sensing. *Sensors*,

17(10), p.2422. <https://doi.org/10.3390/s17102422>.

Bongiovanni, R. and Lowenberg-Deboer, J., 2004. Precision Agriculture and Sustainability. *Precision Agriculture*, 5(4), pp.359–387. <https://doi.org/10.1023/B:PRAG.0000040806.39604.aa>.

Boobalan, J., Jacintha, V., Nagarajan, J., Thangayogesh, K. and Tamilarasu, S., 2018. An IOT Based Agriculture Monitoring System. In: *2018 International Conference on Communication and Signal Processing (ICCSP)*. Chennai, India: IEEE. pp.594–598. <https://doi.org/10.1109/ICCSP.2018.8524490>.

Chiang, M. and Zhang, T., 2016. Fog and IoT: An Overview of Research Opportunities. *IEEE Internet of Things Journal*, 3(6), pp.854–864. <https://doi.org/10.1109/JIOT.2016.2584538>.

FAO, IFADU, UNICEF, WFP and WHO, 2021. *The State of Food Security and Nutrition in the World 2021. Transforming food systems for food security, improved nutrition and affordable healthy diets for all*. [online] Rome. <https://doi.org/10.4060/cb4474en>.

Frau, I., Wylie, S., Byrne, P., Cullen, J., Korostynska, O. and Mason, A., 2019. Detection of Zn in water using novel functionalised planar microwave sensors. *Materials Science and Engineering B: Solid-State Materials for Advanced Technology*, 247, p.114382. <https://doi.org/10.1016/j.mseb.2019.114382>.

Fu, B., 2016. The research of IOT of agriculture based on three layers architecture. In: *2016 2nd International Conference on Cloud Computing and Internet of Things (CCIOT)*. Dalian, China: IEEE. pp.162–165. <https://doi.org/10.1109/CCIOT.2016.7868325>.

Gutierrez, S., Martinez, I., Varona, J., Cardona, M. and Espinosa, R., 2019. Smart Mobile LoRa Agriculture System based on Internet of Things. In: *2019 IEEE 39th Central America and Panama Convention (CONCAPAN XXXIX)*.

Guatemala City, Guatemala. pp.1–6.
<https://doi.org/10.1109/CONCAPANXXXIX47272.2019.8977109>.

GutierrezMiceli, F., GarciaGomez, R., RinconRosales, R., AbudArchila, M., MariaAngela, O., Cruz, M. and Dendooven, L., 2008. Formulation of a liquid fertilizer for sorghum (*Sorghum bicolor* (L.) Moench) using vermicompost leachate. *Bioresource Technology*, 99(14), pp.6174–6180.
<https://doi.org/10.1016/j.biortech.2007.12.043>.

Harnsoongnoen, S., 2021. Metamaterial-Inspired Microwave Sensor for Detecting the Concentration of Mixed Phosphate and Nitrate in Water. *IEEE Transactions on Instrumentation and Measurement*, 70, pp.1–6.
<https://doi.org/10.1109/TIM.2021.3086901>.

Harnsoongnoen, S. and Wanthong, A., 2021. A non-contact planar microwave sensor for detection of high-salinity water containing NaCl, KCl, CaCl₂, MgCl₂ and Na₂CO₃. *Sensors and Actuators, B: Chemical*, 331, p.129355.
<https://doi.org/10.1016/j.snb.2020.129355>.

Harnsoongnoen, S., Wanthong, A., Charoen-In, U. and Siritaratiwat, A., 2019. Microwave Sensor for Nitrate and Phosphate Concentration Sensing. *IEEE Sensors Journal*, 19(8), pp.2950–2955.
<https://doi.org/10.1109/JSEN.2018.2890462>.

Hussain, C.M. and Keçili, R., 2020. Spectroscopic techniques for environmental analysis. In: C.M. Hussain and R. Keçili, eds. *Modern Environmental Analysis Techniques for Pollutants*. Elsevier. pp.133–161. <https://doi.org/10.1016/B978-0-12-816934-6.00006-0>.

International Fertilizer Association, 2019. *Fertilizer Consumption - Historical Trends by Country or Region*. [online] Available at: <https://www.ifastat.org/databases/graph/1_1> [Accessed 25 January 2022].

International Fertilizer Association, 2021. *Public Summary Medium-Term Fertilizer Outlook 2021 – 2025*. [online] *International Fertilizer Association*, Available at: <<https://api.ifastat.org/reports/download/13362>> [Accessed 25 January 2022].

Jilani, M.S., Bakar, A., Waseem, K. and Kiran, M., 2009. Effect of different levels of NPK on the growth and yield of cucumber (*Cucumis sativus*) under the plastic tunnel. *Journal of Agriculture & Social Sciences*, 5(3), pp.99–101.

Joshitha, C., Kanakaraja, P., Kumar, K.S., Akanksha, P. and Satish, G., 2021. An eye on hydroponics: The iot initiative. In: *2021 7th International Conference on Electrical Energy Systems, ICEES*. Chennai, India: IEEE.pp.553–557. <https://doi.org/10.1109/ICEES51510.2021.9383694>.

Jung, D.-H., Kim, H.-J., Cho, W.-J., Park, S.H. and Yang, S.-H., 2019. Validation testing of an ion-specific sensing and control system for precision hydroponic macronutrient management. *Computers and Electronics in Agriculture*, 156, pp.660–668. <https://doi.org/10.1016/j.compag.2018.12.025>.

Keshavarz, R., Lipman, J., Schreurs, D.M.M.-P. and Shariati, N., 2021. Highly Sensitive Differential Microwave Sensor for Soil Moisture Measurement. *IEEE Sensors Journal*, 21(24), pp.27458–27464. <https://doi.org/10.1109/JSEN.2021.3125718>.

Lara, J.C.D., Gutierrez, S. and Rodriguez, F., 2019. Low Cost Greenhouse Monitoring System Based on Internet of Things. In: *2019 IEEE International Conference on Engineering Veracruz (ICEV)*. Boca del Rio, Mexico: IEEE.pp.1–6. <https://doi.org/10.1109/ICEV.2019.8920502>.

Liu, R.-T., Tao, L.-Q., Liu, B., Tian, X.-G., Mohammad, M., Yang, Y. and Ren, T.-L., 2016. A Miniaturized On-Chip Colorimeter for Detecting NPK Elements. *Sensors*, 16(8), p.1234. <https://doi.org/10.3390/s16081234>.

Madanayaka, N. and Thilakarathne, B.L.S., 2021. Implementation IoT (Internet of Things) Based Smart Agriculture Fertilizer System. In: *2nd National Symposium on Agro-Technology and Rural Sciences (NSATRS) 2021*. Hambantota, Sri Lanka: University of Colombo.

Mahmoud, M.S. and Mohamad, A.A.H., 2016. A Study of Efficient Power Consumption Wireless Communication Techniques/ Modules for Internet of Things (IoT) Applications. *Advances in Internet of Things*, 6(2), pp.19–29. <https://doi.org/10.4236/ait.2016.62002>.

Menon, A.G. and Prabhakar, M., 2021. Smart Agriculture Monitoring Rover for Small-Scale Farms in Rural Areas using IoT. In: *2021 International Conference on Innovative Computing, Intelligent Communication and Smart Electrical Systems (ICSES)*. Chennai, India: IEEE.pp.1–10. <https://doi.org/10.1109/icses52305.2021.9633976>.

Mohammadi, S., Nadaraja, A.V., Roberts, D.J. and Zarifi, M.H., 2020. Real-time and hazard-free water quality monitoring based on microwave planar resonator sensor. *Sensors and Actuators, A: Physical*, 303, p.111663. <https://doi.org/10.1016/j.sna.2019.111663>.

Moldoveanu, S.C. and David, V., 2016. *Selection of the HPLC method in chemical analysis*. Elsevier Inc.

Monteiro-Silva, F., Jorge, P.A.S. and Martins, R.C., 2019. Optical sensing of nitrogen, phosphorus and potassium: A spectrophotometrical approach toward smart nutrient deployment. *Chemosensors*, 7(4), p.51. <https://doi.org/10.3390/chemosensors7040051>.

Narang, R., Mohammadi, S., Ashani, M.M., Sadabadi, H., Hejazi, H., Zarifi, M.H. and Sanati-Nezhad, A., 2018. Sensitive, Real-time and Non-Intrusive Detection of Concentration and Growth of Pathogenic Bacteria using Microfluidic-Microwave Ring Resonator Biosensor. *Scientific Reports*, 8(1),

p.15807. <https://doi.org/10.1038/s41598-018-34001-w>.

Omer, A.E., Shaker, G. and Safavi-Naeini, S., 2020. Portable Radar-Driven Microwave Sensor for Intermittent Glucose Levels Monitoring. *IEEE Sensors Letters*, 4(5), pp.1–4. <https://doi.org/10.1109/LSENS.2020.2986208>.

Potdar, R.P., Shirolkar, M.M., Verma, A.J., More, P.S. and Kulkarni, A., 2021. Determination of soil nutrients (NPK) using optical methods: a mini review. *Journal of Plant Nutrition*, 44(12), pp.1826–1839. <https://doi.org/10.1080/01904167.2021.1884702>.

Poursafar, N., Alahi, M.E.E. and Mukhopadhyay, S., 2017. Long-range wireless technologies for IoT applications: A review. In: *2017 Eleventh International Conference on Sensing Technology (ICST)*. Sydney, NSW, Australia: IEEE. pp.1–6. <https://doi.org/10.1109/ICSensT.2017.8304507>.

Prathibha, S.R., Hongal, A. and Jyothi, M.P., 2017. IOT Based Monitoring System in Smart Agriculture. In: *2017 International Conference on Recent Advances in Electronics and Communication Technology (ICRAECT)*. Chennai, India: IEEE. pp.81–84. <https://doi.org/10.1109/ICRAECT.2017.52>.

Random Nerd Tutorials, 2022. *Getting Started with the ESP32 Development Board*. [online] Available at: <<https://randomnerdtutorials.com/getting-started-with-esp32/>> [Accessed 21 March 2022].

Richa, A., Fizir, M. and Touil, S., 2021. Advanced monitoring of hydroponic solutions using ion-selective electrodes and the internet of things: a review. *Environmental Chemistry Letters*, 19(4), pp.3445–3463. <https://doi.org/10.1007/s10311-021-01233-8>.

Rocher, J., Basterrechea, D.A., Parra, L. and Lloret, J., 2019. A new conductivity sensor for monitoring the fertigation in smart irrigation systems. In: P. Novais, J. Lloret, P. Chamoso, D. Carneiro, E. Navarro and S. Omatu, eds.

Ambient Intelligence – Software and Applications – 10th International Symposium on Ambient Intelligence. ISAmI 2019. Advances in Intelligent Systems and Computing. Springer, Cham. pp.136–144.
https://doi.org/10.1007/978-3-030-24097-4_17.

Russel, D.A. and Williams, G.G., 1977. History of Chemical Fertilizer Development. *Soil Science Society of America Journal*, 41(2), pp.260–265.
<https://doi.org/10.2136/SSSAJ1977.03615995004100020020X>.

Saad, C., Mostafa, B., Ahmadi, E. and Abderrahmane, H., 2014. Comparative Performance Analysis of Wireless Communication Protocols for Intelligent Sensors and Their Applications. *International Journal of Advanced Computer Science and Applications*, 5(4), pp.76–85.
<https://doi.org/10.14569/ijacsa.2014.050413>.

Saini, M.K. and Saini, R.K., 2020. Agriculture monitoring and prediction using Internet of Things (IoT). In: *2020 Sixth International Conference on Parallel, Distributed and Grid Computing (PDGC)*. Wagnaghat, India: IEEE. pp.53–56.
<https://doi.org/10.1109/PDGC50313.2020.9315836>.

Sharma, K. and Dhir, N., 2014. A Study of Wireless Networks : WLANs , WPANs , WMANs , and WWANs with Comparison. *International Journal of Computer Science and Information Technology (IJCSIT)*, 5(6), pp.7810–7813.

Silva, A.F., Löfkvist, K., Gilbertsson, M., van Os, E.A., Franken, G.C., Balendonck, J., Pinho, T.M., Boaventura-Cunha, J., Coelho, L., Jorge, P. and Martins, R., 2021. Hydroponics Monitoring Through UV-Vis Spectroscopy and Artificial Intelligence : Quantification of Nitrogen, Phosphorous and Potassium. *Chemistry Proceedings*, 3, pp.181–186.

Sinha, R.S., Wei, Y. and Hwang, S.H., 2017. A survey on LPWA technology: LoRa and NB-IoT. *ICT Express*, 3(1), pp.14–21.
<https://doi.org/10.1016/j.icte.2017.03.004>.

Su, L., Mata-Contreras, J., Vélez, P. and Martín, F., 2017. A Review of Sensing Strategies for Microwave Sensors Based on Metamaterial-Inspired Resonators: Dielectric Characterization, Displacement, and Angular Velocity Measurements for Health Diagnosis, Telecommunication, and Space Applications. *International Journal of Antennas and Propagation*, 2017, pp.1–13. <https://doi.org/10.1155/2017/5619728>.

Uchida, R., 2014. Essential Nutrients for Plant Growth: Nutrient Functions and Deficiency Symptoms. In: J.A. Silva and R. Uchida, eds. *Plant Nutrient Management in Hawaii's Soils, Approaches for Tropical and Subtropical Agriculture*. Manoa: University of Hawaii. pp.31–55.

University of Nebraska–Lincoln, 2015. *Fertilizer History Pt. 1*. [online] INSTITUTE OF AGRICULTURE AND NATURAL RESOURCES. Available at: <https://cropwatch.unl.edu/fertilizer-history-p1> [Accessed 25 January 2022].

Velez, P., Grenier, K., Mata-Contreras, J., Dubuc, D. and Martin, F., 2018. Highly-sensitive microwave sensors based on Open Complementary Split Ring Resonators (OCSRRs) for dielectric characterization and solute concentration measurement in liquids. *IEEE Access*, 6, pp.48324–48338. <https://doi.org/10.1109/ACCESS.2018.2867077>.

Velez, P., Munoz-Enano, J., Grenier, K., Mata-Contreras, J., Dubuc, D. and Martin, F., 2019. Split Ring Resonator-Based Microwave Fluidic Sensors for Electrolyte Concentration Measurements. *IEEE Sensors Journal*, 19(7), pp.2562–2569. <https://doi.org/10.1109/JSEN.2018.2890089>.

Virupaxappa, G. and Thangam, S., 2021. Smart agriculture and role of IOT. In: *2021 Third International Conference on Inventive Research in Computing Applications (ICIRCA)*. Coimbatore, India: IEEE. pp.1–6. <https://doi.org/10.1109/ICIRCA51532.2021.9545042>.

Wibowo, R.R.D.I., Ramdhani, M., Priramadhi, R.A. and Aprillia, B.S., 2019. IoT based automatic monitoring system for water nutrition on aquaponics system. In: *Journal of Physics: Conference Series*. Purwokerto, Indonesia: IOP Publishing.p.012071. <https://doi.org/10.1088/1742-6596/1367/1/012071>.

Yan, Q., Duan, Z., Mao, J., Li, X. and Dong, F., 2012. Effects of root-zone temperature and N, P, and K supplies on nutrient uptake of cucumber (*Cucumis sativus* L.) seedlings in hydroponics. *Soil Science and Plant Nutrition*, [online] 58(6), pp.707–717. <https://doi.org/10.1080/00380768.2012.733925>.

Yee, S.K., Ong, N.T.J., Lim, S.C.J., Mohd Zin, N.S., Dahlan, S.H., Ashyap, A.Y.I. and Soon, C.F., 2021. Microwave sensing of ammonia and iron concentration in water based on complementary double split-ring resonator. *Sensors and Actuators Reports*, 3, p.100044. <https://doi.org/10.1016/j.snr.2021.100044>.

Zarifi, M.H., Farsinezhad, S., Shankar, K. and Daneshmand, M., 2015. Liquid Sensing Using Active Feedback Assisted Co-Planar Microwave Resonator. *IEEE Microwave and Wireless Components Letters*, 25(9), pp.621–623. <https://doi.org/10.1109/LMWC.2015.2451354>.

APPENDICES

Appendix A: MCU program code

```
//mian
#include "oled_display.h"
#include "ads1115.h"
#include "firebase.h"

void convert_to_conc();

#define buttonPin 39

float VCO_vtune = 0;
float PD_vout = 0;
char* fertiliser_type ;
float conc;

void setup() {
  Serial.begin(115200);

  init_oled();
  init_ads1115();
  init_firebase();

  pinMode(buttonPin, INPUT);//tactile button switch

}

void loop() {
  VCO_vtune = read_adc_vco();
  title_display(VCO_vtune);

  // check if the pushbutton is pressed. If it is, the buttonState is HIGH:
```

```

if (digitalRead(buttonPin) == HIGH) {
  delay(30);
  if (digitalRead(buttonPin) == HIGH) {
    while(digitalRead(buttonPin) == HIGH); //wait the tactile button release
    VCO_vtune = read_adc_vco();
    Serial.print("VCO_vtune: "); Serial.println(VCO_vtune);
    PD_vout = read_adc_pd();
    convert_to_conc();
    result_display(fertiliser_type, conc);
    if (fertiliser_type != "invalid"){
      firebase_send_data(fertiliser_type, conc);
    }
    delay(2000);
  }
}
delay(100);
}

```

```

void convert_to_conc(){ //convert pd voltage to concentration
  if (VCO_vtune > 3.919 && VCO_vtune < 3.924) {
    fertiliser_type = "Urea";
    conc = -10.212*PD_vout + 7.6903;
  }else if (VCO_vtune > 5.110 && VCO_vtune < 5.115) {
    fertiliser_type = "MAP";
    conc = 2220.1*PD_vout*PD_vout - 3165.4*PD_vout + 1128.3;
  }else{
    fertiliser_type = "invalid";
    conc = 0;
  }
}
}

```

```

//ads1115.h
#ifndef ADS1115_H
#define ADS1115_H

```



```

void init_ads1115();
float read_adc_vco();
float read_adc_pd();

#endif

#include <Adafruit_ADS1X15.h>

Adafruit_ADS1115 ads;

void init_ads1115 () {

    //ads.setGain(GAIN_ONE);      //ADS1115 1x gain +/- 4.096V 1 bit =
0.125mV
    ads.setGain(GAIN_TWO);      // 2x gain +/- 2.048V 1 bit = 0.0625mV
    //ads.setDataRate(RATE_ADS1115_860SPS); //8, 16, 32, 64, 128, 250, 475,
860 default128

    if (!ads.begin()) {
        Serial.println("Failed to initialize ADS.");
        while (1);
    }
}

float read_adc_vco() {

    int16_t adc0;
    float volts0;

    adc0 = ads.readADC_Differential_0_1();

    volts0 = adc0 * 0.0000625 * 4.9 ; //volts0=ads.computeVolts(adc0);

    return (volts0);
}

float read_adc_pd() {

    int16_t adc1;
    float volts1;

    adc1 = ads.readADC_Differential_2_3();

    volts1 = adc1 * 0.0000625;

    // Specify the number of loops for one measurement.
    const int loops = 20; //40

```

```

// Specify the delay between the loops.
const int loopDelay = 10; //200

// Initialize the used variables.
double totalInputValue = 0;
double averageInputValue = 0;

// Loop to get the average of different analog values.
for (int counter = 1; counter <= loops; counter++) {

    // Read the analog value.
    adc1 = ads.readADC_Differential_2_3();

    // Add the analog value to the total.
    totalInputValue += adc1;

    // Wait some time after each loop.
    delay(loopDelay);
}

// Calculate the average input value.
averageInputValue = totalInputValue / loops;

volts1 = averageInputValue * 0.0000625;

return (volts1);
}

//firebase.h
#ifndef OLED_DISPLAY_H
#define OLED_DISPLAY_H

void init_firebase();
void firebase_send_data(char* fertiliser_type, float conc);

#endif

#include <Arduino.h>
#include <WiFi.h>
#include <Firebase_ESP_Client.h>
#include "time.h" // to get timestamp

//Provide the token generation process info.
#include "addons/TokenHelper.h"
//Provide the RTDB payload printing info and other helper functions.
#include "addons/RTDBHelper.h"

// Insert your network credentials
#define WIFI_SSID "WiFi -2.4G"

```

```

#define WIFI_PASSWORD " WiFi123456"

// Insert Firebase project API Key
#define API_KEY "AIzaSyB25S0k1TzxDeSVqTX3A2qZqj0er-aTFmZ"

// Insert RTDB URLdefine the RTDB URL */
#define DATABASE_URL "https://esp32-b-default-rtdb.asia-southeast1.firebaseio.app/"

/* Define the user Email and password that already registerd or added in your project */
#define USER_EMAIL "user@outlook.com"
#define USER_PASSWORD "qweasdzxc"

//Define Firebase Data object
FirebaseData fbdo;

FirebaseAuth auth;
FirebaseConfig config;

int timestamp;
const char* ntpServer = "pool.ntp.org";

// Parent Node (to be updated in every loop)
String parentPath;

unsigned long getTime();

void init_firebase(){
  //connect to wifi
  WiFi.begin(WIFI_SSID, WIFI_PASSWORD);
  while (WiFi.status() != WL_CONNECTED){
    delay(500);
  }

  // Init and get the time
  configTime(25200, 0 , ntpServer);

  /* Assign the api key (required) */
  config.api_key = API_KEY;

  /* Assign the RTDB URL (required) */
  config.database_url = DATABASE_URL;

  /* Assign the user sign in credentials */
  auth.user.email = USER_EMAIL;
  auth.user.password = USER_PASSWORD;
  /* Assign the callback function for the long running token generation task */
  config.token_status_callback = tokenStatusCallback; //see
  addons/TokenHelper.h

```

```

    Firebase.begin(&config, &auth);
    Firebase.reconnectWiFi(true);
}

void firebase_send_data(char* fertiliser_type, float conc){
    //Get current timestamp
    timestamp = getTime();
    parentPath = "test1/" + String(fertiliser_type) + "/" + String(timestamp);

    Firebase.RTDB.setInt(&fbdo, (parentPath + "/timestamp") , timestamp);

    // Write an Float number on the database path test/conc
    Firebase.RTDB.setFloat(&fbdo, (parentPath + "/conc"), conc);

    //}
}

// Function that gets current epoch time
unsigned long getTime() {
    time_t now;
    struct tm timeinfo;
    if (!getLocalTime(&timeinfo)) {
        return(0);
    }
    time(&now);
    return now;
}

//oled_display.h
#ifndef OLED_DISPLAY_H
#define OLED_DISPLAY_H

void init_oled();
void title_display(float VCO_vtune);
void result_display(float PD_vout);

#endif

#include <Wire.h>
#include <Adafruit_GFX.h>
#include <Adafruit_SSD1306.h>
#include <Fonts/FreeSans9pt7b.h>

#define SDA_2 18
#define SCL_2 19

#define SCREEN_WIDTH 128 // OLED display width, in pixels
#define SCREEN_HEIGHT 64 // OLED display height, in pixels

```

```

// Declaration for an SSD1306 display connected to I2C (SDA, SCL pins)
Adafruit_SSD1306 display(SCREEN_WIDTH, SCREEN_HEIGHT, &Wire1,
-1);

void init_oled(){
  Wire1.begin(SDA_2, SCL_2);
  if (!display.begin(SSD1306_SWITCHCAPVCC, 0x3C)) {
    Serial.println("SSD1306 allocation failed");
    for(;;);
  }
  display.clearDisplay();
}

void title_display(float VCO_vtune) {
  display.setFont(&FreeSans9pt7b);
  display.clearDisplay();
  display.setTextSize(1);
  display.setTextColor(WHITE);
  display.setCursor(0, 15);
  display.print("Vtune : ");
  display.println(VCO_vtune, 3);
  display.drawLine(0, 22, 127, 22, WHITE);
  display.display();
  delay(100);
}

void result_display(char* fertiliser_type, float conc) {
  display.clearDisplay();
  display.setCursor(0, 15);
  display.println(fertiliser_type);
  display.drawLine(0, 22, 127, 22, WHITE);

  display.setCursor(5,40);
  display.println("conc (g/ml) : ");
  display.setCursor(5,60);
  display.println(conc,3);
  display.display();
  //delay(2000);
}

```

Appendix B: Mobile app program code

```

//App.js
import { StatusBar } from 'expo-status-bar';
import { StyleSheet, Text, View, TouchableOpacity, ScrollView } from 'react-native';
import { initializeApp } from 'firebase/app';
import { getDatabase, ref, onValue, set } from 'firebase/database';
import React, { useState, useEffect } from 'react';
import CircularProgress from 'react-native-circular-progress-indicator';
import moment from "moment";
import { InteractiveChart } from "./app/InteractiveChart";
import { NavigationContainer } from '@react-navigation/native';
import { createBottomTabNavigator } from '@react-navigation/bottom-tabs';
import { MaterialCommunityIcons } from '@expo/vector-icons';
import { Entypo } from '@expo/vector-icons';
import { FontAwesome5 } from '@expo/vector-icons';

export default function App() {
  // Initialize Firebase
  const firebaseConfig = {
    apiKey: " AIzaSyB25S0k1TzxDeSVqTX3A2qZqj0er-aTFmZ ",
    authDomain: "esp32-b.firebaseio.com",
    databaseURL: "https://esp32-b-default-rtdb.asia-southeast1.firebaseio.com",
    projectId: "esp32-b",
    storageBucket: "esp32-b.appspot.com",
    messagingSenderId: "37278084142",
    appId: "1:372780841428:web:7410a1f5144488463abe4"
  };

  initializeApp(firebaseConfig);
  const db = getDatabase();

  const [conc, set_conc] = useState(0);
  const [fertilizer_type, set_fertilizer_type] = useState('Urea');
  const [max_conc, set_max_conc] = useState()
  const [his_data, set_his_data] = useState([ { timestamp: 0, conc: 0 },]);

  //Read data
  useEffect(() => {
    readData(fertilizer_type)
  }, []);
  useEffect(() => {
    if (fertilizer_type === 'Urea')
      set_max_conc(0.435);
    if (fertilizer_type === 'MAP')
      set_max_conc(0.200);
  }, [fertilizer_type]);

```

```

function readData(userId) {
  const reference = ref(db, 'test1/' + userId);
  onValue(reference, (snapshot) => {
    const data = snapshot.val();
    convert_his_data(data);
  });
}

function convert_his_data(data) {
  var all_data = [];
  for (var obj_name in data) {
    all_data = [...all_data, { "timestamp": data[obj_name].timestamp, "conc":
data[obj_name].float }];
  }
  set_his_data(all_data);
}

const PrintHis = () => {
  let reverse_his_data = his_data.reverse();
  let time = [];
  for (var obj_name in reverse_his_data) {
    time = [...time, moment(new Date(his_data[obj_name].timestamp *
1000)).format('DD/MM/YYYY HH:mm:ss')];
  }
  return reverse_his_data.map((obj_data, index) => (
    <View key={index}>
      <Text style={{{ fontSize: 18 }}}>{index + 1}~ {time[index]} :
{obj_data.conc} g/ml</Text>
    </View>
  ))
}

function Home() {
  return (
    <View style={styles.container}>

      <View style={{{ flex: 3, alignItems: 'center', justifyContent: 'center' }}}>
        <ButtonLayout
          label="Type of fertilizer"
          values={["Urea", "MAP"]}//, "K2SO4", "MAP"]
          selectedValue={fertilizer_type}
          setSelectedValue={set_fertilizer_type}
          readData={readData}
        >
          <View
            style={styles.box}
          >
            <Text style={styles.labelResult}> {fertilizer_type} :
{his_data[Object.keys(his_data).length - 1].conc} g/ml </Text>

```

```

    </View>
  </ButtonLayout>

  <CircularProgress
    value={his_data[Object.keys(his_data).length - 1].conc}
    maxValue={max_conc}
    radius={120}
    duration={1000}
    progressValueColor={'#258039'}
    progressValueFontSize={40}
    title={fertilizer_type}
    titleColor={'#0081B7'}
    titleFontSize={20}
    valueSuffix={' g/ml'}
    activeStrokeColor={'#8ce68c'}
    activeStrokeSecondaryColor={'#87cdf6'}
    inactiveStrokeOpacity={0.5}
    inactiveStrokeWidth={10}
    activeStrokeWidth={20}
    progressFormatter={(value) => {
      'worklet';
      return value.toFixed(3); // 2 decimal places
    }}
  />
</View>

  <StatusBar style="auto" />
</View>
);
}
function Graph() {
  return (
    <View style={styles.container}>

      <Text style={[styles.labelResult, { fontSize: 28 }]}>
        {fertilizer_type}
      </Text>
      <InteractiveChart data={his_data} />

      <StatusBar style="auto" />
    </View>
  );
}
function History() {
  return (
    <View style={styles.container}>
      <ScrollView>
        <View style={[styles.history]}>
          <Text style={[styles.labelResult, { fontSize: 18 }]}>
            History : {fertilizer_type}
          </Text>
        </View>
      </ScrollView>
    </View>
  );
}

```



```

        </Text>
        <PrintHis />
    </View>
</ScrollView>
<StatusBar style="auto" />
</View>
);
}
const Tab = createBottomTabNavigator();
return (
    <NavigationContainer>
        <Tab.Navigator
            initialRouteName="Home"
            screenOptions={{
                tabBarActiveTintColor: '#19A019',
                tabBarActiveBackgroundColor: '#A0AFA090',
                tabBarInactiveTintColor: '#3D4A3D',
                showLabel: true,
                tabBarStyle: {
                    position: "absolute",
                    bottom: 20,
                    left: 20,
                    right: 20,
                    elevation: 0,
                    backgroundColor: '#A0AFA080',
                    high: 80,
                    borderRadius: 20,
                },
                tabBarLabelStyle: {
                    fontSize: 12,
                },
                headerShown: false,
                tabBarItemStyle: {
                    borderRadius: 20,
                },
            }}
        >
            <Tab.Screen
                name="Home"
                component={Home}
                options={{
                    tabBarLabel: 'Home',
                    tabBarIcon: ({ color, size }) => (
                        <FontAwesome5 name="home" color={color} size={size} />
                    ),
                }}
            />
            <Tab.Screen
                name="Graph"
                component={Graph}

```

```

options={{
  tabBarLabel: 'Graph',
  tabBarIcon: ({ color, size }) => (
    <Entypo name="area-graph" color={color} size={size} />
  ),
}}
/>
<Tab.Screen
  name="History"
  component={History}
  options={{
    tabBarLabel: 'History',
    tabBarIcon: ({ color, size }) => (
      <MaterialCommunityIcons name="history" color={color} size={size}
/>
    ),
  }}
/>
</Tab.Navigator>
</NavigationContainer>
);
}

```

```

const ButtonLayout = ({
  label,
  children,
  values,
  selectedValue,
  setSelectedValue,
  readData,
}) => (
  <View style={{ padding: 10 }}>
    <Text style={styles.label}>{label}</Text>
    <View style={styles.row}>
      {values.map((value) => (
        <TouchableOpacity
          key={value}
          onPress={() => { setSelectedValue(value); readData(value) }}
          style={[
            styles.button,
            selectedValue === value && styles.selected,
          ]}
        >
          <Text
            style={[
              styles.buttonLabel,
              selectedValue === value && styles.selectedLabel,
            ]}
          >
            {value}

```

```

        </Text>
      </TouchableOpacity>
    )})
  </View>
  <View style={{styles.container1}}>
    {children}
  </View>
</View>
);

```

```

const styles = StyleSheet.create({
  container: {
    flex: 1,
    backgroundColor: '#fff',
    alignItems: 'center',
    justifyContent: 'center',
  },

  box: {
    backgroundColor: "powderblue",
    alignSelf: "center",
  },

  row: {
    flexDirection: "row",
    flexWrap: "wrap",
    justifyContent: 'space-between',
  },

  button: {
    paddingHorizontal: 8,
    paddingVertical: 6,
    borderRadius: 14,
    backgroundColor: "#A0AFA0",
    alignSelf: "center",
    marginHorizontal: "1%",
    marginBottom: 6,
    minWidth: "30%",
    textAlign: "center",
  },

  selected: {
    backgroundColor: '#3D4A3D',
    borderWidth: 0,
  },

  buttonLabel: {
    fontSize: 22,
    fontWeight: "700",
    color: "#3D4A3D",
    textAlign: "center",
  },

  selectedLabel: {
    color: "#6BA4FF",

```

```

    },
    label: {
      textAlign: "center",
      marginBottom: 10,
      fontSize: 34,
    },
    container1: {
      marginTop: 8,
    },
    },
    labelResult: {
      textAlign: "center",
      marginBottom: 5,
      marginTop: 5,
      fontSize: 22,
    },
    },
    history: {
      width: 'auto',
      height: '20%',
      backgroundColor: "powderblue",
      alignSelf: "center",
      justifyContent: 'center',
      alignItems: 'center',
      flexWrap: "nowrap",
      flex: 1,
      position: 'relative',
      bottom: 0,
    },
    },
  });

```

```

///app/InteractiveChart.js
// import React, { useEffect, useRef, useState, useMemo } from "react";
import {
  PanResponder,
  Dimensions,
  View,
} from "react-native";
import { AreaChart, XAxis, YAxis } from "react-native-svg-charts";
import Svg, {
  Circle,
  Defs,
  G,
  Line,
  LinearGradient,
  Path,
  Rect,
  Stop,
  Text as SvgText,
} from "react-native-svg";
import * as shape from "d3-shape";

```

```

import * as scale from "d3-scale";
import format from 'date-fns/format'

export const InteractiveChart = ({
  data
}) => {
  const apx = (size = 0) => {
    let width = Dimensions.get("window").width;
    return (width / 750) * size; //750
  };
  const [dateList, setDateList] = useState(data.map((obj_data) => { return
obj_data.timestamp }));
  const [priceList, setPriceList] = useState(data.map((obj_data) => { return
obj_data.conc }));
  const xMin = Math.min(...dateList), xMax = Math.max(...dateList);
  const yMin = 0, yMax = Math.max(...priceList);

  useEffect(() => {
    setDateList(data.map((obj_data) => { return obj_data.timestamp }));
    setPriceList(data.map((obj_data) => { return obj_data.conc }));
  }, [data]);

  const size = useRef(dateList.length);

  const [positionX, setPositionX] = useState(-1); // The currently selected X
coordinate position
  const [posX, setPosX] = useState(-1);

  const panResponder = useMemo(() =>
    PanResponder.create({

      onStartShouldSetPanResponder: (evt, gestureState) => true,
      onStartShouldSetPanResponderCapture: (evt, gestureState) => true,
      onMoveShouldSetPanResponder: (evt, gestureState) => true,
      onMoveShouldSetPanResponderCapture: (evt, gestureState) => true,
      onPanResponderTerminationRequest: (evt, gestureState) => true,

      onPanResponderGrant: (evt, gestureState) => {
        updatePosition(evt.nativeEvent.locationX);
        return true;
      },
      onPanResponderMove: (evt, gestureState) => {
        updatePosition(evt.nativeEvent.locationX);
        return true;
      },
      onPanResponderRelease: () => {
        setPositionX(-1);
      },
    }), [data, xMax, xMin]// dependency list
  );

```

```

const updatePosition = (x) => {
  const YAxisWidth = apx(40);
  const x0 = apx(0); // x0 position
  const chartWidth = apx(750) - YAxisWidth - x0;
  const xN = x0 + chartWidth; //xN position
  const xDistance = chartWidth / (xMax - xMin); // The width of each
coordinate point
  if (x <= x0) {
    x = x0;
  }
  if (x >= xN) {
    x = xN;
  }

  let value = (((x - x0) / xDistance) + xMin + 1).toFixed(0);
  setPosX(((x - x0) / xDistance));

  const closestIndex = (num, arr) => {
    let curr = arr[0], diff = Math.abs(num - curr);
    let index = 0;
    for (let val = 0; val < arr.length; val++) {
      let newdiff = Math.abs(num - arr[val]);
      if (newdiff < diff) {
        diff = newdiff;
        curr = arr[val];
        index = val;
      }
    };
    };
    return index;
  };
  value = closestIndex(value, data.map((obj_data) => { return
obj_data.timestamp }));

  setPositionX(Number(value));
};

const CustomGrid = ({ x, y, ticks }) => (
  <G>
  {
    // Horizontal grid
    ticks.map((tick) => (
      <Line
        key={tick}
        x1="0%"
        x2="100%"
        y1={y(tick)}
        y2={y(tick)}
        stroke="#EEF3F6"
      />

```

```

    ))
  }
  {
    // Vertical grid
    data.map((value, index) => (
      <Line
        key={index}
        y1="0%"
        y2="100%"
        x1={x(data[index].timestamp)}
        x2={x(data[index].timestamp)}
        stroke="#EEF3F6"
      />
    ))
  }
</G>
);

const CustomLine = ({ line }) => (
  <Path
    key="line"
    d={line}
    stroke="#5EDE58"
    strokeWidth={apx(5)}
    fill="none"
  />
);

const CustomGradient = () => (
  <Defs key="gradient">
    <LinearGradient id="gradient" x1="0%" y="0%" x2="100%"
y2="100%">
      {<Stop offset="0%" stopColor="#8ce68c" stopOpacity={0.3} />}
      {<Stop offset="100%" stopColor="#87cdf6" stopOpacity={0.5} />}
    </LinearGradient>
  </Defs>
);

const Tooltip = ({ x, y, ticks }) => {
  if (positionX < 0) {
    return null;
  }

  const date = (format((dateList[positionX] * 1000), 'DD MMM YY
HH:mm:ss'));

  return (
    <G x={x(data[positionX].timestamp)} key="tooltip">
      <G

```

```

        x={posX > (xMax - xMin) / 2 ? -apx(200 + 10) : apx(10)}
//positionX,size.current->PosX,(xMax - xMin)
        y={y(priceList[positionX]) - apx(30)}
    >
        <Rect
            y={-apx(15 + 15 + 10) / 2}
            rx={apx(22)} // borderRadius
            ry={apx(22)} // borderRadius
            width={apx(230)}
            height={apx(60)}
            stroke='#3D4A3D80'
            fill="#A0AFA080"
        />

        <SvgText x={apx(20)} y={apx(5)} fill='#2270C7' opacity={0.9}
fontSize={apx(24)}>
            {date}
        </SvgText>
        <SvgText
            x={apx(20)}
            y={apx(20 + 10)}
            fontSize={apx(24)}
            fontWeight="bold"
            fill='#6BA4FF'
        >
            {priceList[positionX]} g/ml
        </SvgText>
    </G>

    <G x={x}>
        <Line
            y1={apx(0)}
            y2={apx(570)}
            stroke="rgba(54, 148, 126, 0.7)"
            strokeWidth={apx(3)}
            strokeDasharray={[8, 4]}
        />

        <Circle
            cy={y(priceList[positionX])}
            r={apx(20 / 2)}
            stroke="#3D4A3D80"
            strokeWidth={apx(4)}
            fill="#A0AFA0"
        />
    </G>
</G>
);
};

```



```

const CustomDot = ({ x, y, data }) => {
  return data.map((value, index) => (
    <Circle
      key={index}
      cx={x(value.timestamp)}
      cy={y(value.conc)}
      r={3}
      stroke={'#3D4A3D80'}
      fill={'#A0AFA080'}
    />
  ))
}

const verticalContentInset = { top: apx(50), bottom: apx(40), left: apx(5),
right: apx(5) };

return (
  <View
    style={{
      backgroundColor: "#DDD",
      alignItems: "stretch",
    }}
  >
    <Svg height="40" width={apx(750)}>
      <SvgText
        fill="#A0AFA0"
        stroke="#3D4A3D"
        strokeWidth={apx(3)}
        fontSize={apx(50)}
        fontWeight="800"
        x={apx(375)}
        y={apx(45)}
        textAnchor="middle"
      >
        Conc vs Time
      </SvgText>
    </Svg>

    <View
      style={{
        flexDirection: "row",
        width: apx(750),
        height: apx(570),
        alignSelf: "stretch",
      }}
    >
      <YAxis
        style={{
          width: apx(60),
        }}

```

```

    data={data}
    yAccessor={({ item }) => item.conc}
    min={yMin}
    max={yMax}
    contentInset={verticalContentInset}
    svg={{ fontSize: apx(25), fill: "#617485" }}
  />
  <View style={{
    flex: 1,
  }} {...panResponder.panHandlers}>
    <AreaChart
      style={{ flex: 1 }}
      data={data}
      yAccessor={({ item }) => item.conc}
      xAccessor={({ item }) => item.timestamp}
      yscale={scale.scaleLinear}
      yMin={yMin}
      yMax={yMax}
      curve={shape.curveLinear}
      contentInset={{ ...verticalContentInset }}
      svg={{ fill: "url(#gradient)" }}
    >
      <CustomLine />
      <CustomGrid />
      <CustomGradient />
      <Tooltip />
      <CustomDot />
    </AreaChart>
  </View>
</View>
<XAxis
  style={{
    alignSelf: "stretch",
    marginTop: apx(5),
    marginBottom: apx(1),
    width: apx(750),
    height: apx(150),
  }}
  data={data}
  xAccessor={({ item }) => item.timestamp}
  formatLabel={(value, index) => {
    return (format((dateList[index] * 1000), 'HH:mm:ss'));
  }}
  contentInset={{
    left: apx(66),
    right: apx(30),
  }}
  svg={{
    fontSize: apx(25),
    fill: "#111485",

```

```
        y: apx(25),  
        originY: 30,  
        rotation: -40,  
    }}  
    />  
</View>  
);  
}
```

Appendix C: Web app program code

```

//App.js
import { StatusBar } from 'expo-status-bar';
import { StyleSheet, Text, View, TouchableOpacity, ScrollView } from 'react-native';
import { initializeApp } from 'firebase/app';
import { getDatabase, ref, onValue, set } from 'firebase/database';
import React, { useState, useEffect } from 'react';
import moment from "moment";
import { InteractiveChart } from "./app/InteractiveChart";
import { NavigationContainer } from '@react-navigation/native';
import { createBottomTabNavigator } from '@react-navigation/bottom-tabs';
import { MaterialCommunityIcons } from '@expo/vector-icons';
import { Entypo } from '@expo/vector-icons';
import { FontAwesome5 } from '@expo/vector-icons';

export default function App() {
  // Initialize Firebase
  const firebaseConfig = {
    apiKey: " AIzaSyB25S0k1TzxDeSVqTX3A2qZqj0er-aTFmZ ",
    authDomain: "esp32-b.firebaseio.com",
    databaseURL: "https://esp32-b-default-rtdb.asia-southeast1.firebaseio.com",
    projectId: "esp32-b",
    storageBucket: "esp32-b.appspot.com",
    messagingSenderId: "37278084142",
    appId: "1:372780841428:web:7410a1f5144488463abe4"
  };

  initializeApp(firebaseConfig);
  const db = getDatabase();

  const [conc, set_conc] = useState(0);
  const [fertilizer_type, set_fertilizer_type] = useState('Urea');
  const [max_conc, set_max_conc] = useState()
  const [his_data, set_his_data] = useState([ { timestamp: 0, conc: 0 },,]);

  //Read data
  useEffect(() => {
    readData(fertilizer_type)
  }, []);
  useEffect(() => {
    if (fertilizer_type === 'Urea')
      set_max_conc(0.435);
    if (fertilizer_type === 'MAP')
      set_max_conc(0.200);
  }, [fertilizer_type]);

  function readData(userId) {

```

```

const reference = ref(db, 'test1/' + userId);
onValue(reference, (snapshot) => {
  const data = snapshot.val();
  convert_his_data(data);
});
}

function convert_his_data(data) {
  var all_data = [];
  for (var obj_name in data) {
    all_data = [...all_data, { "timestamp": data[obj_name].timestamp, "conc":
data[obj_name].float }];
  }
  set_his_data(all_data);
}

const PrintHis = () => {
  let reverse_his_data = his_data.reverse();
  let time = [];
  for (var obj_name in reverse_his_data) {
    time = [...time, moment(new Date(his_data[obj_name].timestamp *
1000)).format('DD/MM/YYYY HH:mm:ss')];
  }
  return reverse_his_data.map((obj_data, index) => (
    <View key={index}>
      <Text style={{fontSize: 18 }}>{index + 1}~ {time[index]} :
{obj_data.conc} g/ml</Text>
    </View>
  ))
}

function Home() {
  return (
    <View style={styles.container}>

      <View style={{flex: 3, alignItems: 'center', justifyContent: 'center' }}>
        <ButtonLayout
          label="Type of fertilizer"
          values={"Urea", "MAP"}
          selectedValue={fertilizer_type}
          setSelectedValue={set_fertilizer_type}
          readData={readData}
        >
          <View
            style={styles.box}
          >
            <Text style={styles.labelResult}> {fertilizer_type} :
{his_data[Object.keys(his_data).length - 1].conc} g/ml </Text>
          </View>
        </ButtonLayout>

```

```

    </View>

    <StatusBar style="auto" />
  </View>
);
}
function Graph() {
  return (
    <View style={styles.container}>

      <Text style={[styles.labelResult, { fontSize: 28 }]}>
        {fertilizer_type}
      </Text>
      <InteractiveChart data={his_data} />

      <StatusBar style="auto" />
    </View>
  );
}
function History() {
  return (
    <View style={styles.container}>
      <ScrollView>
        <View style={styles.history}>
          <Text style={[styles.labelResult, { fontSize: 18 }]}>
            History : {fertilizer_type}
          </Text>
          <PrintHis />
        </View>
      </ScrollView>
      <StatusBar style="auto" />
    </View>
  );
}
const Tab = createBottomTabNavigator();
return (
  <NavigationContainer>
    <Tab.Navigator
      initialRouteName="Home"
      screenOptions={{
        tabBarActiveTintColor: '#19A019',
        tabBarActiveBackgroundColor: '#A0AFA090',
        tabBarInactiveTintColor: '#3D4A3D',
        showLabel: true,
        tabBarStyle: {
          position: "absolute",
          bottom: 20,
          left: 20,
          right: 20,
          elevation: 0,

```

```

        backgroundColor: '#A0AFA080',
        high: 80,
        borderRadius: 20,
    },
    tabBarLabelStyle: {
        fontSize: 12,
    },
    headerShown: false,
    tabBarItemStyle: {
        borderRadius: 20,
    },
  },
}
}
}
</Tab.Navigator>
</NavigationContainer>
);
}

const ButtonLayout = ({

```

```

label,
children,
values,
selectedValue,
setSelectedValue,
readData,
}) => (
  <View style={{ padding: 10 }}>
    <Text style={styles.label}>{label}</Text>
    <View style={styles.row}>
      {values.map((value) => (
        <TouchableOpacity
          key={value}
          onPress={() => { setSelectedValue(value); readData(value) }}
          style={[
            styles.button,
            selectedValue === value && styles.selected,
          ]}
        >
          <Text
            style={[
              styles.buttonLabel,
              selectedValue === value && styles.selectedLabel,
            ]}
          >
            {value}
          </Text>
        </TouchableOpacity>
      ))}
    </View>
    <View style={[styles.container1]}>
      {children}
    </View>
  </View>
);

```

```

const styles = StyleSheet.create({
  container: {
    flex: 1,
    backgroundColor: '#fff',
    alignItems: 'center',
    justifyContent: 'center',
  },

  box: {
    backgroundColor: "powderblue",
    alignSelf: "center",
  },

  row: {
    flexDirection: "row",

```



```
    flexWrap: "wrap",
    justifyContent: 'space-between',
  },
  button: {
    paddingHorizontal: 8,
    paddingVertical: 6,
    borderRadius: 14,
    backgroundColor: "#A0AFA0",
    alignSelf: "center",
    marginHorizontal: "1%",
    marginBottom: 6,
    minWidth: "30%",
    textAlign: "center",
  },
  selected: {
    backgroundColor: '#3D4A3D',
    borderWidth: 0,
  },
  buttonLabel: {
    fontSize: 22,
    fontWeight: "700",
    color: "#3D4A3D",
    textAlign: "center",
  },
  selectedLabel: {
    color: "#6BA4FF",
  },
  label: {
    textAlign: "center",
    marginBottom: 10,
    fontSize: 34,
  },
  container1: {
    marginTop: 8,
  },
  labelResult: {
    textAlign: "center",
    marginBottom: 5,
    marginTop: 5,
    fontSize: 22,
  },
  history: {
    width: 'auto',
    height: '20%',
    backgroundColor: "powderblue",
    alignSelf: "center",
    justifyContent: 'center',
    alignItems: 'center',
    flexWrap: "nowrap",
    flex: 1,
```

```
position: 'relative',  
bottom: 0,  
},  
});
```

LIST OF PUBLICATIONS

Lim, Z.Y., Mun, H.K., Kwan, B.H., 2022. *Real-time liquid fertilizer concentration measurement based on planar microwave sensor*. In: 17th International Engineering and Computing Research Conference (eureca). Taylor's University, Lakeside Campus, 29 June 2022.